Spectral Characterization of Cytochromes CYP11A1 (aka P450scc) Active Site and Catalytic Intermediates

Qianhong Zhu
Marquette University

SPECTRAL CHARACTERIZATION OF CYTOCHROMES CYP11A1 (*aka* P450scc) ACTIVE SITE AND CATALYTIC INTERMEDIATES

By

Qianhong Zhu, B.Sc., M.S.

A Dissertation submitted to Faculty of the Graduate School,
Marquette University,
in Partial Fulfillment of the Requirements for
the Degree of Doctor of Philosophy

Milwaukee, Wisconsin

May 2015

ABSTRACT

SPECTRAL CHARACTERIZATION OF CYTOCHROMES CYP11A1 (*aka* P450scc) ACTIVE SITE AND CATALYTIC INTERMEDIATES

Qianhong Zhu, B.Sc., M.S.

Marquette University, 2015

The Cytochromes P450 are monooxygenases which use dioxygen and endogenous reducing equivalents to generate highly reactive intermediates capable of performing several types of oxidative transformations, most commonly, hydroxylations via the so-called Compound I species. There are two main kinds of mammalian P450s: those functioning in drug metabolism and those that facilitate steroid biosynthesis. Steroidogenic P450s participating in the biosynthesis of steroid hormones are involved in a number of different pathways. CYP11A1, one of the steroidogenic P450s also known as P450scc, is the enzyme that converts cholesterol to pregnenolone through side chain cleavage between carbon 20 and 22. The overall process is a three step reaction. The two intermediates, 22(R)-hydroxycholesterol and 20R,22R-dihydroxycholesterol, bind more tightly than either cholesterol or pregnenolone. One of the most interesting aspects of the enzymatic cycle is that, while the first two reactions involve substrate hydroxylations, presumably proceeding through the Compound I species, the third reaction involves a side chain cleavage reaction that has been proposed to occur through Compound I attack on the diol fragment of the 20R,22R-dihydroxycholesterol.The present work employs resonance Raman (rR) spectroscopy to structurally characterize the enzyme active site structure. Also, in order to obtain a generally useful calibration procedure to permit reliable rR-based evaluation of the percentage of HS and LS population for CYP11A1 and other P450s, a method was developed to relate HS/LS populations to measured intensities of spin state markers based on well-behaved CYP101 reference samples. These cross section values from P450cam high spin and low spin are used to determine the spin population in CYP11A1 complex with three different substrates and evaluate the effect of Adx binding. The work also clarifies certain confusing issues that had arisen from previously published spectroscopic studies of ferric and ferrous-CO states. Most significantly, the present work provides the first rR spectroscopic characterization of the oxy adducts for the three substrate-bound forms, providing some insight into the active intermediates involved in the three sequential reactions.

ACKNOWLEDGEMENTS

Qianhong Zhu, B.Sc., M.S.

My heartfelt thanks go to Professor James R. Kincaid for his continued mentorship throughout my time in his research group. I will forever be grateful for his guidance and his major contribution to my career development. I would like to also express my appreciation to my Committee members, Professors Daniel S. Sem, Michael. D. Ryan and Adam Fiedler for useful discussions throughout my studies, writing of this dissertation and being flexible in time for my research meeting, annual review and thesis defense. I am so grateful to Professor Michael, D. Ryan for kindly offering his UV-vis instrument in my research. Also I am thankful to Dr. James Anderson, Dr. Pinfen Yang and Dr. Daniel S. Sem for their help during the purification CYP11A1 and offering me to use their equipment in their lab. I would also like to thank Dr. Piotr Mak for his guidance, help, his patience and time during my research time. Without his help, I could not finish my research. My sincere gratitude is also extended to my group members, Drs. K. Czarnecki and P. Mak for introducing me to resonance Raman spectroscopy and continued technical advice and support. Also thanks to my peer group members, Ying Wang, Remigio Usai, Yinlin Liu, for their help.

Finally, I would like to express my heartfelt thanks to my mom for her unconditional support and help for my academic success. Also I would like to thank my little son for his company during all my time in Milwaukee and his love. I also would like to thank my family members and friends for believing in me and encouraging me continuously.

TABLE OF CONTENTS

LIST OF FIGURES

LIST OF TABLES

1 General Introduction

1.1 Heme proteins

Proteins are metalloproteins which contain an iron protoporphyrin IX (structure showed in Figure 1.1.1) as a cofactor. These types of proteins play very important roles in mammalian life. They can serve as oxygen transporter and storage[1], as a catalyst in a difficult reaction[2], as electron transporter[3] or for NO synthesis[4]. There are four main classes of heme proteins. 1) Globins serve as oxygen transporter and storage. Hemoglobin (Hb) in blood cells serves as oxygen transporter from high oxygen concentration in lung tissue to low oxygen concentration in bodily tissues. Myoglobin (Mb) in muscle can store oxygen until the cells need it.[1] 2) Electron transport proteins include cytochrome b_5 and other cytochromes.[3] 3) Nitrophorins serve as NO carrying protein.[5,6] 4) The last type, classified as oxidoreductases, is used as catalyst which can use O_2 or H_2O_2 to oxidize the substrates, for example P450s, peroxidases, etc.[4]

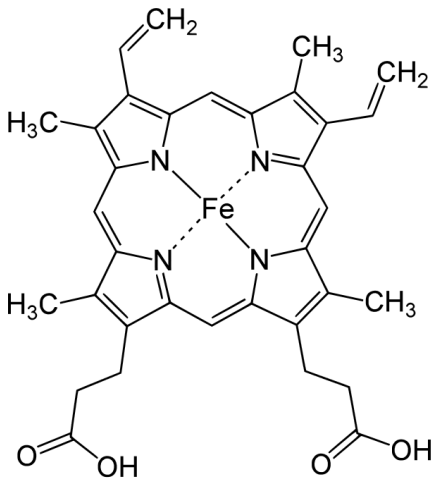

Figure 1.1.1 Structure of iron protoporphyrin IX

1.1.1 Globins

There are two main globins: hemoglobin (Hb) and myoglobin (Mb).[1] Myoglobin is found in the muscle tissue which stores oxygen until the cells use it. Myoglobin is a monomer, a relatively small molecular weight (~16 kDa), which contains only one heme in one isolated polypeptide.[7] The oxygen binds to the heme group, which serves as the sixth ligand, the trans-axial (so-called proximal) ligand of the myoglobin being an imidazole fragment of a histidyl residue. Comparing hemoglobin and myoglobin, hemoglobin is a tetramer which consists of four myoglobin-like subunits, two of them called α subunits and another two called β subunits, each of them containing a heme group.[7] The ribbon diagrams of myoglobin and hemoglobin are shown in Figure 1.1.2.

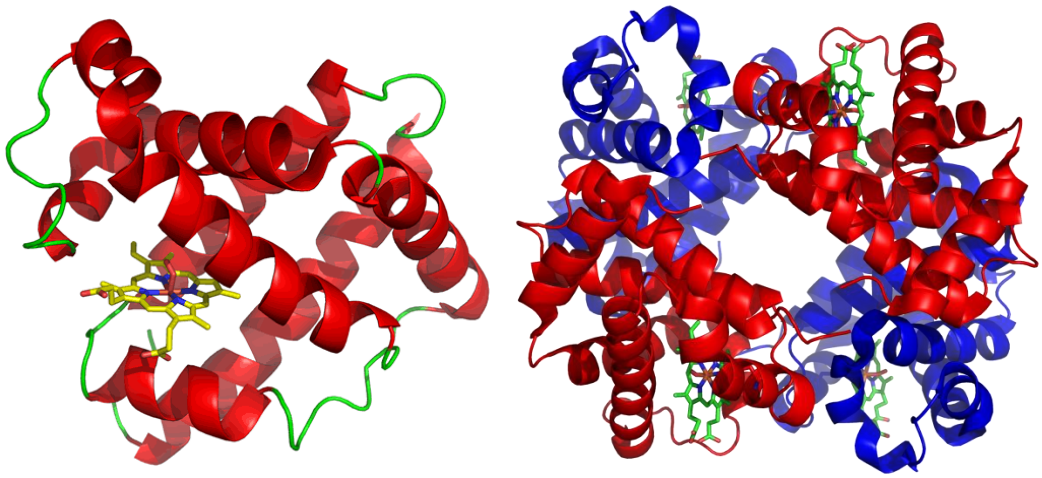

Figure 1.1.2 Ribbon diagram of myoglobin (left) and hemoglobin (right) with its α and β subunits represented in red and blue. [7]

With the conformational difference between Mb and Hb, their ability to bind oxygen is quite different. Myoglobin binds with oxygen according to a hyperbolic curve typical of at a simple bi-molecular chemical equilibrium. On the other hand, the curve for oxygen binding to Hb exhibits a sigmoidal (so-called "S-shaped") curve that is characteristic of allosteric ligand binding, where early oxygen binding steps induce a global conformational change that enhances the affinity of remaining empty heme sites. This behavior is depicted in Figure 1.1.3, which shows the oxygen binding curves for Mb and Hb.[8] As can be seen, at low oxygen pressure characteristic of bodily tissues, the binding affinity of Hb for oxygen is lower than that of Mb while at high oxygen pressure, as exists in the lung, the binding affinity of Hb and Mb are comparable. This process allows hemoglobin to more efficiently carry oxygen from the lung to the cell tissue.

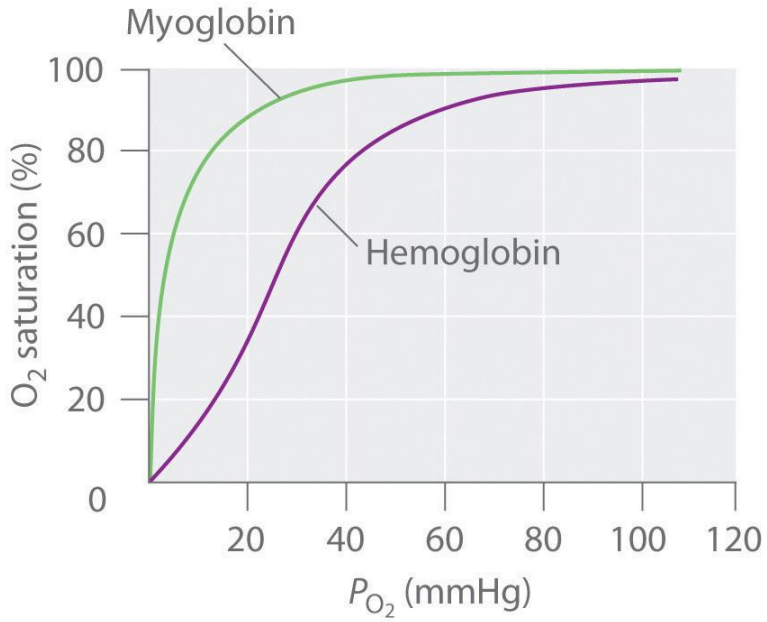

Figure 1.1.3 The oxygen binding curve by myoglobin and hemoglobin[8]

Though this description of the functional properties of hemoglobin allosteric binding is commonly accepted, the precise molecular transformations that give rise to this allostery are still not fully understood and are the subject of continuing interest. In fact, recently our group has been collaborating with that of Professor Spiro's group at the University of Washington and I have succeeded in preparing judiciously designed hybrid hemoglobins to facilitate these studies, the results for a hybrid containing mesoheme and protoheme (i.e., $[\alpha_{meso}\beta_{proto}]_2$ and $[\alpha_{proto}\beta_{meso}]_2$) having been recently published in the *Journal of the American Chemical Society*,[9] with ongoing similar studies of the Fe/Co hybrids expected to conclude in the near future Though not included in this dissertation, which is devoted to studies of Cytochromes P450, the experimental details involved in preparing these hybrids are included in Appendices section of this dissertation.

1.1.2 Cytochromes

Heme proteins which serve as electron transfer proteins belong to a large family of cytochromes that are responsible to produce ATP. The cytochromes are classified to four groups according to the binding mode with heme: *a*, *b*, *c*, *d* and *f*. [10] Among these four groups, Cyt*b* containing proto heme and Cyt*c* containg a proto heme which is covalently bound with protein are the most studied cytochromes.

The Cyt*b* can be found in the mitochondrion of eukaryotes and in aerobic prokaryotes. It is an integral membrane protein, also known as bc1 complex, which has two heme groups with around 400 amino acid residues.[11] The molecular weight is about 40 kDa. Cyt*c* can be found in inner membrane of the mitochondria which is a small protein with 103-112 amino acid residues. The molecular weight is around 12 kDa.[3]

The electron transfer process involves a heme oxidation state change between Fe(II) and Fe(III). Cytochromes are performing reduction (from Fe(III) to Fe(II)) and oxidation (from Fe(II) to Fe(III)) reactions during the electron transfer process.[12] This reaction is involved in the process generating ATP, which is for intracellular energy transfer.

1.1.3 Nitrophorin

Nitrophorin (NP) is one type of NO-carrying heme protein which can be found in the saliva of the blood feeding insects, the kissing bug (*Rhodnius prolixus*) and the bedbug (*Cimex lectularius*).[5,6] The adult Rhodnius prolixus contains at least four NPs which are designated to NP1-4,depending on their relative abundance in the glands which have been widely studied.[6] The NPs in the kissing bug bind with histamine and NO when NO releases, the histamine will be scavenged by coordination to the heme Fe while the NPs in bed bugs bind with two NOs, one to the heme and the another one to the cysteine which serves as the ligand when NO is absent. This requires the bond cleavage between the Fe and S from the cysteine group.

Under physiological conditions, the neurotransmitter, NO, is oxidatively generated from arginine by nitric oxide synthase (NOS), with the soluble guanylate cyclase (sGC) acting as the NO receptor. NPs serve as a group of NO-carrying protein which enter the salivary gland then cause the diffusion of the NO with NOS then NO molecular binds with the NP instead. The low pH (5-6) [13] environment in the saliva helps stabilize the NP-NO complex with Fe(III) which makes this diffusion and binding with NP more favorable. NPs are insect protein and they will interact with the blood environment when they are sucking blood. The pH environment will change in blood at ~7.4 versus the saliva 5-6.[13] This drastic pH change causes some conformational change in some NPs which lead to the diffusion of NO from NPs. Then the NO receptor (sGC) binds with NO. [5,6] The NP is used for transport the NO molecular.

1.1.4 Heme oxidoreductases

Heme-containing oxidoreductases are the main proteins studied in our lab. They can catalyze a wide range of reactions; for example, hydroxylation, bond cleavage, aromatization, etc.[2] The reactions of interest in our lab are catalyzed through oxidation reaction on the substrates using O_2 or H_2O_2. There are many types of enzymes which are capable of catalyzing oxidation reactions; for example, peroxidases, NOS, heme dioxygenases, heme-thiolate haloperoxidases and P450s.[4] Since P450s will be discussed in next sections in a very detailed way, in this section basic summaries of some other oxidative heme enzymes are presented.

1.1.4.1 Peroxidases

Due to the easy preparation of horseradish peroxidase (HRP), this type of enzyme became the first studied heme enzyme since 1903.[14] The molecular weight of a peroxidase is 30-150 kDa[15] with a histidine residue attached to the heme Fe through Fe-N bond. The ribbon diagram of HRP is shown in Figure 1.1.4.

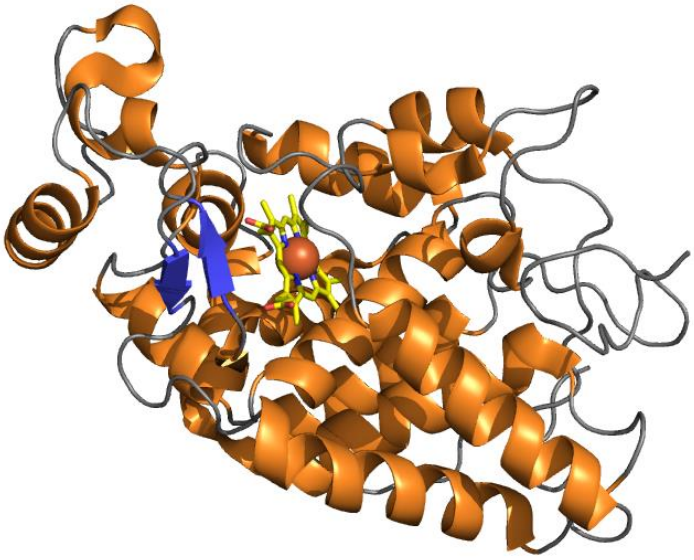

Figure 1.1.4 The ribbon diagram of horseradish peroxidase (HRP) [14]

Peroxidases can catalyze a wide range of reactions under the presence of peroxide such as oxidize the polymerisation of phenols and aromatic amines. The peroxidase reaction will go through a cycle similar with P450s.[4,15] The first step of the cycle is that the peroxide, H_2O_2, removes one electron from Fe (III) and a second electron from porphyrin to generate an unstable intermediate called compound I which is a ferryl heme π cation radical, where one electron has been removed from the heme porphyrin

framework and another from the ferric iron to generate an oxo-Fe(IV) fragment, the peroxide being reduced to H_2O. In the second step, the electron donor substrate donates an electron to compound I which becomes compound II, a ferryl heme moiety, where the porphyrin radical has been reduced. In the last step, compound II is further reduced by a second substrate, regenerating the Fe(III) state. This process will produce another free radical and a molecular of H_2O. The substrates for HRP like peroxidase are usually phenols and aromatic amines. The scheme of this process is shown in Figure 1.1.5.

1. $Fe^{3+}R + H_2O_2 \longrightarrow Fe^{4+}{=}O\ R^{\cdot+} + H_2O$

   Compound I

2. $Fe^{4+}{=}O\ R^{\cdot+} + SH \longrightarrow Fe^{4+}{=}O\ R + S^{\cdot}$

   Compound II

3. $Fe^{4+}{=}O\ R + SH \longrightarrow Fe^{3+}\ R + S^{\cdot} + H_2O$

Figure 1.1.5 Catalytic cycle scheme of peroxidase (S: substrate) [4]

1.1.4.2 Nitric oxide synthase (NOS)

Nitric oxide synthase (NOS) catalyzes the synthesis of NO from arginine through two consecutive cycles.[4,16] This type of enzyme can be found in many species, like mammals, fish, birds, invertebrates, and plants, bacteria.[17] The most well studied NOSs are from mammals. There are three main types of NOS isozymes according to the gene sequence: neuronal NOS (nNOS) found in neuronal tissues in nervous system, inducible NOS (iNOS) found in macrophages in immune system, endothelial NOS (eNOS) found in endothelial cells in cardiovascular system.[18]

The NOS has a cysteine in the proximal side and hydroxylates substrates through a general P450 like cycle.[4,18] In the resting state, NOS bound with BH_4, the heme is primary five coordinate with small component in six coordinate. Upon binding of the substrate, $_L$-arginine (Arg), or N^{ω}-$_L$-hydroxyarginine (NOHA), the heme becomes fully five coordinate. The general mechanism is shown in Figure 1.1.6. In the first step, the BH_4 bound NOS in the resting state (I) is reduced by one electron from NADPH. The second step, this ferrous species binds with an oxygen molecule which forms ferrous-oxy complex (III). The third step, this ferrous-oxy complex structurally rearranges to ferric superoxide complex (IV) which is more reasonable for electron density distribution. These three steps are exactly the same as P450s which you will see in the P450 mechanism cycle part. The forth step, the superoxide complex accepts an electron and a proton from BH4 to generate hydroperoxy complex (V). The electron from BH4 will reduce complex (IV) to a cationic pterin radical which is eventually reduced by a reductase domain and regenerate BH4. This step is different in P450s, which accept

electron from NADPH again and proton is from the surrounding environment, H_2O or amino acid residues. Then the hydroxyperoxy complex is quickly protonated to form a very reactive π cation radical species, compound I (VI) with releasing of a water molecule. This complex insert the oxygen molecule to substrate Arg to form NOHA then the complex is back to its resting state.

Through the second cycle, the complex formation from I-V is the same as the first cycle. The hydroxyl complex (V) reacts with substrate NOHA, generated from the first cycle, to generate NO and L-citrulline. The NO and L-citrulline then depart the active site for next physiological process in other place.

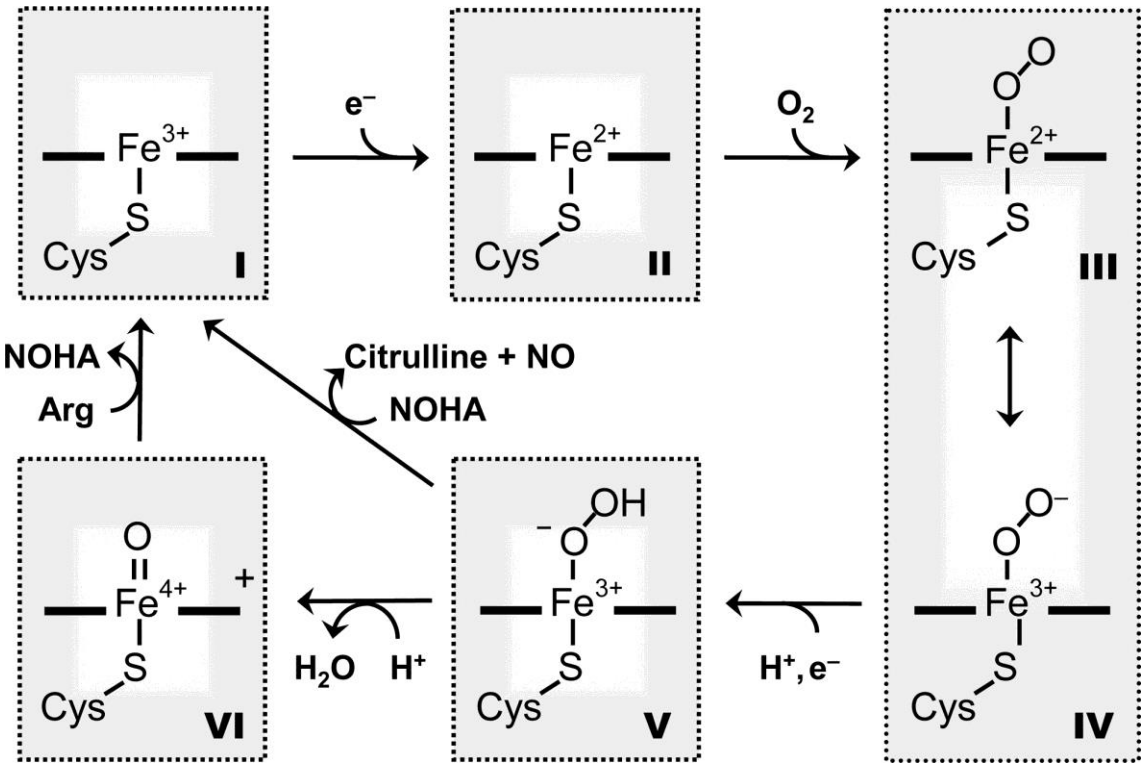

Figure 1.1.6 The mechanism of NOS reaction cycle[18]

1.1.4.3 Heme oxygenase

Heme oxygenase (HO) is one type of heme protein which catalyzes the heme degradation in order to release non-toxic heme fragments.[4,19] Hemoglobin is the main source of heme. The heme groups from about 6-8 g of hemoglobin (molecular weight 64 kDa) are degraded daily; i. e., degradation of 300 mg (molecular weight 656 g/mol) of protoheme.[4] There are many types of HOs found in human, rat and bacteria. Human HO-1 was is the first structure reported. The heme in HO is sandwiched between the proximal and distal helices, as shown in Figure 1.1.7, with a histidine group on the proximal side.

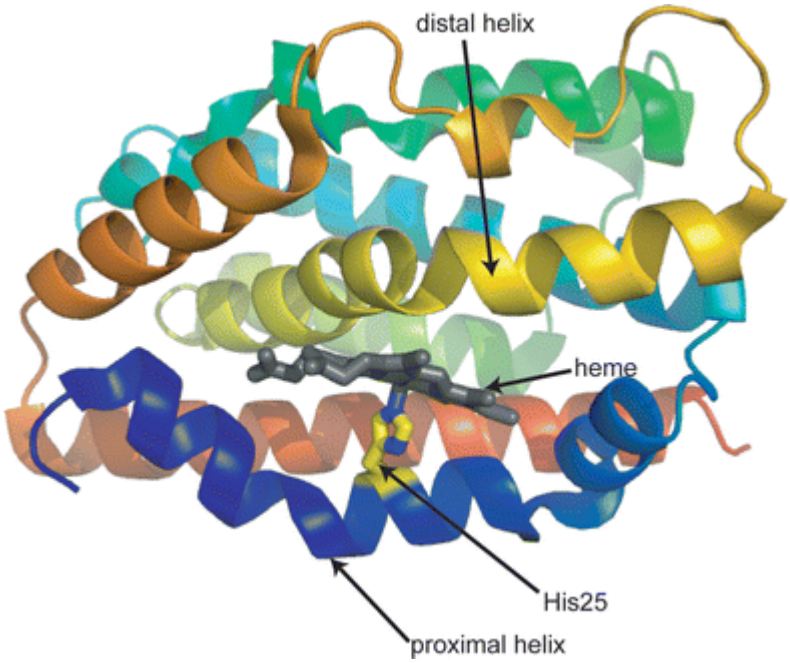

Figure 1.1.7 The ribbon diagram of heme oxygenase[20]

The heme oxygenase system consist a heme oxygenase and a NADPH contained P450 reductase. The mechanism involves three cycles to generate biliverdin.[4] The first step of the overall reaction is to form α-meso-hydroxyheme. The ferric heme Fe(III) is reduced to Fe(II) by one electron donated from NADPH contained P450 reductase. Then it binds with oxygen molecular to form oxy complex, most reasonably formulated as ferric superoxide Fe(III)-O-O^{-1}. This complex accepts another electron from the reductase and a proton from a water molecule in the active site to form ferric hydroperoxide species Fe(III)-O-OH. Then the terminal oxygen reacts with the α-meso-carbon of the porphyrin to generate the ferric a-meso-hydroxyheme. Figure 1.1.8 shows the detailed mechanism of heme degradation.

The second step is the verdoheme generation. The α-meso-hydroxyheme can be depronated to generate an Fe(II) radical with two resonance structures. This complex can go through two pathways to generate verdoheme. In the first pathway, the Fe(II) radical species can first accept an electron and then with bind with molecular oxygen and react, releasing CO to form verdoheme. The other pathways is that the Fe(II) radical species first binds with oxygen and reacts, releasing CO, and then is reduced by one electron to generate verdoheme. Even though the pathways are different, the two steps of binding with oxygen and being reduced by one electron are the same in the two pathways, as can be seen in Figure 1.1.8.

The mechanism of last step, verdoheme to biliverdin, is not well understood. The proposed mechanism shown in Figure 1.1.8 is according to intermediates seen from the QM/MM calculation and crystallography studies.[21,22] After generation, the reaction cycle is done then the biliverdin will be released from the active site of the protein.

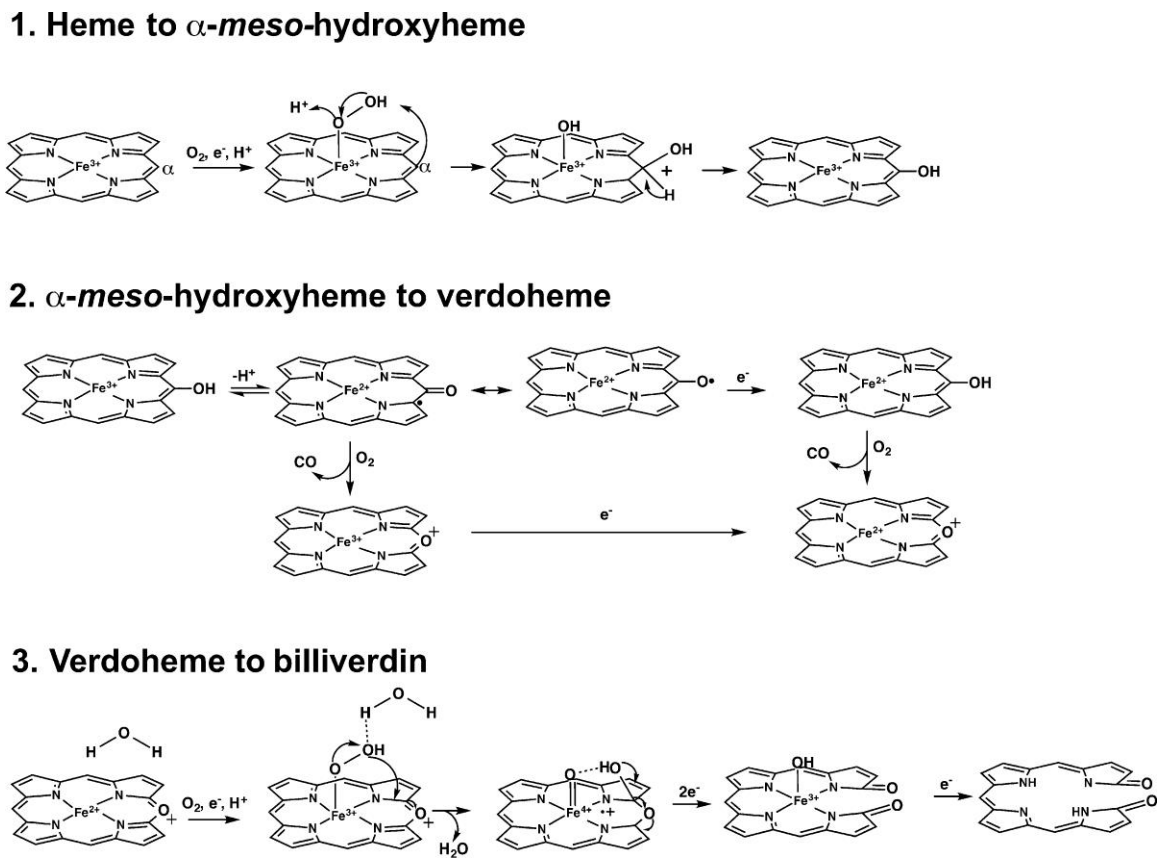

Figure 1.1.8 Mechanism of heme degradation[4]

1.1.4.4 Heme-thiolate haloperoxidases

Heme-thiolate haloperoxidases are among the most versatile biocatalysts in the heme protein family.[4,23] Among all these types of enzymes, the most well-known one is chloroperoxidase (CPO), which belongs to haloroperoxidase family, which can oxidize chloride (Cl^-), bromide (Br^-) and/or iodide (I^-), but not fluoride (F^-). Figure 1.1.9 shows some of the halogenations catalyzed by CPO.[23] As can be seen, CPO can catalyze oxidation of not only Cl, but also other halogens.

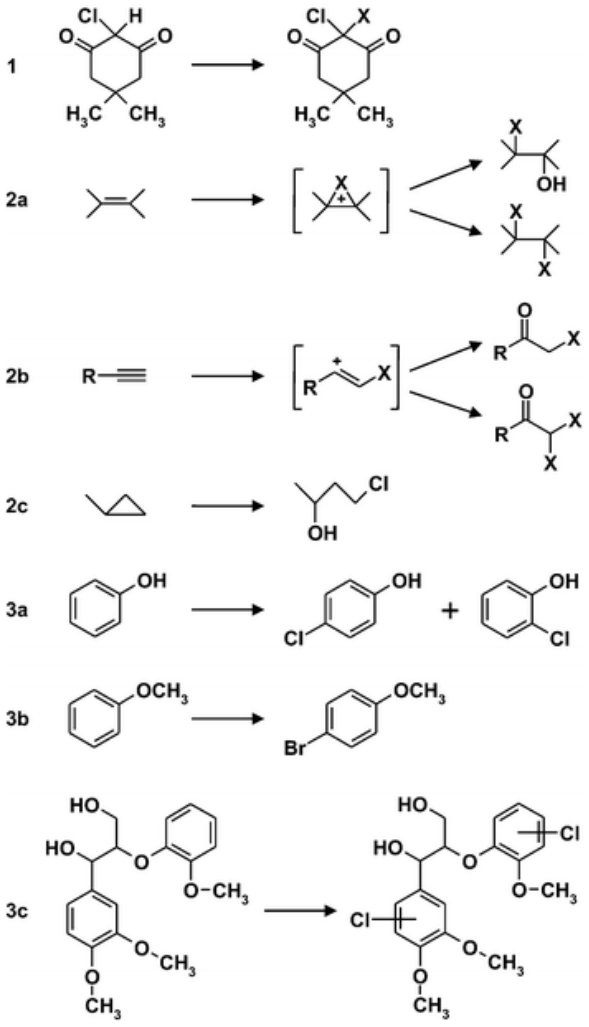

Figure 1.1.9 Halogenation catalyzed by CPO [23]

Besides halogenation, CPO can catalyze many types of reactions, for example, olefin oxidation, oxygenation insertion, sulfoxidation, etc.[23] The Figure 1.1.10 shows all the reactions can be catalyzed by CPO.

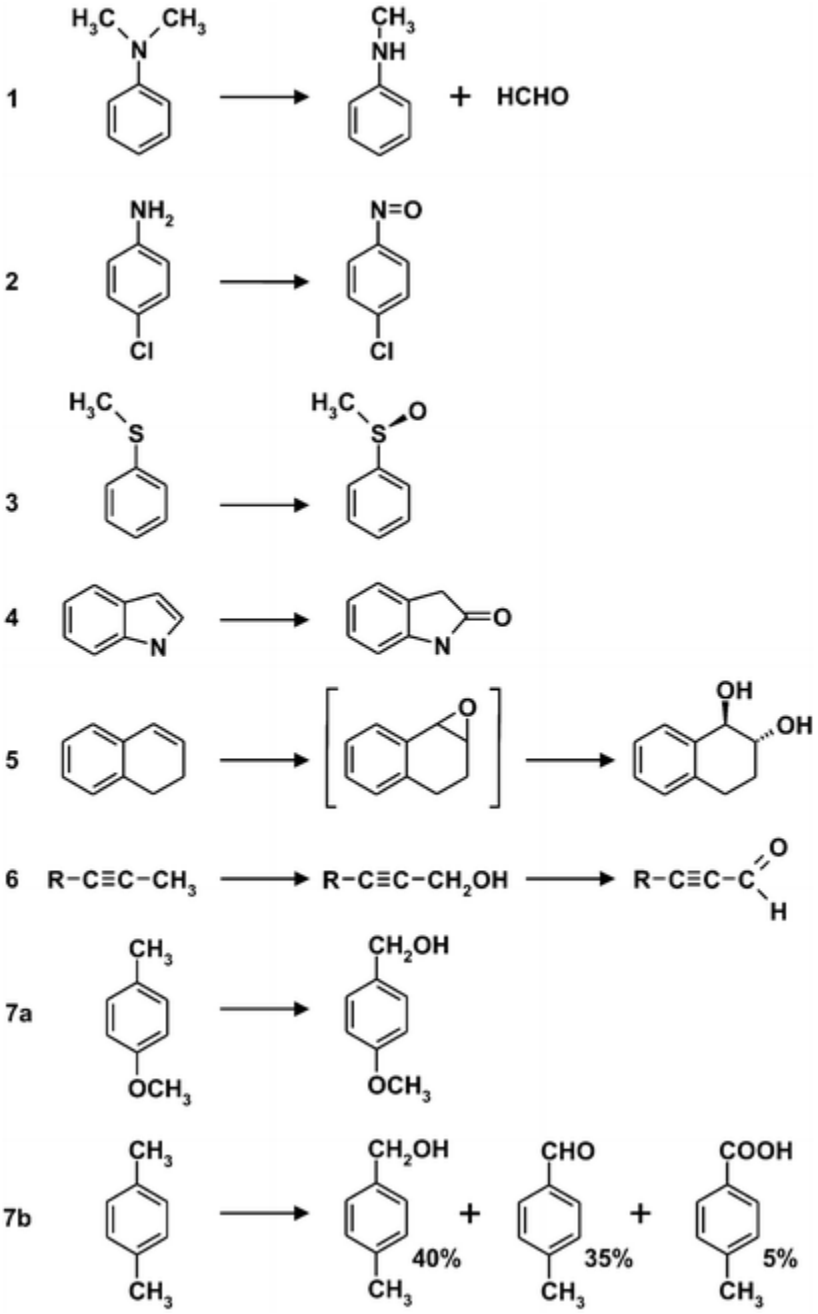

Figure 1.1.10 non-halogenation reactions catalyzed by CPO [23]

Since CPO can catalyze a wide range of reactions, it becomes a very flexible catalyst compared with other heme enzymes. The proposed mechanism of the oxidation cycle[23] is shown in Figure 1.1.11. In the first step the resting state **(1)**, Fe(III) bound with S from cysteine on the proximal side, binds H_2O_2, then goes through a bond cleavage of O-O and release a H_2O molecule to generate the reactive π cation radical species, compound I **(2)**. This process needs two electrons transferred from the heme. Compound I is a very reactive species which can react with various types of substrates.

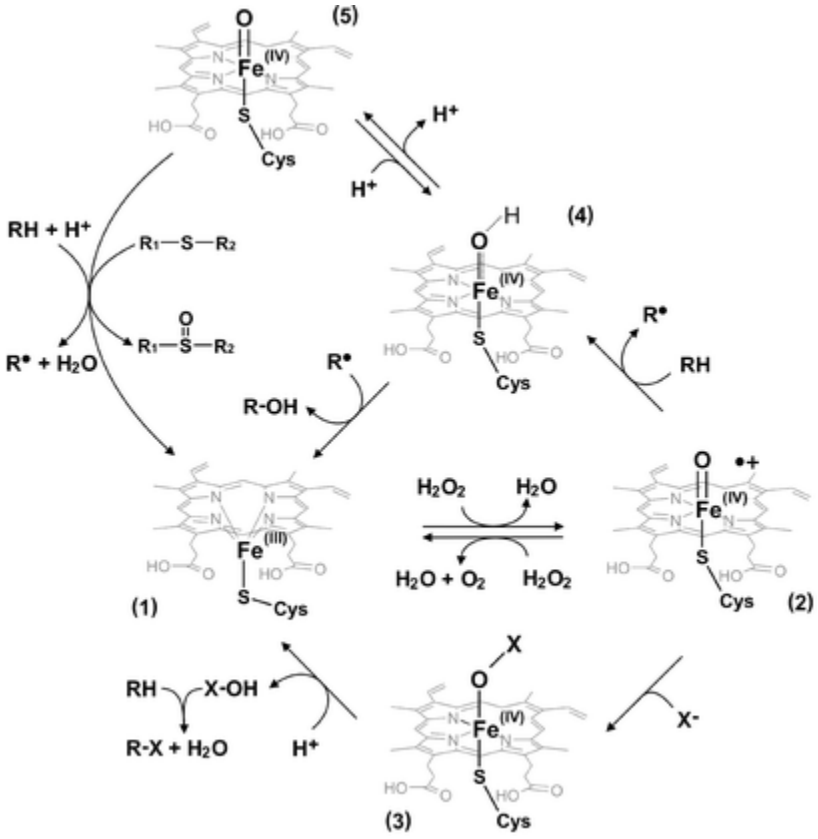

Figure 1.1.11 Catalytic cycle of haloroperoxidase [23]

1.2 Cytochrome P450s

1.2.1 Discovery of P450s

In 1955 Axelrod[24] and Brodie[25] first discovered that the oxygenase enzyme system in the endoplasmic reticulum of the liver. In 1958, Garfinkel[26] and Klingenberg[27] reported the special CO bound pigment in the liver microsomes which showed a strong Soret absorption maximum at 450nm in the UV absorption spectrum (Figure 1.2.1). This special type of enzyme was named Cytochrome P450 according to its characteristic absorption feature.

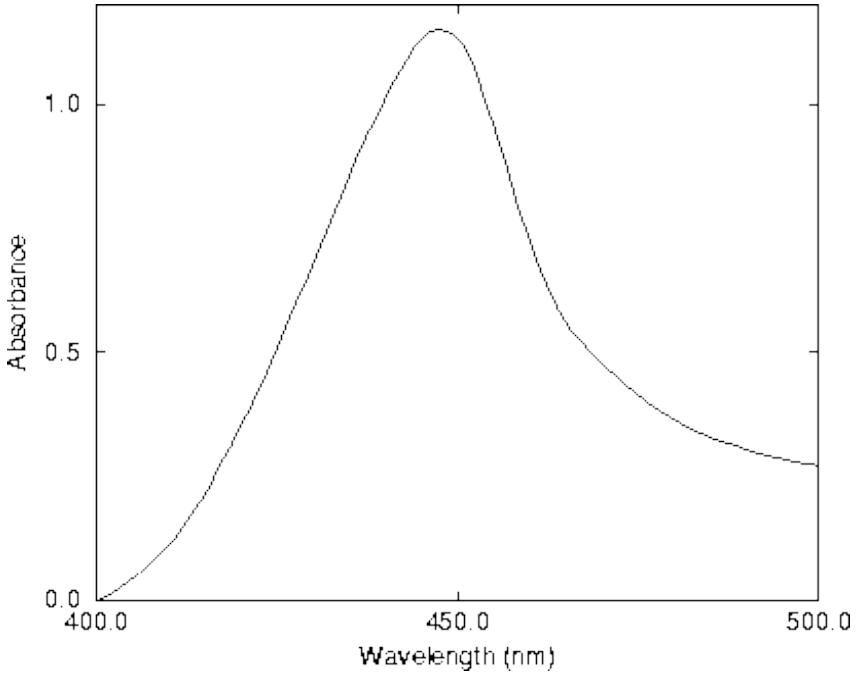

Figure 1.2.1 Absorption spectrum of Cytochrome P450-CO complex showing the characteristic Soret peak at ~ 450 nm [26,27]

The electron spin resonance spectroscopy identified that protein is a low spin ferric form hemoprotein.[28] In 1964, this liver microsomes pigment was purified and the properties were tested which proved the heme group was bound with a thiolate residue through S atom.[29–32] This gives the reason that the strong absorption feature came from the charge transfer of Fe-S bound.[33] Resonance Raman spectroscopy also provided definitive evidence that S was the cysteine residue which was covalently bond with the Fe in the heme group.[33–35]

Because P450s can hydroxylate very different kinds of compounds and give specific stereochemistry configuration by using atmospheric oxygen,[36] research on P450s covers a broad spectrum of scientific interests (Figure 1.2.2).[37]

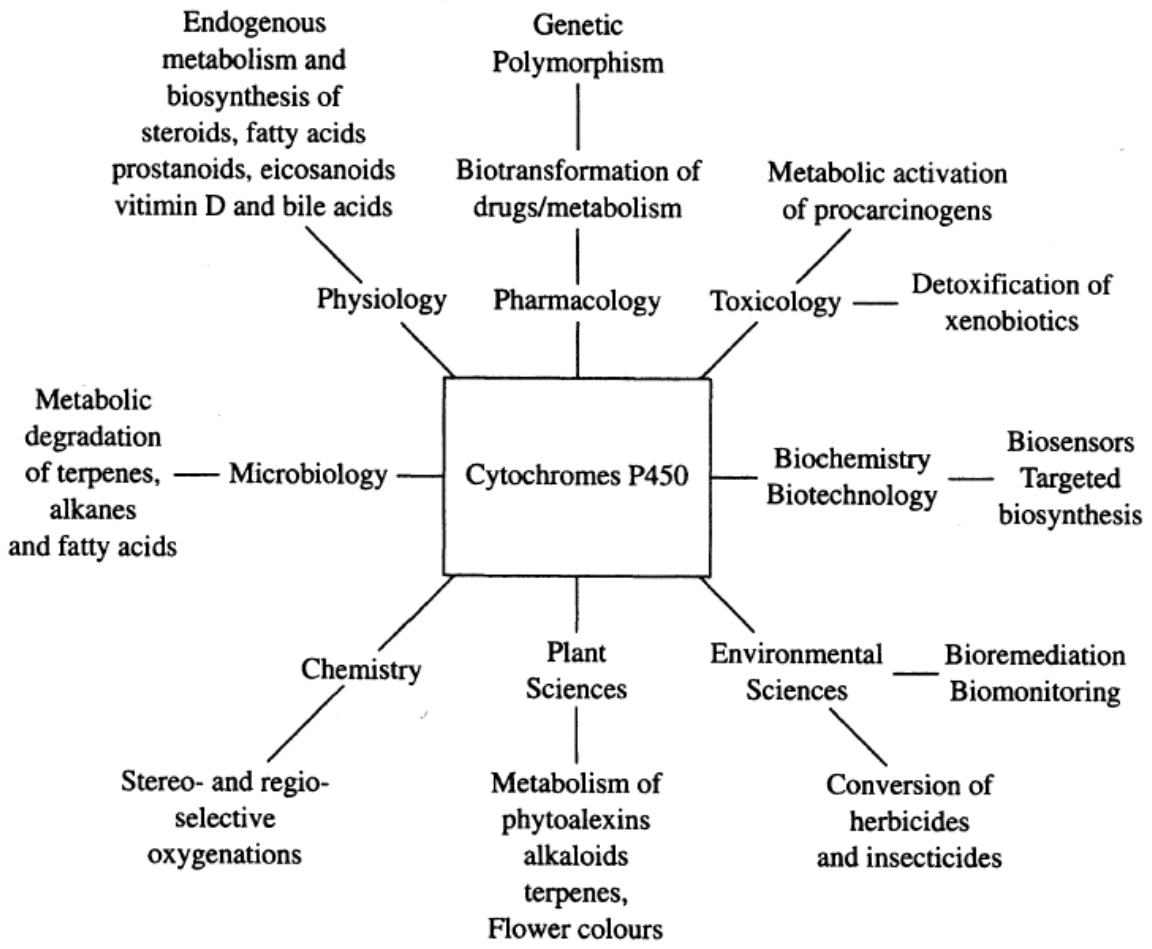

Figure 1.2.2 P450 research fields and its application [37]

1.2.2 Nomenclature

There was no problem when there were only few P450 crystal structures. Name was given by its substrate, for example, P450cam (also known as CYP101), or its function, P450scc (also called CYP11A1), etc. However, as more and more P450 enzymes have been discovered and characterized, it became apparent that the number of P450 genes and proteins is very large so it became necessary to develop a nomenclature system. The systematic naming took place since 1989 according to the gene evolution.[38] The nomenclature system uses symbol CYP as an abbreviation for Cytochrome. An alphanumerical code is used for P450 families, subfamilies and individual proteins.[37] Example is given below:

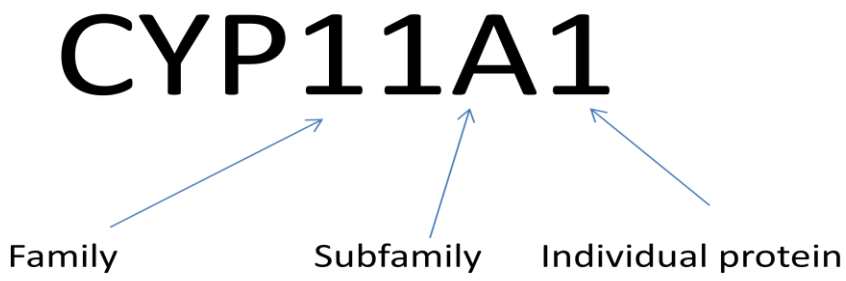

Figure 1.2.3 Systematic nomenclature for P450s, examples given as CYP11A1

1.2.3 Catalytic cycle

P450s can catalyze impressive range of reaction, such as ring expansion and carbon-carbon bond cleavage.[36] In order to better understand the impressively diverse chemical reactivity accessible to these enzymes, we need to better understand what exactly is happening at the active site; i.e., what types of species are encountered in the catalytic cycles of these enzymes. The enzymatic cycle shows the process and intermediates generated during one cycle (Figure 1.2.4). Some enzymes can do multiple cycles and then release the product, for example CYP11A1 which converts cholesterol to pregnenolone through three consequential cycles.[39,40]

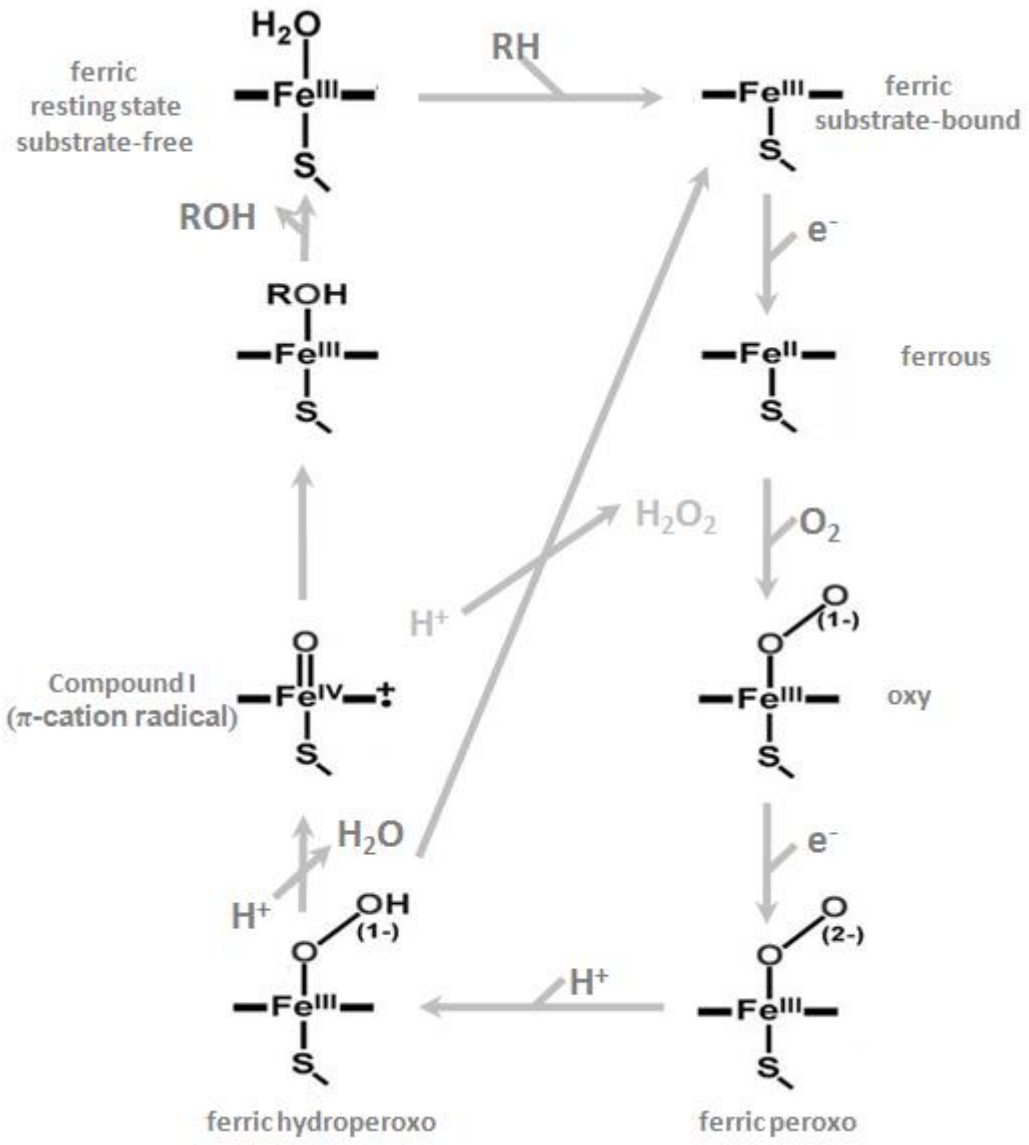

Figure 1.2.4 Catalytic cycle for general P450s

The cycle takes place from the resting state which is substrate free form. The heme iron in this state is a low spin (LS) ferric form and its sixth ligand is a water molecule from the water cluster in the distal pocket. The binding of a suitable substrate, such as camphor in case of CYP101, causes disruption of the distal pocket network of water molecules and displacement of the ligated water to generate a 5-coordinated heme with consequent stabilization in the high spin (HS) state.

Now, the reduction potential of the HS heme increase which leads to facilitate electron transfer from the natural (or artificial) reductase to the substrate bound P450 through redox partner, with the resultant ferrous state remaining in high spin (HS).[34,41,42] This relatively electron rich Fe(II) in its high spin (HS) state combines with the electron deficient dioxygen molecule.[43] Based on a wealth of supportive spectroscopic evidence, this Fe(II)-O_2 complex is most reasonably formulated as a ferric-superoxide species, Fe(III)-O-O^{-}.[42,44]

A second electron is transferred from a reductase also via electron transport system, the redox partner. Then it generates a negatively charged ferric peroxo group which is Fe(III)-O-O^{2-}. This species can be quickly protonated by local transferred hydrogen from water or surrounding amino acid side chain. Then it becomes ferric hydroperoxo Fe(III)-(O-OH^{-}). This complex can be further protonated, by a local donor, at the distal oxygen atom, promoting O-O bond cleavage, generating a highly reactive species, commonly called P450 Compound I. This species is best formulated as an Fe(IV) oxo species with the second oxidizing equivalent generating a heme based π-cation radical localized over the porphyrin macrocycle.[2,42] Compound I is very reactive, but has been generated by artificial means and characterized in 2010.[45]

This extremely potent oxidizing species reacts with substrate to regenerate a ferric heme which, upon release of product and reorganization of the active site water molecules, returns to the ferric low spin (LS) resting state. This cycle can be interrupted by different conditions, and then end up at ferric substrate bound or ferrous form as shown in Figure 1.2.4.

Spin state equilibrium: It is generally known that the binding of substrate will convert the enzyme to high spin, but there are many cases that only partially convert to HS, for example, CYP11A1 with substrate cholesterol showing partial HS and LS. DFT calculation discovered that there is very small difference between the energy of water-bound resting heme state and that of methytriazolate-bound CYP121.[46] This leads to the conclusion that the existence of two equilibrium binding modes between the water ligand and substrate is possible.[46] Also the study of CYP121 binding with the antifungal drug, fluconazole (FLU), shows that an additional H-bonding interaction in the active site residues leads to low spin binding mode.[47] Another important type of substrate are inhibitors. A so-called "Type 2" substrate/inhibitor provides a donor group that allows the substrate or inhibitor to coordinate to the heme iron, through Fe-N bond; for example, 1-alkoxy-4-nitrobenzenes and 1,4-phenylenesiisocyanide bound to CYP1A1, which is six-coordinated complex.[48] This shows low spin.

One of the very effective techniques to study those intermediates is resonance Raman spectroscopy.

1.3 Resonance Raman

Raman Spectroscopy technique was discovered by an Indian scientist C.V. Raman in 1928.[49] It is used to study vibrational modes, rotational modes or other low-frequency modes in a system. It is done by scattering light from an intense source, in modern times a laser. Almost all of the photons are scattered with no change in energy; this is called Rayleigh scattering.[49] However, some of photons will interact with the sample and be scattered at longer wavelengths, losing some energy to the sample, with the acquired energy generating a vibrationally excited state of the molecule (Raman scattering); i.e., analysis of the scattered light will reveal weak side bands whose frequency difference from that of the incident laser corresponds to the energy associated with a vibrational transition. Thus, the data one obtains is a spectrum directly analogous to what one obtains from an IR spectrum. If an incident photon encounters a molecule that is already in an excited vibrational level, it can gain energy form the molecule and be scattered as a higher energy photon; this is called ”anti-Stokes Raman scattering”. According to the Boltzman distribution, the excited vibrational states are not well populated at room temp and this population diminishes as the energy of the vibration increases. So, generally, observations are made on the so-called Stokes Raman bands. All of the scattered light will be focused by a collection lens and focused onto the entrance slits of a monochromator; the single monochromator used in our lab is equipped with a CCD detector. The setup is shown in Figure 1.3.1.

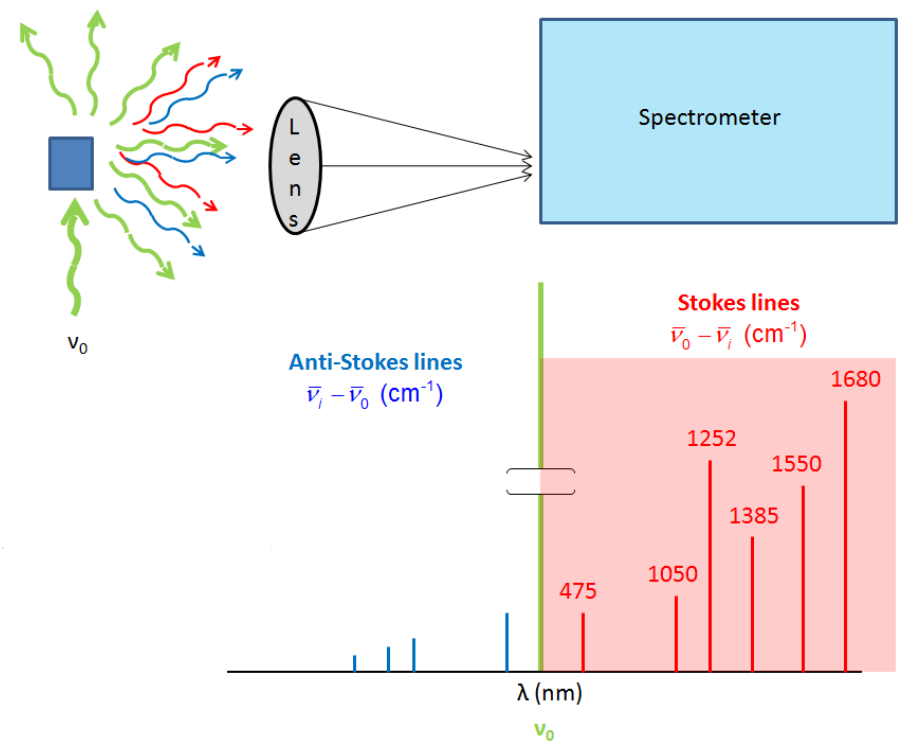

Figure 1.3.1 Raman scattering spectroscopy

Because Raman scattering is a very weak process with low probability of photon and molecule energy exchange, to obtain good quality spectra, it is required to have a concentrated sample; e.g., 1Molar. This is the major problem with this method of ordinary Raman spectroscopy, low sensitivity. However, if a given sample possesses a strong electronic absorption band, using a laser line in resonance with that electronic absorption band can lead to great enhancements of the vibrational modes of the chromophoric molecule, an effect forming the basis for “resonance Raman spectroscopy”, which is now widely used and is the main techniques being used in this work.

A great illustration of resonance Raman spectroscopy is shown in Figure 1.3.2. Compare tris-phenanthroline Fe(II) complex of divalent ion with sulfate ion as a non-enhanced internal standard. The complex has an intense ($\varepsilon \sim 10^4\ M^{-1}\ cm^{-1}$) MLCT transition which shows the absorption band around 510 nm. With 647.1nm excitation, far from the MLCT maximum, the Raman spectrum is dominated by sulfate ion, SO_4^{2-}, with ν(S-O) at 981cm^{-1}. From inspection of the other three spectra, when the excitation lines approach the MLCT maximum, the characteristic modes of the coordinated ligand are strongly enhanced, dominating the spectrum even though the concentration of the complex is 1000 times less than that of the sulfate.[50]

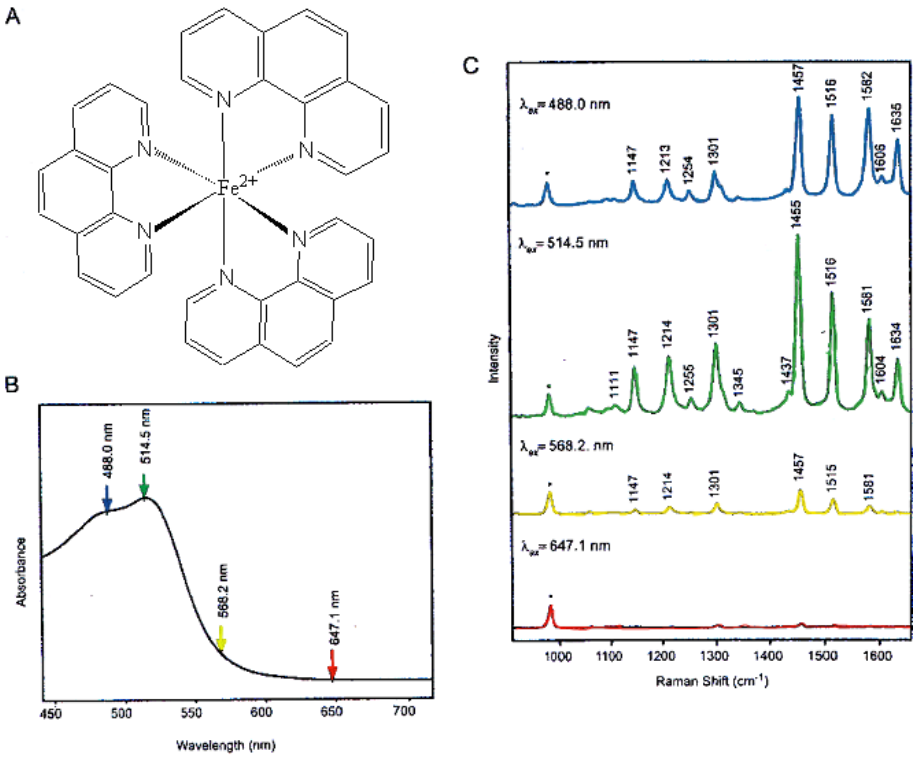

Figure 1.3.2 (A) structure of tris-phenanthroline Fe(II); (B) Absorption spectroscopy of tris-phenanthroline Fe(II); (C) Resonance Raman spectroscopy with different excitation laser lines

This great enhancement permits selective interrogation of chromophoric groups buried within complex molecular and biological matricies. For example, hemoglobin has four heme groups buried deeply in the protein with molecular weight at 64 KDa.[51] The electronic absorption spectrum of human hemoglobin and the structure of heme group are shown in Figure 1.3.3. When the laser line is between 220 nm - 280 nm, the vibrational modes from four aromatic amino acids, Tyrosine, Phenylalanine, Tryptophan, and Histidine, can be observed because only these four amino acids have electronic absorption bands in this region.[44] On the other hand, if the excitation line is near the strong Soret ($\varepsilon \sim 10^5\ M^{-1}cm^{-1}$) or Q ($\varepsilon \sim 10^4\ M^{-1}cm^{-1}$) π-π^* bands of the heme, then the modes from the heme group will be selectively enhanced, in other words, we will be able to observe the modes associated only with the active site heme group.[44,52]

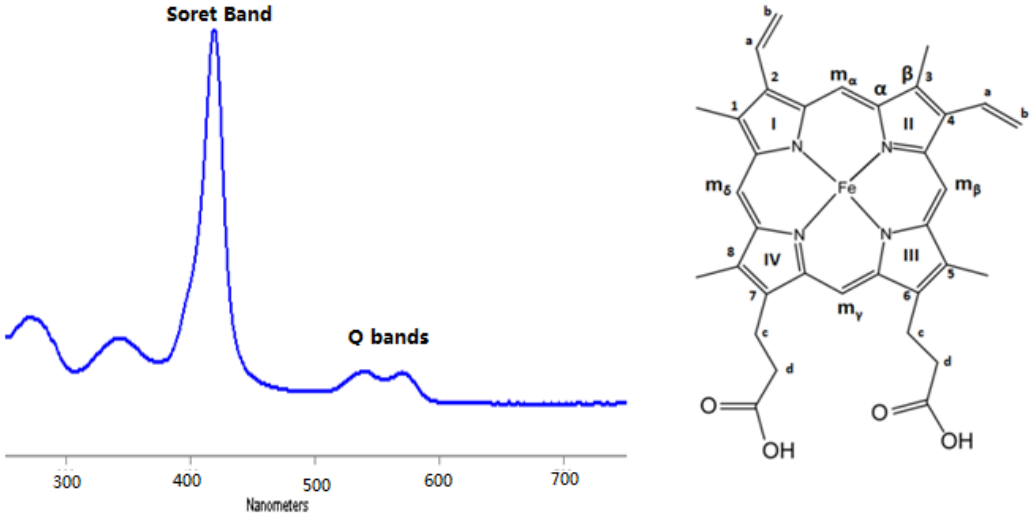

Figure 1.3.3 Electronic absorption spectroscopy of human being hemoglo bin and the structure of heme group

Now we can apply the resonance Raman spectroscopy to the study of Cytochrome P450s. Champion and his coworkers trapped the oxy form intermediate of CYP101 by using resonance Raman with $^{16}O_2$ and $^{18}O_2$ isotope label. The bending mode, δ(Fe-O-O), was published in 1999.[53] By subtracting, the two stretch modes ν(O-O) and ν(Fe-O) can be clearly seen.[42,53,54] Figure 1.3.4 shows the spectrum of oxy-CYP101 and its oxygen isotope labels measured by 356 nm and 413 nm excitation lines. As it shows that by subtracting, one can clearly observe the Raman shift arising from the oxygen isotope labeling. The relative intensity of ν(O-O) increases while ν(Fe-O) decreases as compared with ν_4 when the excitation line changes from 356 nm to 413 nm. This application of isotope labeling helps us to see the weak modes, or the modes buried within the envelope of strong heme modes.

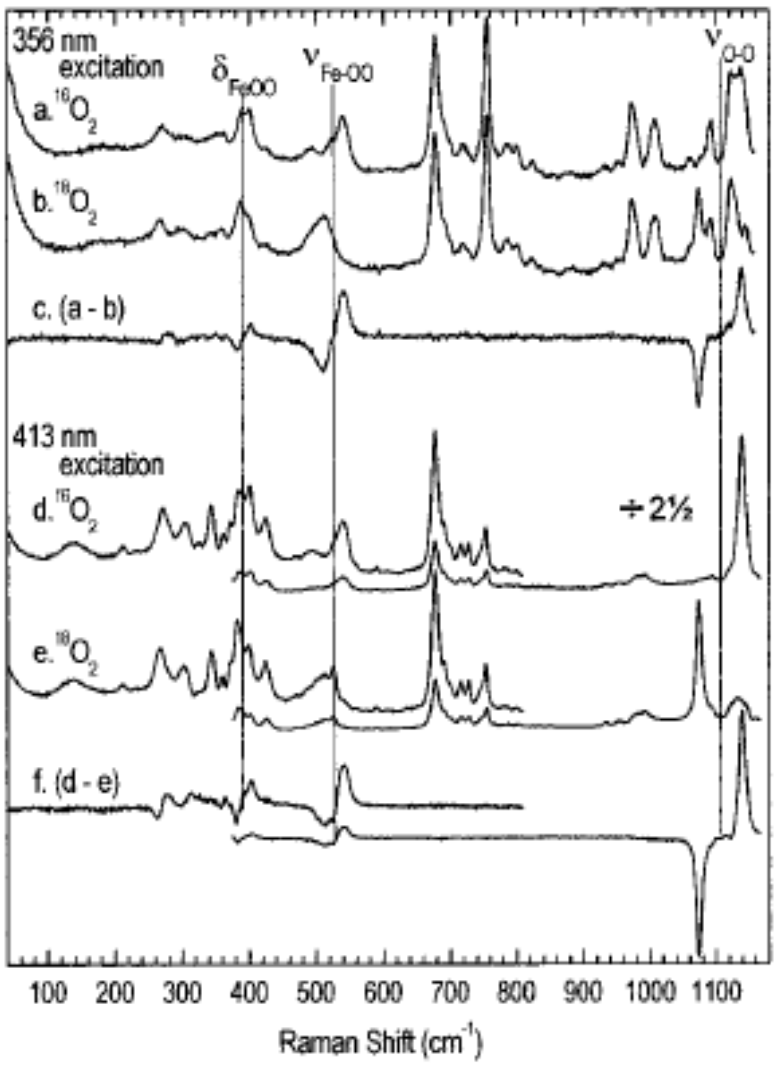

Figure 1.3.4 Resonance Raman Shift by isotopic labeling of O_2 of oxy-CYP101 at excitations of 356 nm (a-c) and 413 nm (d-f) [53]

In addition to studying the oxy intermediate by resonance Raman, it is also possible to trap other "oxy intermediates"; for example, the ferric peroxo, hydroperoxo, or even Compound II. People realized The oxy intermediate is the most stable intermediate compared with later intermediates,[42] but after addition of an electron to form a ferric-peroxo species, in most situations, proton transfer from active site surroundings is very efficient, promoting rapid reaction, with the complex quickly returning to its resting state. So, the cycle just quickly finishes after adding an electron to the oxy intermediate, with no intermediates being seen under physiological conditions. The only way to trap and interrogate these fleeting intermediates is to only allow the electron to transfer but restrict the proton transfer. The only effective method to accomplish this is a method called cryoradiation by gamma ray which was pioneered by Martyn Symons in 1980s.[55] The method has been elegantly refined and used extensively by Brian Hoffman, Stephen Sligar and coworkers.[54,56] The procedure for doing this is summarized below and shown in Figure 1.3.5.

Step 1: The heme protein is prepared in a buffer (H_2O or D2O) containing 20-30% glycerol, which ultimately is the free electron source. Using a reducing agent, such as $Na_2S_2O_4$, the heme is reduced from Fe(III) to Fe(II), then $^{16}O_2$ or $^{18}O_2$ is bubbled through the solution and quickly frozen in liquid N_2 to make sure the sample does not auto-oxidize. At this stage, oxy-hemeprotein has formed, as is then confirmed using resonance Raman spectroscopy with Soret excitation.

Step 2: One electron can be added to this oxy-hemeprotein by irradiating the sample under ^{60}Co gamma ray source which will generate electrons from glycerol environment. The source is available at Notre Dame Radiation Laboratory. At this stage,

ferric peroxoanion is formed via migration of electrons, which can migrate at 77K, while other species, including protons, are not so mobile. The resonance Raman spectrum of this trapped peroxo- species can be collected at this point.

Step 3: The ferric hydroperoxo complex can be generated at this point by annealing at different temperatures/times and monitoring the rR spectrum for changes associated with formation of a hydroperoxo species. In the case of the simple CYP101 system, this proton transfer step is so efficient, even at 77Km this it was not possible to trap the peroxo form. However, employing the D251N mutant, which has a restricted proton transfer, [54,57] after annealing at 145 K to get rid of the excess radicals generated by gamma ray irradiation, it was indeed possible to observe the rR spectrum of the peroxo form of this CYP101mutant.[58] Subsequent annealing to 187 K allowed proton movement to the heme site yielded the rR spectrum of the hydroperoxo form.[54] The precise annealing temperature is more easily determined by using EPR which can detect the change from peroxo to hydroperoxo much faster than resonance Raman, 10 minutes verse a few hours of measurements. At this stage, ferric hydroperoxo is formed and the rR spectrum can be acquired.

Step 4: Ideally if annealing further, Compound I will be formed but this species is too reactive to be seen yet.

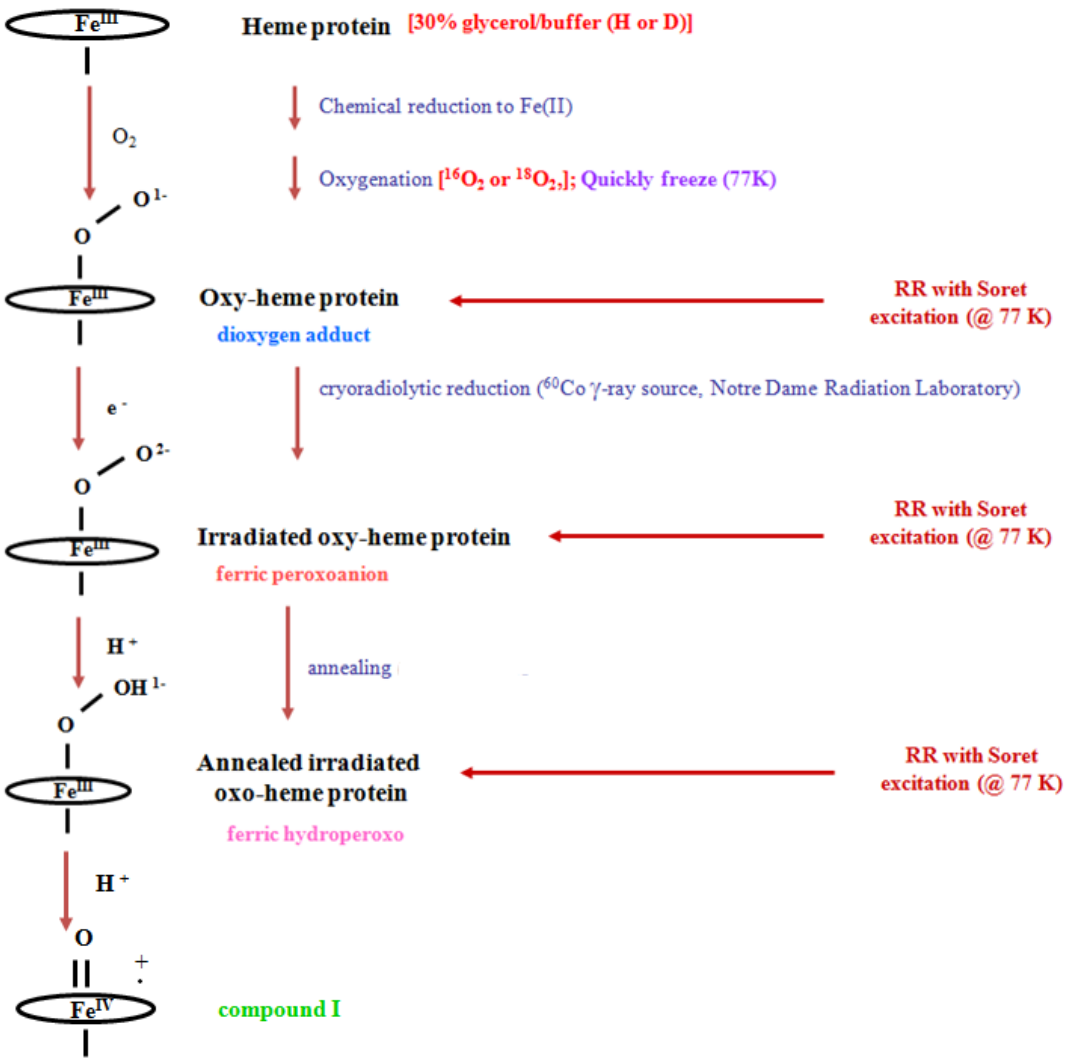

Figure 1.3.5 Process of cryoreduction and annealing to generate intermediates at different stage

A brief set up for RR spectroscopy is shown in Figure 1.3.6. That equipment will allow us to measure samples at 77K all the time. The container, where the sample will be kept, is filled with liquid N_2, and people who measure the sample can refill the liquid N_2 easily when the liquid N_2 is evaporated. Samples can be measured with different laser lines and different frequency by adjusting the monochromator spectrometer. Annealing process is done by placing the sample in desired temperature cold bath and incubating for a certain time. The efficiency of annealing is confirmed by resonance Raman.

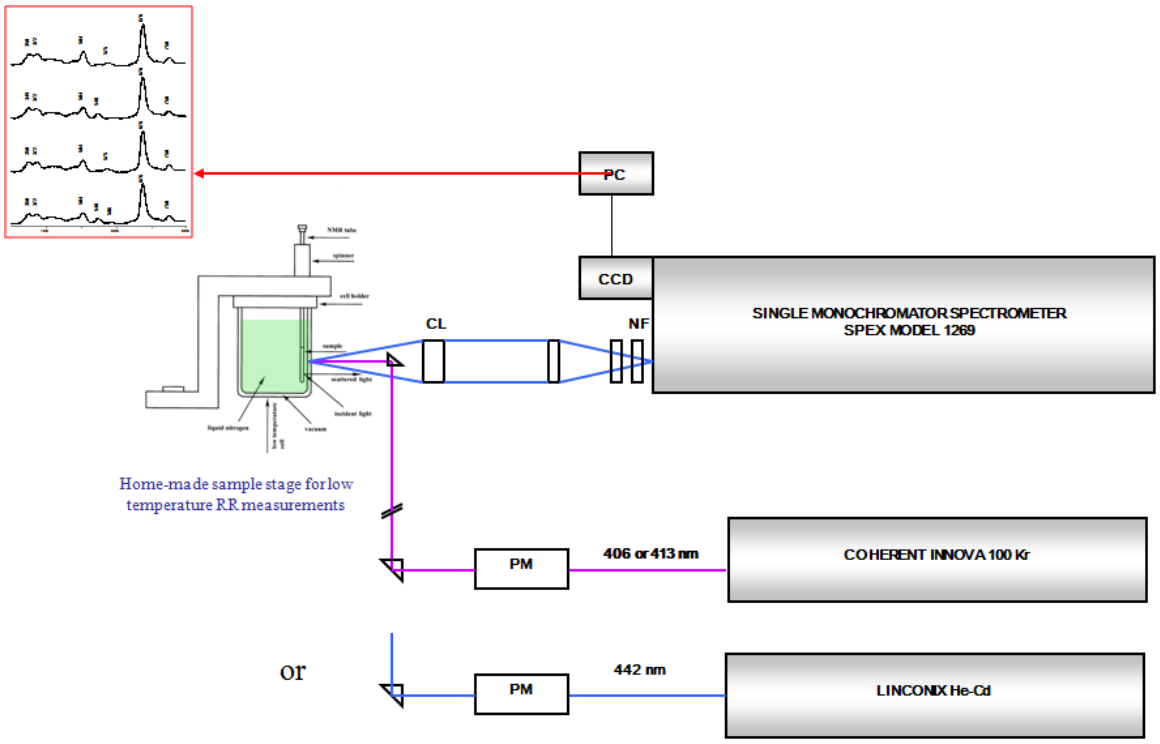

Figure 1.3.6 Cryogenic resonance Raman measurements instrumental setup

According to the CYP101 absorption spectra, which are shown in Figure 1.3.7, it is known that the oxy-CYP101 has peak at 415 nm while hydroperoxo-CYP101 and peroxo-CYP101 both have an absorption feature at around 440 nm.[54]

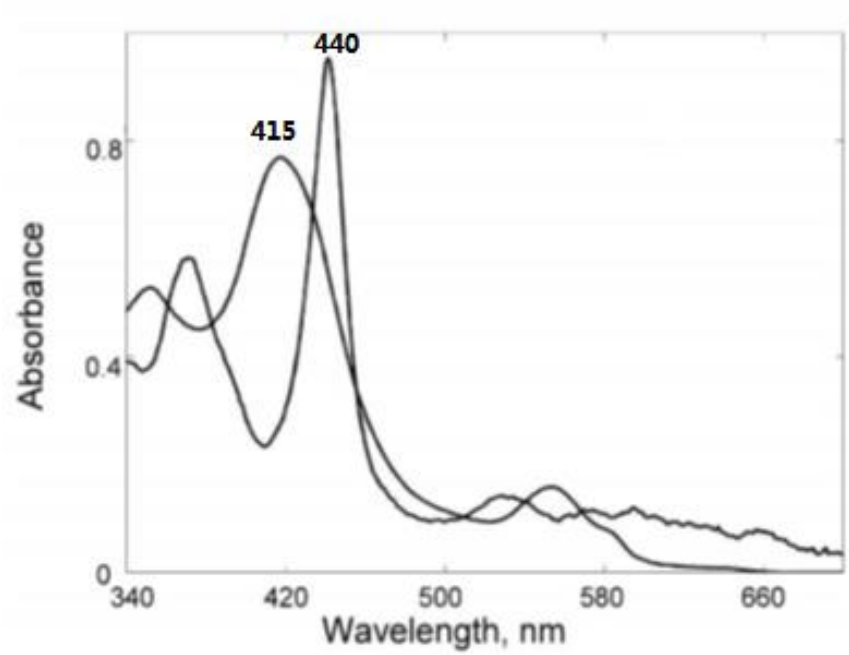

Figure 1.3.7 Absorption Spectra of CYP101 before and after cryoreduction[54]

From the absorption spectrum for CYP101, the Soret is at 415 nm for oxy sample and 440 nm for peroxo and hydroperoxo samples. The excitation line 442 nm from He:Cd laser was used to measure peroxo and hydroperoxo complexes which were generated after cryo-irradiation and annealing. After gamma irradiation, resonance Raman spectrum is shown in Figure 1.3.8. From the difference spectrum done by subtracting, it clearly shows H/D shift which means the sample is sensitive to H_2O or D_2O. From the peroxo-CYP101 structure, this complex should not be sensitive to H or D buffer because the proton has not transferred to the complex yet. The only reason for this to happen is that the proton is already transferred to the peroxo-CYP101 complex so the intermediate trapped here is the hydroperoxo-CYP101. The proton shuttle for this enzyme system is so efficient. It delivers electron even at 77 K.[59]

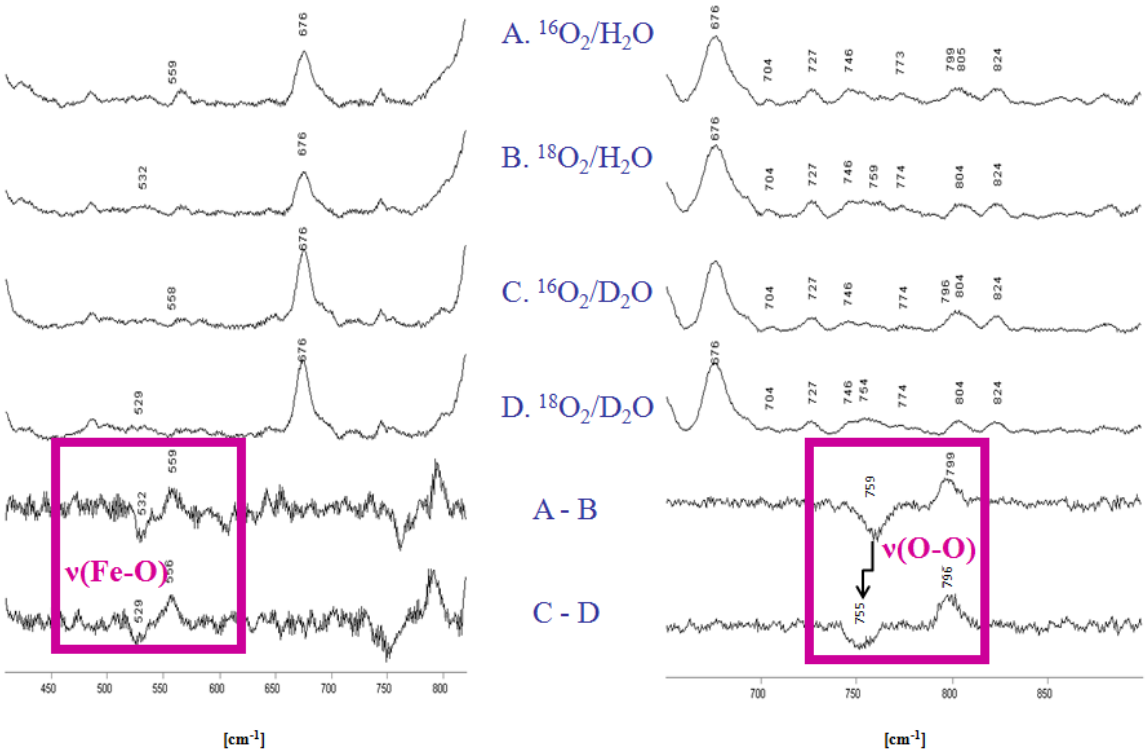

Figure 1.3.8 Resonance Raman spectra of CYP101 after gamma irradiation by using 442 nm excitation line.

Better method needs to be introduced to restrict or slow down the proton transfer. In 2008, Denisov et al discovered that asparatic acid 251 and threonine 252 are fragments in a so-called proton shuttle, which transfers proton to the oxy forms. Mutation from aspartic acid 251 to asparagine (D251N) will break or slow down the proton transferring process.[60] Figure 1.3.9 shows the proton shuttle and the active site with absorption spectroscopy. From the absorption spectroscopy, peroxo-CYP101 and hydroperoxo-CYP101 are showing differently. That means peroxo-CYP101 can be observed after gamma irradiation at 77K which process only allows an electron to move and with the slow down proton transfer shuttle done by mutation from aspartic acid 251 to asparagine restricts the proton transfer to the complex. With further annealing at 185K, one proton transfers to the complex so the hydroperoxo-CYP101 is formed and observed.[54,60] Resonance Raman has been used to characterize the trapped peroxo and hydroperoxo intermediates.

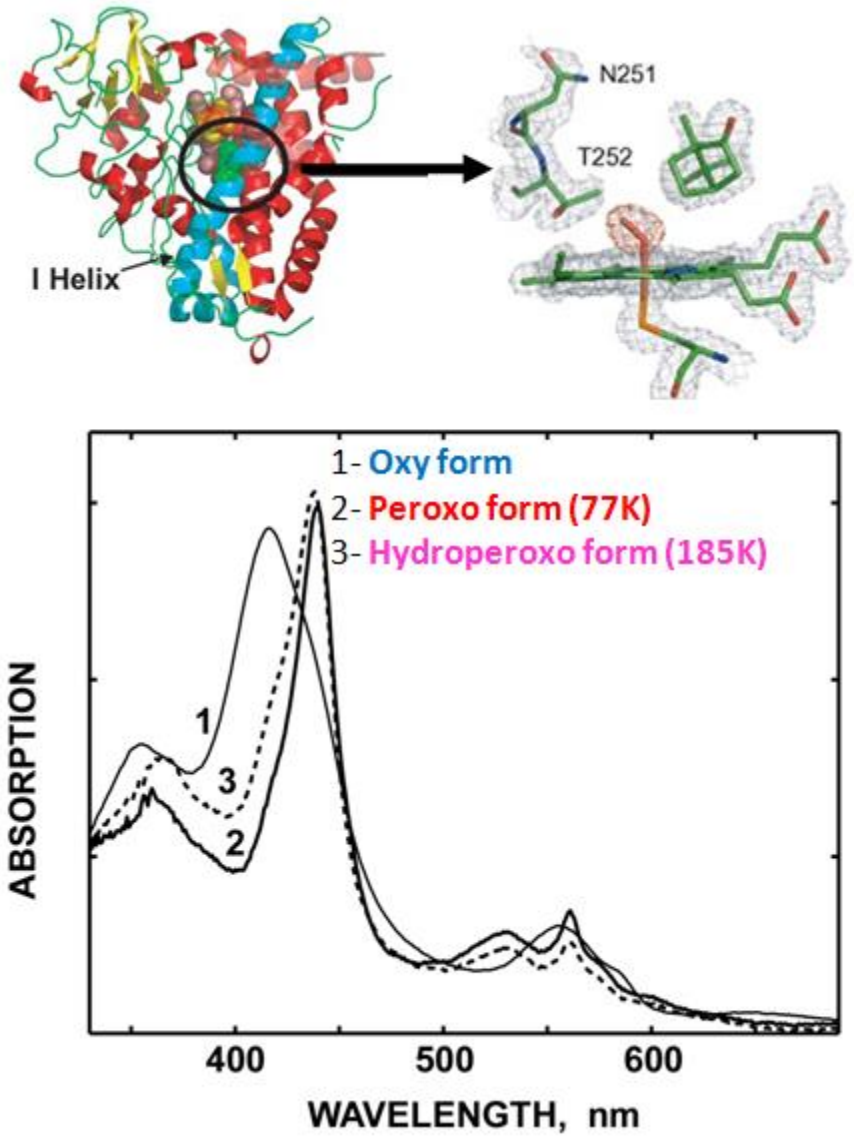

Figure 1.3.9 Mutation with proton shuttle view in the active site and its absorption spectroscopy

The Figure 1.3.10 shows the resonance Raman spectroscopy taken at 4°C and 77K for the oxy-CYP101 mutant. Comparing the spectra taken at two different temperatures, the shift at 1134 cm^{-1} has two modes shown at 77K spectra but not observed at 4°C. This observation impressively shows that there are two oxy modes in the active site, one associated with hydrogen bonding, another one not, as they can be seen compared with the difference between D_2O and H_2O buffer. These two modes are because of the presence of an H-bond donor in the hem distal pocket, with the H-bonded form showing a lower ν(O-O) stretching mode, shifted by ~10 cm^{-1}.[58]

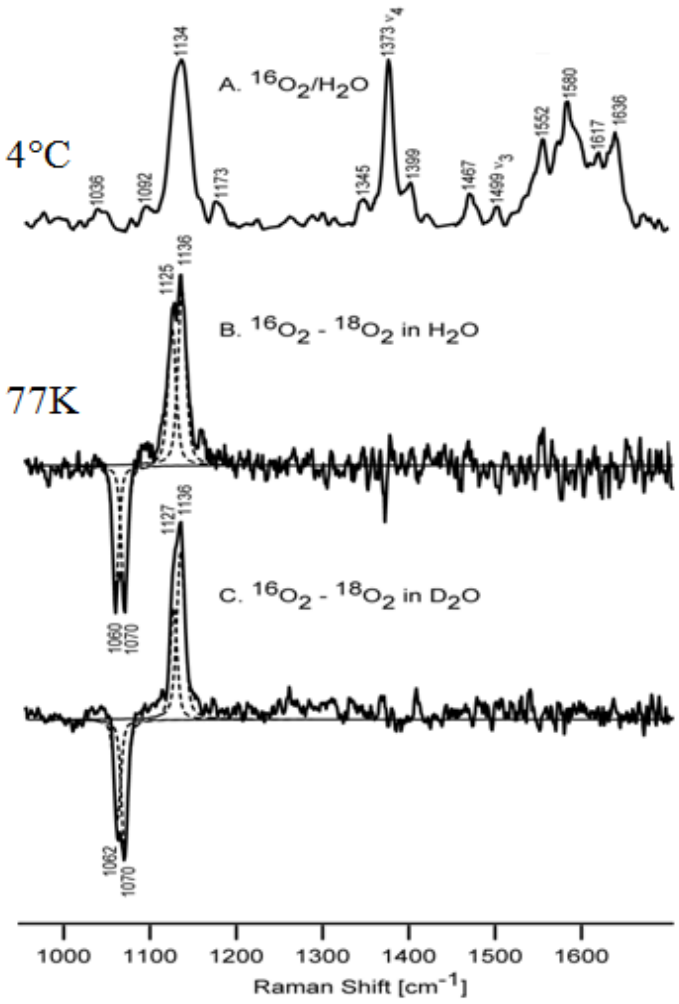

Figure 1.3.10 Resonance Raman spectroscopy at 4°C and 77K with D_2O and H_2O buffer

The Figure 1.3.11 shows the spectrum after gamma irradiation and after annealing. After gamma irradiation, one electron transfers to the complex and peroxo-CYP101 is form. From the left spectrum in Figure 1.3.11, stretching mode of O-O bound does not have the H/D shift. After annealing to 185K, at this temperature allows the proton transfers to the complex and forms hydroperoxo-CYP101, so H/D shift is observed. [60]

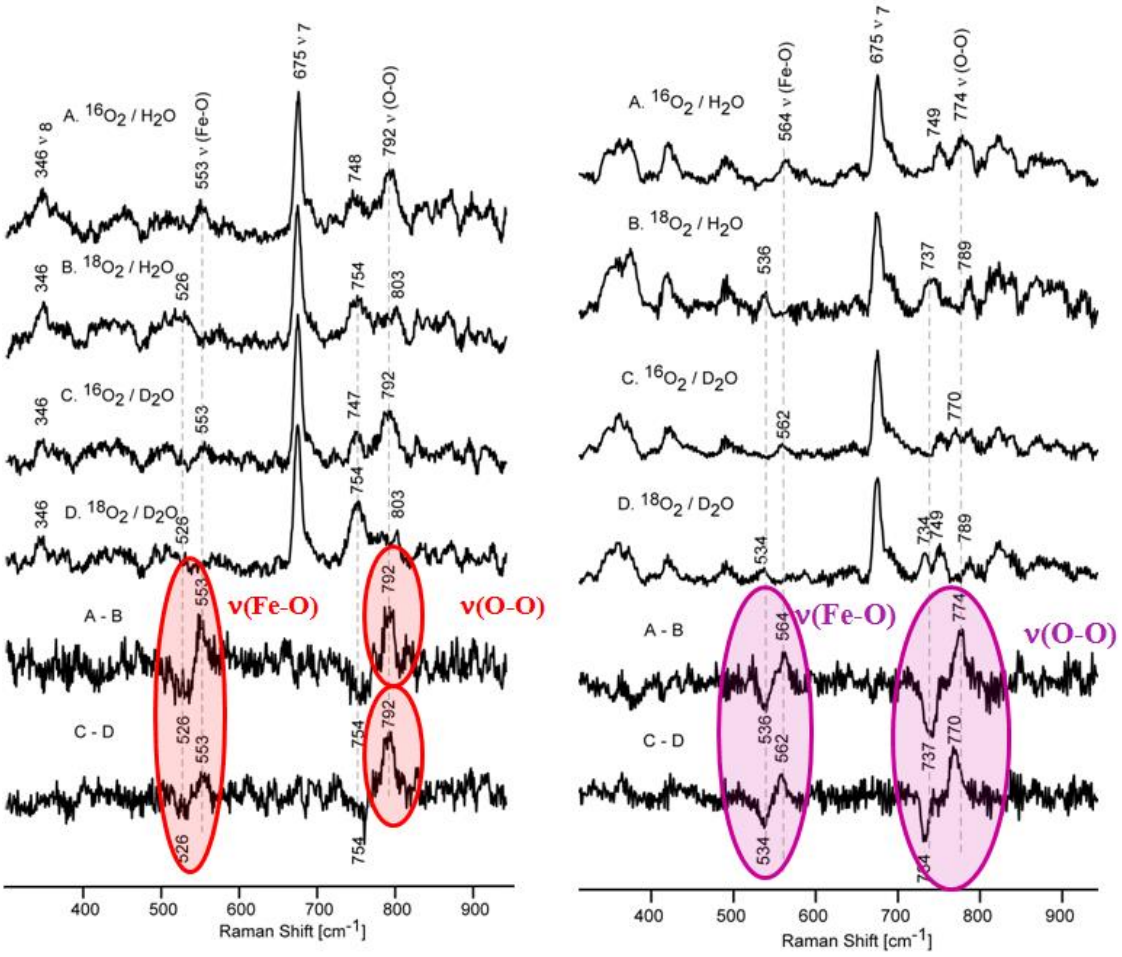

Figure 1.3.11 Resonance Raman spectroscopy taken after gamma irradiation (left) but not annealing and after annealing at 185K (right)

Nano-disc technology[61] has been introduced because there are some membrane bound enzymes, for example Cyt P450 2B4 and its reductase, Cyt b5 and its reductase (Figure 1.3.12). These membrane bound enzymes have hydrophobic tails which bound tightly with the membrane anchors so they are not soluble in aqueous, in other words, they will tend to aggregate after dissolving in aqueous solution through the hydrophobic tails.

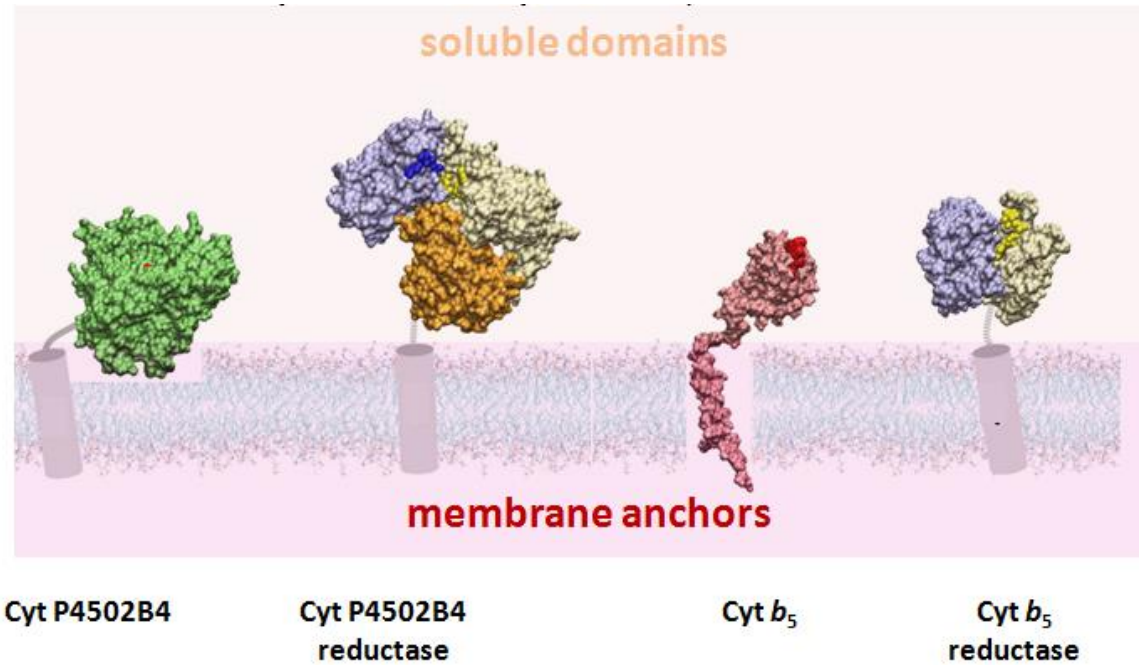

Figure 1.3.12 Membrane bound protein with hydrophobic tail bound with membrane

Nano-disc is made to avoid the aggregation. This technique was developed and employed by Stephen Sligar and coworkers.[61,62] The nano-disc is made of phospholipid bilayers which are assembled by two membrane scaffold proteins. The schematic view of nano-disc is shown in Figure 1.3.13 left. The middle one is the membrane bound enzyme incorporated in nano-disc. If the reductase of one enzyme is membrane bound also then both enzyme and its reductase can incorporate within a single nano-disc as shown in the right. The redox partner of CYP11A1, Adx, binds with CYP11A1 through the proximal side so Adx is not membrane bounded.

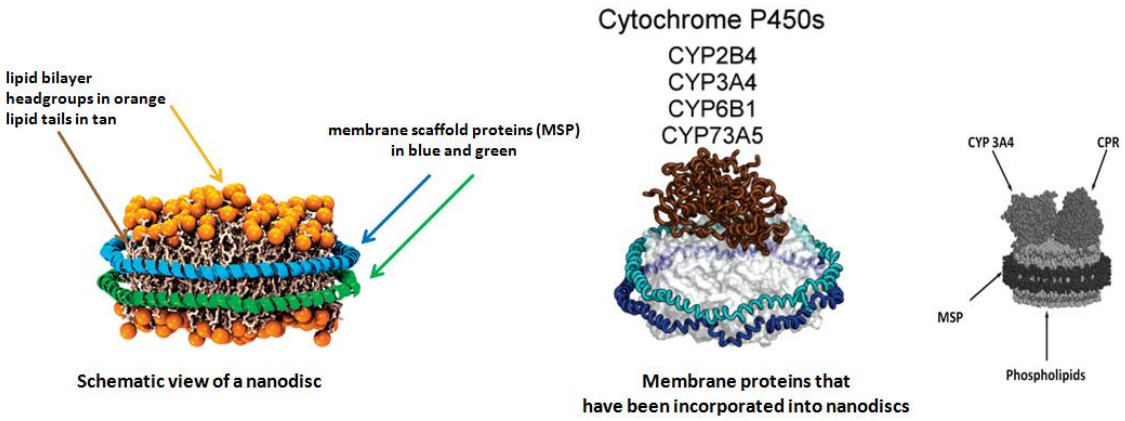

Figure 1.3.13 (left) nano-disc lipid bilayer with membrane scaffold proteins; (middle) mammalian P450s incorporated with nano-disc; (right) P450 and its reductase incorporated with nano-disc

The great advantage of this nano-disc technique can be very effectively demonstrated by resonance Raman spectroscopy. Results are shown in Figure 1.3.14. The top two spectra were taken with the samples in the conventional media, which are 50 mM phosphate buffer, 20 % glycerol, 0.1% Emulgen 913, 1 mM DTT. As can be seen, both samples contain a mixture of HS and LS species and there is almost no spin conversion upon addition of the substrate testosterone (TST). After making the enzyme incorporated with nano-disc, the substrate-free sample shows almost purely LS form, as expected, and upon adding a large amount of TST, there is a conversion to ~ 75% percent of high spin.[63] Other effects may involved when using detergent, for example, detergent can denature the protein; glycerol can have some impact on the spin state conversion.[64]

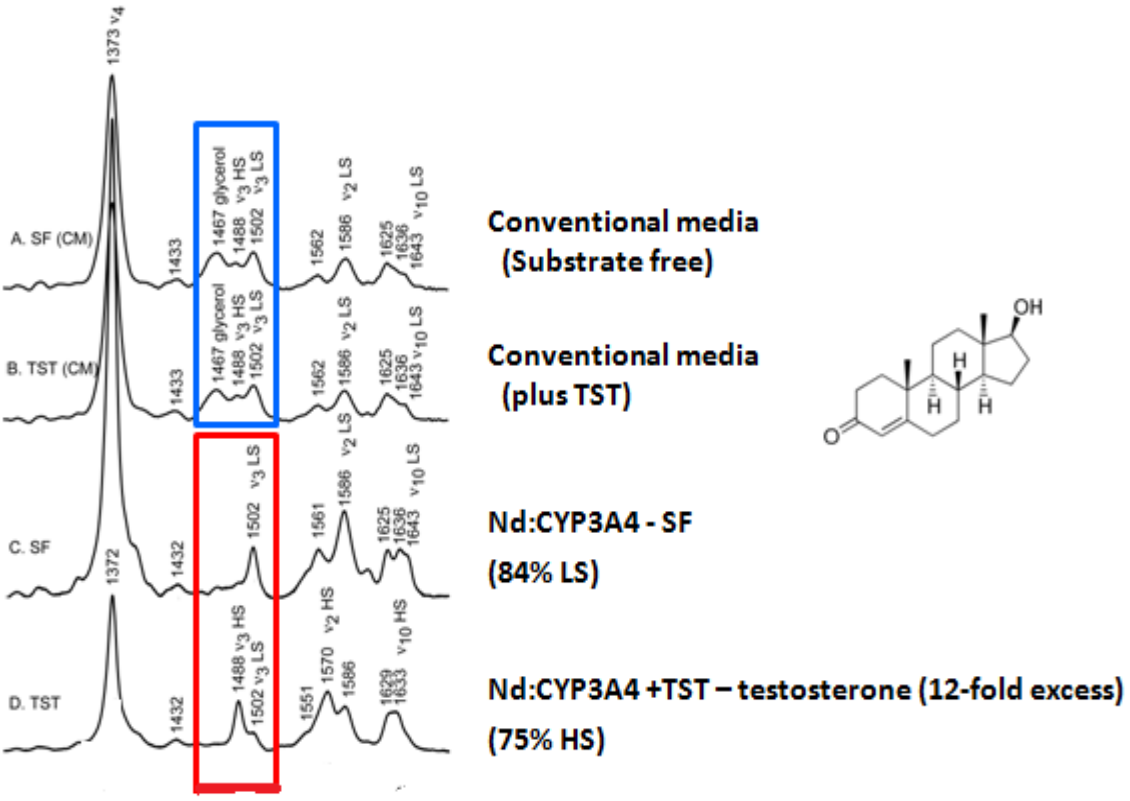

Figure 1.3.14 Spin population change after substrate bound in conventional media and nano-disc incorporated methods

1.4 Overview of my research

The main goal of this research is to characterize the stable and unstable intermediates of CYP11A1. For stable species of CYP11A1 (i.e., ferric state and ferrous-CO state) there are two high spin (HS) substrates and one low spin (LS) substrate. In order to evaluate the heme structural change and spin population change when CYP11A1 binds with three natural substrates in the ferric state, we used CYP101 as a reference protein to obtain a generally useful calibration procedure to permit reliable rR-based evaluation of the percentage of HS and LS population for CYP11A1 complex with different substrates and with the redox partner Adx.

CYP101 is an ideal reference because CYP101 gives 96% LS when it is substrate free and 95% HS when it binds with natural substrate camphor. In Section 2, a detailed description will be given of how this method was developed and tested to show its ability to evaluate HS/LS population ratios for several different P450s.

2 Using resonance Raman cross-section data to estimate the spin-state populations of cytochromes P450

2.1 Introduction

The cytochromes P450 (CYPs) are heme-based monooxygenases responsible for the oxidative metabolism of a huge number of relatively inert substrates, including pharmaceuticals and other xenobiotics, and for the biosynthesis of essential steroid products.[2,42,65–67] Substrate binding initiates the enzymatic cycle by triggering a crucial low spin (LS) to high spin (HS) state change facilitating reduction to the ferrous heme intermediate that rapidly binds oxygen; subsequent transfer of an electron and two protons transfer generates the highly reactive π cation radical Compound I.[68] The resting state gives a LS which is believed that Fe is six coordinated with H_2O from a water cluster as ligand. Binding with substrate will kick off the water molecular and then Fe becomes five coordinated. In many cases, enzymes or proteins will not give a 100% of high spin or low spin when binding with substrate or not. Or situation will be that no spin state change during binding of substrate. One reason for that could be the aggregation of the protein which blocks the entrances for substrates entering the active site. Another reason will be the substrate serves as a sixth ligand of Fe. Other situation will be that binding of substrates does not show a full change which is more interesting to study what is exactly happened in the active site. No matter which situation, it is very important to know how much HS or LS of the protein or enzyme complex. [2,42,69,70]

Resonance Raman (rR) spectroscopy can effectively document the presence of HS or LS states of the ferric heme by appearance of distinctive frequencies observed at

~1485 cm^{-1} for high spin marker and 1500 cm^{-1} for low spin marker.[44,71,72] Resonance Raman can also allow to check samples at different condition, for example, pH dependent samples, temperature dependent samples, ionic strength affected samples, etc. All these benefit people to check enzyme or protein at different stage by rR quickly. Given recent advances in producing and stabilizing these extremely important enzymes,[60,61,73] it is anticipated that applications of rR to these proteins will now expand considerably. The purpose of this work is to provide a systematic approach to utilize rR spectroscopy to reliably estimate spin-state populations for different substrate/enzyme combinations. Cytochrome CYP101, an ideal reference protein, exhibits an almost complete spin-state conversion upon binding its natural substrate, camphor, switching from 96% LS to 95% HS.[74]

2.2 Methods and experiments

2.2.1 Expression of CYP101

The 10g LB Agar was mixed with 250 ml of deionized water in a plastic flask. The solution was then shaken to let the powder dissolve. The solution was microwaved untill small bubbles formed, and then shaken well. This process was repeated until the solution becomes clear. The solution was then placed in the hood and cooled down. When the solution was not hot, the antibiotic ampicillin was added to the solution to get final concentration of ampicillin at 100 µg/ml. About 20 ml of the solution was poured in the previous labeled Petri Dish. The Petri Dish was left in the hood for a while to let the solution become a solid gel. After the solution became solid gel, an autoclaved wooden stick was used to apply a small amount of CYP101 in BL21 *E. coli* cells which were purchased from Biolabs. The cell was spreaded using autoclaved glass beads. The cell was then incubated at 37 °C for overnight to allow the cells to grow.

Preparation of the 2YT culture media: 1 L of 2YT culture media was made with 16 g of bacto tryptone, 10 g of bacto yeast and 5 g of NaCl, then adding water up to 1 L. The 2YT was placed in the plastic culture flask and then autoclaved. The 2YT media was cooled down and then the antibiotic ampicillin was added to a concentration of 100 µg/ml. A one percent solution of ampicillin contained 2YT media was placed in the small flask. A wooden stick was used to transfer one clone of the CYP101 cells from the Petri Dish to the small flask. The sample was incubated at 37 °C in the shaker with shaking rate of 250 rpm for overnight.

The 2YT culture was warmed in the large container and culture containing ampilcillin, which had been growing over night in the small flask, was transferred back to the large container. The cultures were incubated at 37 °C with a shaking rate of 250 rpm until an OD_{600} (the optical density of the culture at 600 nm) of 0.8-1.0 was reached. The bacterial growth was slowed down by reducing the speed of shaking to 190 rpm and the temperature was reduced to 24 °C. The cells were induced to express CYP101 by addition of 1 mL of 1 M IPTG to 1 L 2YT media culture and δ-ALA (to a final concentration of 30 μM). The δ-ALA is the first precursor of heme biosynthesis. Solid $FeCl_3$ was added to the container to reach a concentration of 80 mg/L.

After 21 hrs of induction, 0.2 g/L of camphor was added to each of the large flasks to yield a final concentration of 1 mM followed by 2 hour incubation at room temperature with shaking at 190 rpm. The cells were harvested by centrifuging at 8,000 rpm for 10 minutes. The wet cells were weighed and stored in a -80 °C freezer. The yield of the cells was about 10 g/L media.

2.2.2 CYP101 purification

The lysis buffer was made at a ratio of 1 g of wet cell with 3 mL of lysis buffer. The lysis buffer contained 50 mM Tris buffer pH=7.4, 25 mM KCl, 1 mM camphor, 1 mM phenylmethylsulfonylfluoride (PMSF), 1 µM leupeptin, 1 µM antipain, 1 µM pepstatin, 32 units/mL DNase, 3 units/mL RNase and 1 mg/mL lysozyme. The wet cells were mixed with lysis buffer. The mixture was placed on the shaker with slowly shaking at 4 °C for 30 minutes to allow the wet cells to fully disperse in the buffer. The mixture was transferred to a 50 mL plastic beaker for sonication. The cells were then sonicated 5 times for 1 minute, each at a power of 6 and a 50% duty cycle. During the sonication process the cells were kept on ice and were allowed to cool for 5 minutes between cycles. After sonication, the sample was centrifuged for 10 minutes at 8,000 rpm 4 °C to remove the cell debris, which stuck on the wall and the bottom of the centrifuge bottle. The supernatant was centrifuged for 2 hours at 20,000 rpm under 4 °C. Crude CYP101 was obtained.

The crude CYP101 was concentrated under high pressure of N_2 with a concentrating device using the membrane transmited only molecules of MW <50,000. The buffer was exchanged with 50 mM Tris buffer pH=7.4, 25 mM KCl, 1 mM camphor; i.e., the appropriate running buffer for the subsequent chromatographic separation. The concentrated sample was applied to a DE53 column previous equilibrated with the above mentioned buffer. The column was eluted with the same buffer until there was no colored eluent. The CYP101 bound on the top of the column shown a brown band. The protein was then eluted by means of a linear salt gradient with 50 mM Tris buffer pH=7.4, 0-300

mM KCl, 1 mM Camphor until the all the brown band was eluted. The protein was collected as 2 mL fractions. The UV spectrum was checked and samples with Rz (A_{391}/A_{280}) > 0.5 were pooled together for further purification.

The Rz > 0.5 fractions were concentrated to 500 µM. The of $(NH_4)_2SO_4$ was added to CYP101 to reach the $(NH_4)_2SO_4$ concentration to 75 mg/mL with slow addition and constant stirring to avoid precipitation**.** Then the entire sample was loaded to a phenyl sepharose hydrophobic column, which had been previously equilibrated with 50 mM Tris buffer pH=7.4, 50 mM KCl, 1 mM camphor and 25% $(NH_4)_2SO_4$ (143 g/L). The column was washed with the same buffer. The protein was then eluted by means of a linear salt gradient with 50 mM Tris buffer pH=7.4, 50 mM KCl, 25%-0% $(NH_4)_2SO_4$, 1 mM camphor. The protein was collected as fractions. The UV spectrum was checked and samples with Rz (A_{391}/A_{280}) > 1.0 were pooled together for further purification.

The Rz > 1.0 fractions were concentrated to 500 µM. Then they were loaded on a P-100 Biogel column with 100 mM PB pH=7.4, 100 mM KCl, 1 mM camphor. CYP101 was collected as 1 mL fractions. The UV spectrum was checked and samples with Rz (A_{391}/A_{280}) > 1.6 were pooled together. Pure CYP101 was obtained, concentrated to 500 µM and stored in a -80 °C freezer for future use.

2.2.3 Preparation of substrate free CYP101

The substrate free form of CYP101 was prepared by passing pure CYP101 through a Sephadex G25 column slowly with 50 mM MOPS (morpholino-propane sulfonic acid) adjusted pH to 7.4 by using 50 mM phosphate buffer to pH=7.4. The purity of substrate-free CYP101 was checked by UV spectroscopy. If there is any trace left of absorption at 391 nm, then the sample was passed through the G25 column again. The MOPS buffer was removed by passing the protein through a separate Sephadex G25 column, which had been equilibrated with 100 mM PB pH=7.4, 100 mM KCl. The purified substrate free samples needed to be processed and analyzed at the same day in order to minimize the P420 formation during the experimental process.

2.2.4 Resonance Raman spectroscopy with CYP101

Resonance Raman spectrum were obtained by using a Spex 1269 spectrometer equipped with Spec-10 LN-cooled detector (Princeton Instruments, NJ). The excitation line used to measure CYP101 with substrate and substrate free was 406.7nm from a Kr^+ laser. Fenchone was used to calibrate the spectrum, which was processed by Grams/32 AI software (Galactic Industries, Salem, NH). Rayleigh scattering was removed with a Notch filter. The power used to measure both substrate free and substrate bound sample is 15 mW. The spectrum was obtained at room temperature with a slit of 150 μm. Each spectrum was scanned 30 times at high frequency and low frequency. The NMR tube containing sample was gently spun under house N_2 gas which avoided the over-heating on the sample by continuous laser beam shining on the sample.

The substrate free and substrate bound sample were prepared by pairs. The buffers were made in 100 mM PB pH=7.4, 100 mM KCl with 500 mM sulfate for CYP101 substrate free and CYP101 substrate bound. The buffer was separated into two parts, one was for CYP101 substrate free, and the other one was for the CYP101 substrate bound. For the CYP101 substrate bound part, camphor was added to make the camphor concentration equal to 5 mM.

Second, a CYP101 substrate free sample was made and distributed to 6 small vials, each vial containing 10 μL with protein concentration at 400 μM. So each vial had the same protein concentration. These 6 vials were grouped into two groups. Each group had 3 vials. The 120 μL of substrate free buffer was added to one group of vials to make the sulfate (SO_4^{2-}) contained substrate free samples. The same amount of substrate bound

buffer was added to another group of vials to make the sulfate (SO_4^{2-}) contained camphor-bound sample. By doing this, all the vials had the same concentration of CYP101 and sulfate ion.

Total sample volume was 130 µL and the detailed sample information is summarized below:

SF1, SF2, SF3: 10uL of ~400mM substrate free CYP101 in 100 mM PB pH=7.4, 100 mM KCl buffer + 120uL buffer of 100 mM PB pH=7.4, 100 mM KCl, 0.50Na2SO4;

SB1, SB2, SB3: 10uL of ~400mM substrate free CYP101 in 100 mM PB pH=7.4, 100 mM KCl buffer + 120uL buffer of 100 mM PB pH=7.4, 100 mM KCl, 0.50Na2SO4, 5 mM camphor.

2.3 Results and discussion

2.3.1 Expression and purification of CYP101

The expression and purification of CYP101 is described in Section 2.2. The UV-Visible absorption spectra of the pure (Rz = 1.60) CYP101 and the reduced CO form of CYP101 are shown in Figure 2.3.1. Optical data of CYP101 has Soret band at 391 nm; the previously reported ε_{mM} =102.[75]

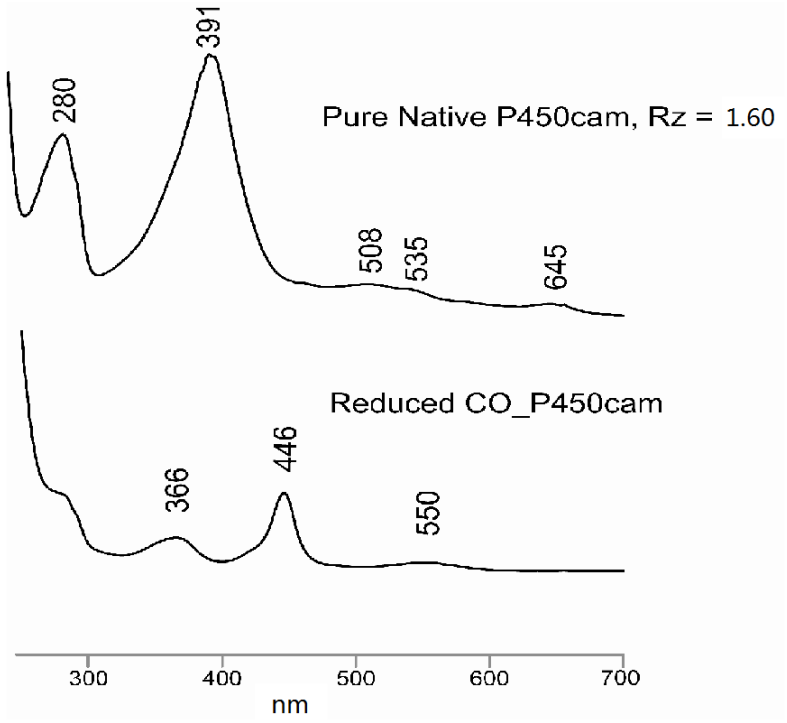

Figure 2.3.1 UV-Vis absorption spectra of native CYP101 and its reduced CO form

The procedure to prepare CYP101 was described in Section 2.2.3. The overlap of UV-Visible absorption spectra of the pure (Rz = 1.60) CYP101 and its substrate free form are shown in Figure 2.3.2. Optical data of CYP101, substrate-free form, showed the Soret band at 417 nm, with ε_{mM} =119.[76] The intensity of CYP101 substrate at 417 nm is higher than the intensity of CYP101 at 391 nm.

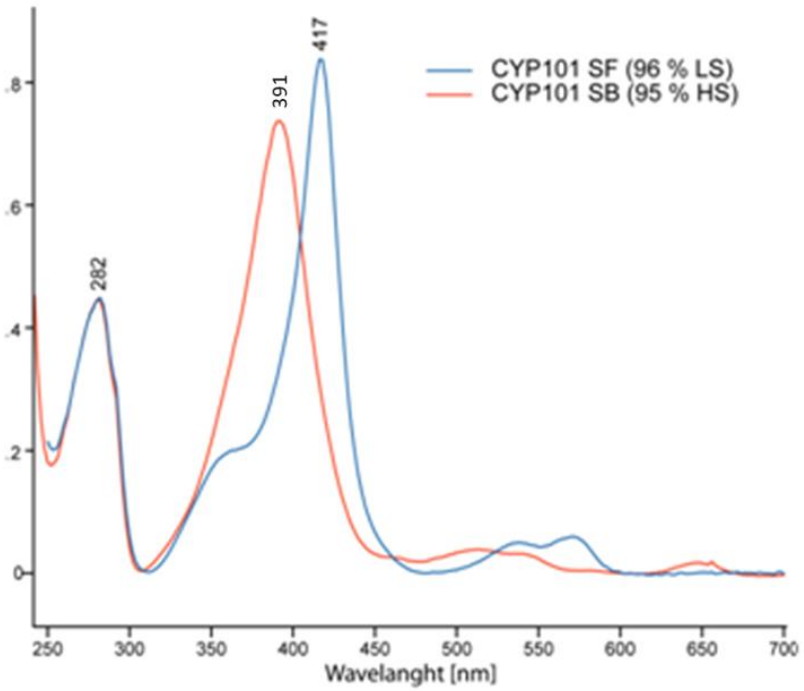

Figure 2.3.2 UV-vis spectrum of overlap CYP101 substrate bound and CYP101 substrate free

2.3.2 Determination of Relative Resonance Raman Spin-State Marker Intensities for substrate-free and Camphor-bound CYP101

As was described in earlier sections, efforts are being made to explore the possibility that resonance Raman spectroscopy might serve as a self-sufficient technique to determine spin-state populations for cytochromes P450, possibly as a generally useful method for a variety of P450s. The basic idea is to use an internal standard to determine accurate estimates of the relative intensities of the major marker bands for spin-state; i.e., the ν_3 for the substrate-bound high spin (HS) state, occurring at ~1485 cm^{-1} and the ν_3 for the substrate-free low-spin (LS) state, which appears near 1500 cm^{-1}. The strategy is to employ a (non-resonance enhanced) internal standard, Na_2SO_4, in both solutions so as to give a standard band with fixed frequency and intensity.

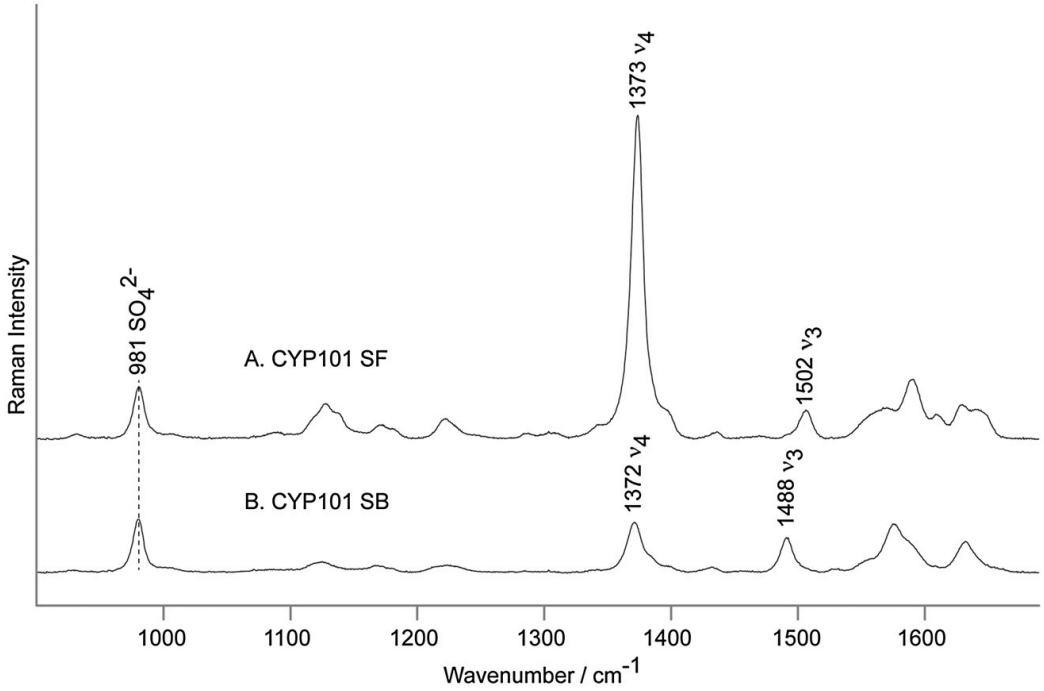

Figure 2.3.3 The resonance Raman spectra of ferric CYP101 substrate-free sample (A) and substrate-bound (B) sample. Spectra measured with 406.7nm excitation line and normalized to the sulfate band at 981 cm^{-1}

The results, shown in Figure 2.3.3, the spin-state change is observed as a shift of ν_3 from 1502 cm^{-1} (LS) to 1488 cm^{-1} (HS). To estimate relative rR cross sections for the substrate-free (SF) and substrate-bound (SB) samples, three samples of these two forms, each containing 0.500M internal standard Na2SO4, were measured, and their spectra were analyzed using the following peak fitting procedure. The $SO4^{2-}$ bands at 981cm^{-1} (and all heme modes) were found to fit best with a 30% Gaussian/70% Lorentzian function. The average band width for the sulfate mode for all six spectra was 10.1 cm^{-1}; the resulting band widths of the spin-marker bands were 11.5 cm^{-1} (1488 cm^{-1}) and 11.3 cm^{-1} (1502 cm^{-1}).

For the normalized the ν_3, we can obtain 9 number ratios of Y_{HS}/Y_{LS} by comparing the area of ν_3 in substrate bound with that in substrate free form. Noting that SF CYP101 is 96% LS, and the camphor-bound CYP101 is 95% HS,[74] the operative relative intensity values, Y_{LS} and Y_{HS}, were derived by dividing the raw relative intensities by 0.96 and 0.95 factors, respectively. Results were listed in Table 2.3.1 for excitation line 406.7 nm and 413.1 nm.

Table 2.3.1 The calculated ratios of relative peak areas (Y_{HS}/Y_{LS}) for a series of substrate-bound and substrate-free samples of CYP101. The spectra were measured with 406.7 and 413.1 nm excitation lines

406.7 nm		413.1 nm	
SB1/SF1	1.23	SB1/SF1	1.17
SB1/SF2	1.13	SB1/SF2	1.15
SB1/SF3	1.23	SB1/SF3	1.16
SB2/SF1	1.28	SB2/SF1	1.19
SB2/SF2	1.18	SB2/SF2	1.17
SB2/SF3	1.29	SB2/SF3	1.18
SB3/SF1	1.30	SB3/SF1	1.25
SB3/SF2	1.20	SB3/SF2	1.23
SB3/SF3	1.30	SB3/SF3	1.24
average:	1.24 ± 0.06	average:	1.19 ± 0.04

The average is 1.24 for excitation line 406.7 nm and 1.19 for excitation line 413.1 nm, indicating a slightly higher, but significant, difference in the ratios at the two excitation lines. Although of borderline significance, this smaller value of 1.19 is reasonable, because the 413.1 nm line is closer to resonance with the Soret band of the LS sample (417 nm). In order to expand the potential applications of this procedure, these ratios were also calculated for the ν_4 and ν_7 modes with both excitation lines listed in Table 2.3.2. These data can be used to normalize spectra in different regions. One can apply the Y_{HS}/Y_{LS} ratio of 0.21 ± 0.013 for the intense ν_4 mode when normalizing high-frequency spectra, and in the low frequency region, one could utilize the 0.38 ± 0.020 ratio for ν_7 mode.

Table2.3.2. The calculated cross section ratios between substrate-bound and substrate-free samples for the ν_7, ν_3 and ν_4 modes, measured with 406.7 and 413.1 nm excitation lines

Mode	Y_{HS}/Y_{LS}	
	406.7 nm	413.1 nm
ν_7	0.38 ± 0.020	0.216 ± 0.003
ν_3	1.24 ± 0.06	1.19 ± 0.04
ν_4	0.21 ± 0.013	0.135 ± 0.005

Given that the electronic spectra of both the HS and LS states of the bacterial CYPs correspond well with those of mammalian CYPs, it is reasonable to expect that the value of 1.24 derived here for CYP101 should be valid for the spectra of mammalian CYPs. To evaluate this issue, the derived 1.24 value was applied to calculate the percentage of spin-state conversion upon substrate binding of several mammalian CYP available in our laboratory; i.e., CYP2B4, ND:CYP3A4, and ND:CYP17.[77–79] The percentages of LS and HS states calculated from rR spectra (406.7nm excitation) using the method presented earlier were compared with the percentages independently derived by other workers from available UV–Visible data (Table 2.3.3).

Table 2.3.3 The calculated percentage of spin-state populations in various cytochromes P450 measured with 406.7nm excitation line and using the Y_{HS}/Y_{LS} ratio of 1.24 ν_3 modes

Protein	Resonance Raman		UV-Vis	
	% High Spin	% Low Spin	% High Spin	% Low Spin
CYP2B4 + Butylated hydroxytoluene	94	6	93[a]	7[a]
CYP3A4 SF	5	95	11[77]	89[77]
+ Testosterone	74	26	80-92[77,78]	8[77,78]
+ Bromocryptine	80	20	93[77]	7[77]
+ Erythromycin	19	81	22[77]	78[77]
CYP17				
+ Progesterone	94	6	97[a]	3[a]
+ 17-hydroxyprogesterone	59	41	62[a]	38[a]

Note: [a] was from personal communication

As can be seen, the data matched quite well for CYP2B4 with butylated hydroxytoluene, CYP3A4 both SF and with erythromycin, as well as CYP17 with progesterone, and 17-hydroxyprogesterone. The value obtained here for the testosterone-bound ND:CYP3A4 falls within the range reported for the measurements with UV–Visible spectrophotometry; as discussed more thoroughly in several earlier works dealing with substrate-binding equilibria and spin-state conversion for these systems,[77–79] the percentage LS to HS conversion is not linearly related to the number of bound substrates and is further complicated by the fact that substrate access to enzyme also depends on partitioning of the substrate into the lipid bilayer of the nanodisc. Similar complications can also be encountered for the bromocryptine-bound samples of the ND:CYP3A4 system and may account for the slightly larger, but not unreasonable, discrepancy seen here; i.e., 80% vs 93%.[80]

2.4 Summary

The cross section ratio in this study is 1.24 for excitation line 406.7 nm and 1.19 for excitation line 413.1 nm. One can use these two numbers to calculate the spin population through resonance Raman data of ferric data measured by 406.7 nm or 413.1 nm lines. This method eases the way of determining the substrate binding, substrate exchange, redox partner binding, etc from the spin population change. The cross section ratio also helps to demine the change in different ionic strength buffer, pH dependence, etc. In section 3, I used this data to determine the spin population change of CYP11A1 when binding with different substrates, Adx effect, and ionic strength effect.

3 Biophysical studies of CYP11A1, ferric, ferrous-CO and oxy-forms with effect of redox partner Adx

3.1 Introduction

3.1.1 Mammalian P450s

Mammalian P450s are mainly membrane bound or incorporated P450s.[2] P450s metabolize thousands of xenobiotics. According to the substrates that P450s metabolize, there are two main kinds of P450s: steroidogenic P450s and drug metabolism P450s.

Drug metabolism P450s can metabolism about 75% of the drugs in the market.[2,81] Among those drug metabolism P450s, CYP3A4 metabolizes around 50%, both CYP2C19 and CYP2D6 metabolize around 13% each. Figure 3.1.1 shows the main enzymes which metabolize the marketed drugs and main CYPs metabolizing marketed drugs.[81]

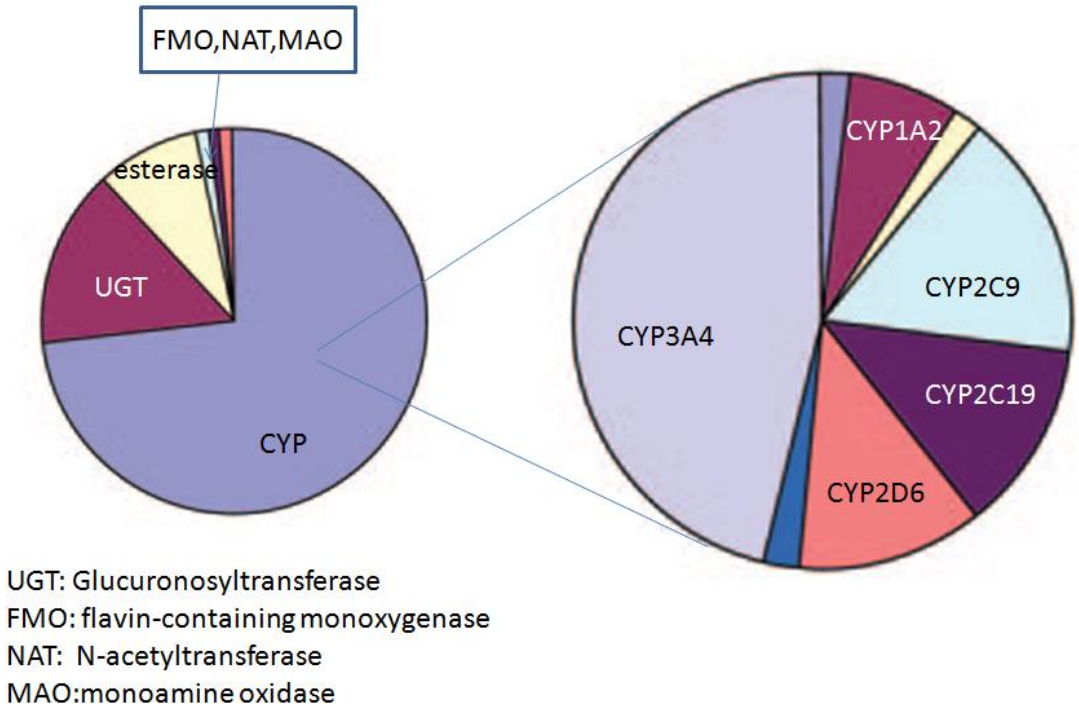

Figure 3.1.1 (left) main enzymes metabolize marketed drugs; (right) main CYPs metabolize marketed drugs

Comparing the active sites of steroidogenic P450s and drug metabolism P450s, the size of the typical active site in drug metabolizing P450s is much larger than in the cases of the steroidogenic P450s. For example the size of active site in CYP3A4 is 1386 $Å^3$ while for CYP11A1 is only about 600 $Å^3$.[39,40,63]

A given drug metabolizing P450s can bind and process a wide range of structurally different substrates and some can bind up to several substrate molecules simultaneously, while steroidogenic P450s can only bind one substrate molecule at a time, with high specificity for the natural substrate. Drug metabolizing P450s typically perform multiple and relatively non-specific hydroxylations on a bound substrate, whereas steroidogenic P450s generally perform multiple highly regio- and stereo-specific hydroxylations or other oxidative transformations on the single natural substrate. For

example CYP11A1 converts cholesterol to pregnenolone through three-hydroxylation cycles.[42]

3.1.2 CYP11A1 (aka P450scc)

Steroid hormones help control metabolism, inflammation, immune functions, salt and water balance, development of sexual characteristics, and the ability to withstand illness and injury. The steroid hormones are produced through multiple pathways which go through six different P450s: CYP11A1, CYP17, CYP21, CYP11B1, CYP11B2, and CYP19. Figure 3.1.2 shows the pathways and the function of each P450.[2]

The steroid hormones synthesis starts from the conversion of cholesterol to pregnenolone which is catalyzed by CYP11A1. This is the first step and the rate determining step.[2] The product, pregnenolone, is produced by the side cleavage between C20 and C22. The pregnenolone is the precursor of the following steps which are catalyzed by CYP17, CYP21, CYP11B1, CYP11B2, and CYP19.

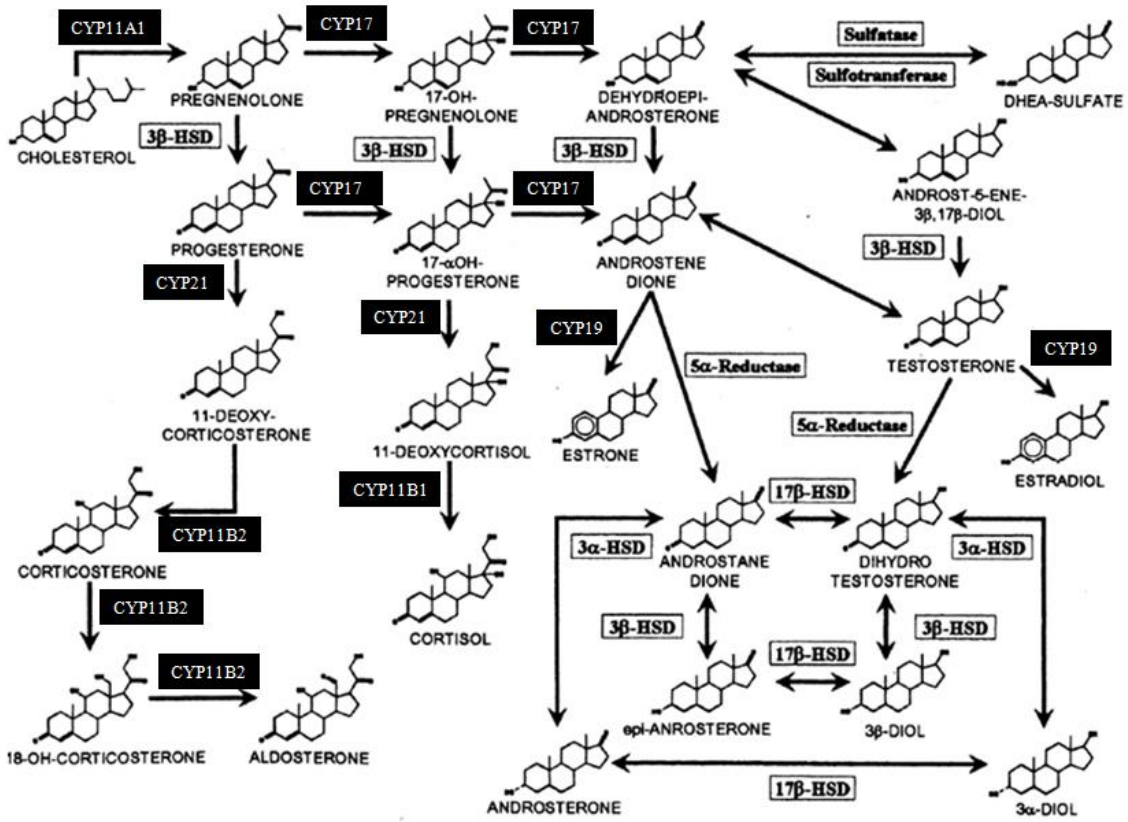

Figure 3.1.2 Biosynthesis of steroid hormones[82]

Steroidogenic cytochromes P450 play important roles in the synthesis of steroid hormones that are essential for maintenance of mammalian life.[2,42] Ultimately, all of these crucial hormones are generated from a common parent hormone, pregnenolone. The pregnenolone is derived from cholesterol in a complex process mediated by the multifunctional steroidogenic P450, CYP11A1. The CYP11A1 is an inner mitochondrial protein of the adrenal cortex also known as cytochrome P450scc. The CYP11A1 catalysis the side cleavage process occurring between C20 and C22 of the cholesterol (Figure 3.1.3). CYP11A1 converts cholesterol to pregnenolone which triggers the first step of steroid synthesis.[40] This is the rate limiting step in the steroid synthesis pathway.[2] The

whole process is catalyzed by CYP11A1 through three sequential steps illustrated in Figure 3.1.3, where the first two steps convert cholesterol (CH) to 22R-hydrocholesterol (22R-OHCH) and then to 20R,22R-dihydroxycholesterol (20R,22R-DiOHCH), with the third stage leading to a bond cleavage between C20 and C22, thereby forming the key product, pregnenolone, and another small molecule, 4-methylpentanal (also called isocaproaldehyde).[39,40] Accumulation of isocaproaldehyde will decrease the viability of Y1 cells,[83] which are responsible for producing 20αdihydroxyprogesterone and 11β,20α-dihydroxyprogesterone in the steroid synthetic process.[84]Aldose reductases (AR), cytosolic monomeric enzymes that belong to the aldo-keto reductase (AKR) superfamily, are able to reduce isocaproaldehyde.[85] This superfamily can reduce carbonyl groups from natural or synthetic substrates, including aliphatic and aromatic aldehydes, ketones, keto prostaglandins, ketosteroids and xenobiotics.[85] It has been established that in mice Akr1b7 is the main isocaproaldehyde reductase and that Akr1b3 serves as a minor reductase for this side-product. [83,85–88]

The well established enzymatic cycle of cytochromes P450 is initiated by substrate-binding to a low-spin ferric "resting state", which possesses an axial water ligand associated with a distal pocket water cluster. Entry of the substrate disrupts the water cluster and displaces the bound axial water ligand, generating a high spin ferric heme, whose elevated reduction potential triggers acceptance of an electron that, in the case of CYP11A1, is provided by NADPH associated adrenodoxin reductase (AdR) and delivered by an Fe-S cluster contained in adrenodoxin (Adx). This resultant ferrous species binds molecular oxygen present within the immediate environment to form a dioxygen adduct, which is most properly formulated as a ferric superoxide species,

Fe(III)-(O-O^{-}).[2,42] Delivery of another electron from the AdR/Adx reductase ensemble then produces a ferric peroxo intermediate, Fe(III)-(O-O^{2-}). While there exist special situations where this ferric peroxo species can react directly with electron- deficient fragments of a given substrate, generally, it is converted by rapid, sequential delivery of two heme pocket protons to first form a transient hydroperoxo- species and then, with the delivery of the second proton, undergo efficient O-O bond cleavage to generate an extremely potent oxidant, known as Compound I, which is most accurately formulated as a ferryl heme π cation radical; i.e., [(Porphyrin$^{+\cdot}$) Fe(IV)=O].[41,45,68,89–92] This species is capable of direct hydroxylation of many types of substrate.[93] The first and second steps of the 3-stage CYP11A1-catalyzed conversion of cholesterol to pregnenolone are classical hydroxylations reasonably assumed to proceed through Compound I.[42] The operative mechanism for the third step, involving a more elaborate C-C bond cleavage process, is still a subject of some debate regarding the details of the Compound I mediated transformation.[40,94–102]

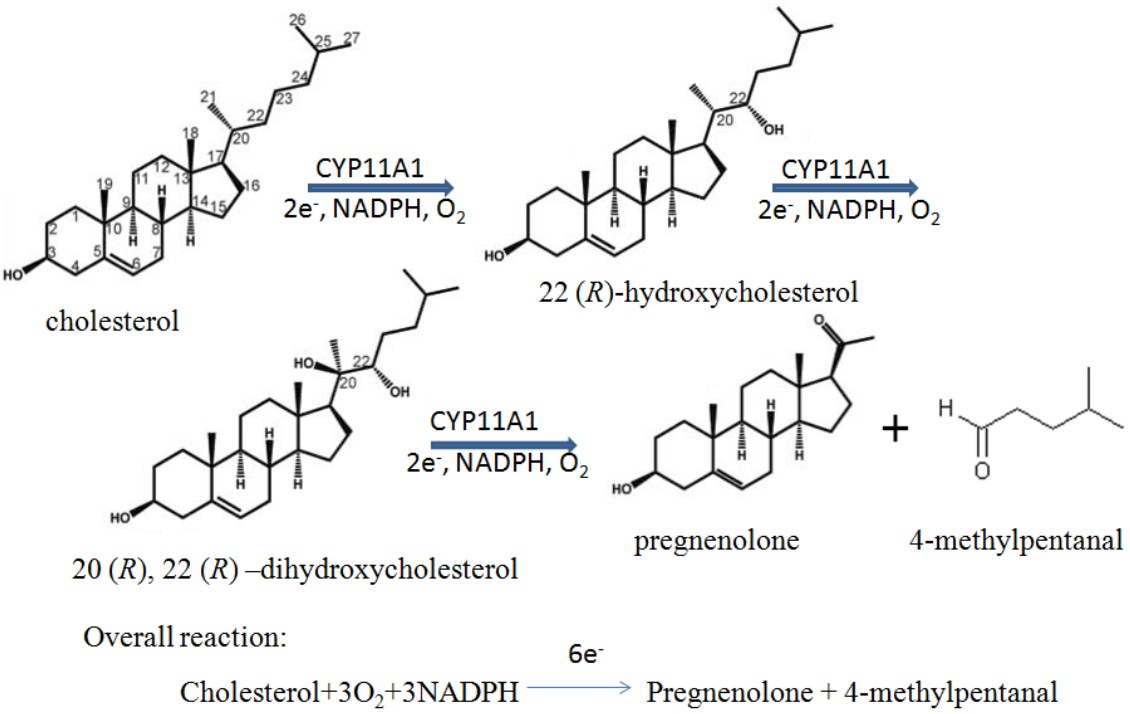

Figure 3.1.3 Conversion process from cholesterol to pregnenolone through CYP11A1

Because the F-G loop and A' helix of CYP11A1 is partially associated with membrane, it is not soluble in aqueous solution. Crystal structures with intermediates were hard to form until 2011. Strushkevich et al. published a crystal structure of adrenodoxin (Adx) bound to CYP11A1 proximal position shown in Figure 3.1.4. Only few amino acids of CYP11A1 are associated with the membrane, so the enzyme is not as tightly bound with the membrane as those enzymes possessing a substantial hydrophobic tail.[40] This is consistent with the former model hypothesis. The pocket of the active site is a banana-shaped tunnel with volume of the cavity is around 625 A^3. The substrate, cholesterol, enters the active site pocket from the top opposite with the Adx and the product, pregnenolone, leaves the pocket from the top also. The shape and length of the

tunnel shows that the substrate movement is translational when the intermediates move toward or away from the active site.

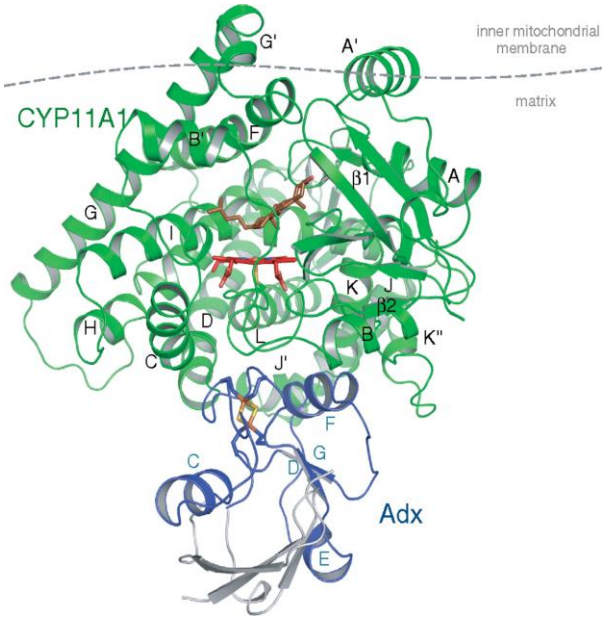

Figure 3.1.4 Crystal structure of CYP11A1-Adx complex[40]

Strushkevich et al[40] also published the superposition of active site with cholesterol, 22R-OHCH and 20R, 22R-DiOHCH, shown in Figure 3.1.5. From the superposition figure and the crystal structure, the distance of C22 to the heme Fe is 4.3 Å and that from C20 to heme Fe is 4.5 Å. However, modeling indicates that the distance between the hydrogen at C22 and the oxyferryl oxygen is 2.3 Å, whereas the hydrogen at C20 is slightly away with a distance of 2.6 Å. That explains the reason why the first hydroxylation takes place at C22 position to generate 22R-OHCH. After the first cycle, the C22 position moves towards the heme-Fe a little compared with C22 in cholesterol. This movement brings the H at C20 position closer to the heme-Fe, which allows the hydroxylation at C20 position during the second cycle to generate 20R, 22R-DiOHCH.

After the second cycle, the whole chain moves back to original position. The heme-Fe locates right between the C20 and C22. This position insures the cleavage between C20 and C22 during third cycle even though the detailed cleavage mechanism still remains unknown.

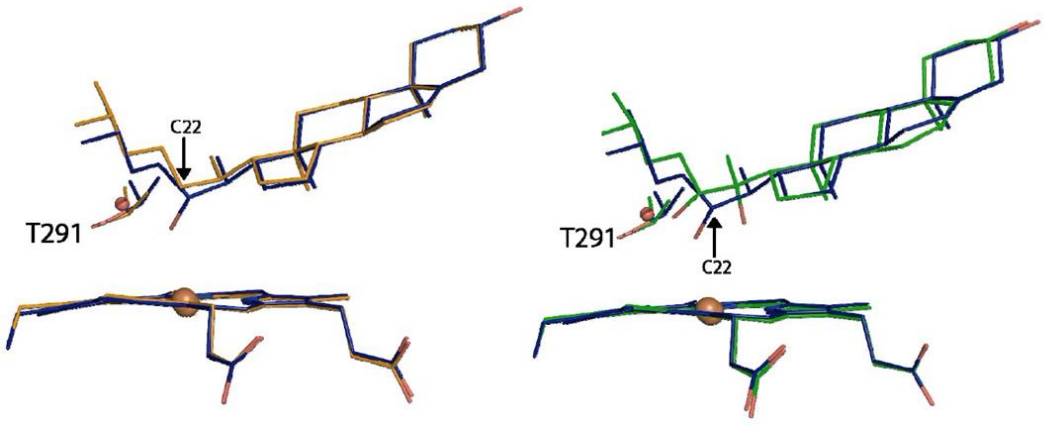

Figure 3.1.5 (left) Superposition of cholesterol and 22R-OHCH above the heme; (right) superposition of 22R-OHCH and 20R, 22R-DiOHCH[40]

Interestingly both Strushkevich et al[40] and Mast et al[39] published the crystal structure of CYP11A1 with substrate 22R-OHCH, which shows almost full low spin in ferric state. The most likely reasons are: 1) the water molecule in the active site is still bound to the heme Fe as a sixth ligand; 2) the O of the hydroxyl group from the 22R-OHCH substrate serves as the sixth ligand. Strushkevich et al indicated that continuous electron density was observed between Fe and the O from C22 hydroxyl group and the distance was 2.6 Å.[40] Mast et al also showed the distance was 2.56 Å which was very likely a covalent bond.[39,59] Further study needs to be done to provide more evidence before a definitive conclusion can be reached.[51]

Mast et al[39] measured electronic absorption spectra of the ferrous CO form with different substrates and without substrate (seen in Figure 3.1.6). The interesting thing is that there is no band at around 450nm for CYP11A1 bound with 22R-OHCH; i.e., they argue that CO doesn't bind. The explanation offered for why this complex apparently binds dioxygen, but not CO, is because of the steric effect; i.e.,the angle of Fe-C-O is 180º, while the angle of Fe-O-O is only about 108º, allowing the O-O to bind end-on without interference by the C-OH fragment of the substrate.[39] However, these results are surprising in light of the fact that rR and FTIR spectroscopic studies, published years before,[103] had provided solid evidence for the stability of the Fe-CO adduct of CYP11A1 bound with 22R-OHCH. As will be discussed below, perhaps the reason the early spectroscopic data was not considered definitive was that the data acquired in that work yielded interpretations that were somewhat ambiguous (vide infra).

Of direct relevance to this seemingly conflicting evidence are studies published by Tuckey and Kamin,[104] who found out that the order of binding affinity of CO to CYP11A1 is: substrate free > cholesterol >20(S)-hydroxycholesterol > 22R-OHCH, and then 20R, 22R-DiOHCH. The results presented by Tuckey and Kamin verified that CO can bind in this case, but has a much lower affinity; i.e., both spectroscopic and functional studies had shown that CO was hard to bind with CYP11A1 when 22R-OHCH was the substrate.[97,100]

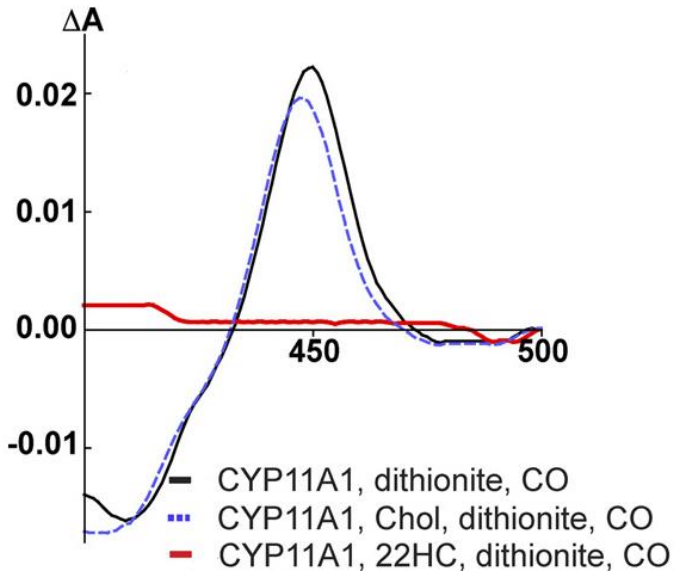

Figure 3.1.6 Reduction of CYP11A1 with sodium dithionite substrate free (black line), cholesterol (dashed line), 22HC (red line)[39]

The previously published resonance Raman studies of CYP11A1 dealt with the CO adducts of CYP11A1 bound with different substrates (including 22R-OHCH) and the substrate-free form (Figure 3.1.7).[98,99] As mentioned above, these workers detected the Fe-C stretching frequency for the CO forms with *all* of the substrates, including 22R-OHCH, while Mast et al[39] had concluded that CO can't bind with CYP11A1 with this latter substrate. On the other hand, though the spectroscopic data confirm CO binding to the sample containing the R22-OHCH substrate,[98,99] the observed sets of Fe-C and C-O stretching frequencies do not adhere to the well-established inverse correlation between these two modes.[72] Usually high C-O stretching frequency will correspond to low Fe-CO stretching frequency,[44] but that correlation was not observed here. More importantly, it is interesting to note that, in the case of the CO adduct with the R22-OHCH substrate, only one ν(Fe-C) stretch was observed, while *two* ν(C-O) stretches were seen in the FTIR

spectrum. For these reasons, new vibrational spectroscopic studies of the these systems are carried out in the present work, as will be later presented and discussed.

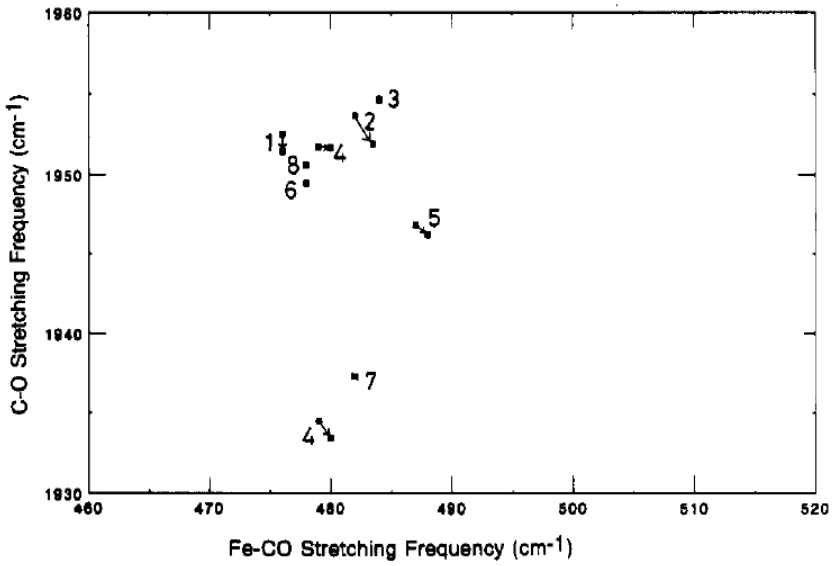

Figure 3.1.7 CO forms of CYP11A1 bound with different substrates: (1) substrate free; (2) cholesterol; (3) 25-OH-cholesterol; (4) 22(R)-OH-cholesterol; (5) 22(S)-OH-cholesterol; (6) 20(S)-OH-cholesterol; (7) 20(R),22(R)-dihydroxycholesterol; (8) 22-ketocholesterol. Effects of reduced adrenodoxin binding are indicated by arrows. [103]

Tsubaki et al[105] also used resonance Raman to check the effects of adrenodoxin and cholesterol. They concluded that with cholesterol only there was only about 70% spin conversion from low spin to high spin, but that that after adding of adrenodoxin, there was full conversion to high spin. In the spectra shown in Figure 3.1.8, ν_{10} (1638 cm^{-1}), ν_3 (1503 cm^{-1}) and ν_2 (1584 cm^{-1}) are spin state sensitive modes indicating ferric low spin state. From those spin state markers, it is argued that the sample in the middle trace is a mixture of high spin and low spin, where ν_{10} shifted to 1620 cm^{-1}, ν_2 shift to 1567 cm^{-1}, ν_3 shifted to 1485 cm^{-1}, all indicating high spin. However, it is important to note that, of these spin state markers, only the ν_3 mode is normally in an isolated region of the spectrum and acts as a reliable marker; in the present case the HS component of that mode is overlapped by the strong glycerol band present, making evaluation of spin state population difficult. Therefore, these studies are to be repeated in the present work, as described later. The lower trace, obtained from CYP11A1 with substrate CH and redox partner Adx, which was interpreted to show almost high spin, though the presence of overlapping modes can hinder an accurate interpretation.

In the low frequency region, only two Raman peaks are seen at 346 cm^{-1} and 380 cm^{-1}, while others are from glycerol. Oxidized adrenodoxin has Raman lines at 289 cm^{-1}, 346 cm^{-1} and 381 cm^{-1}. It is hard to tell the structural change upon binding of Adx or different substrates from the low frequency data, because the major heme modes are obscured by the peaks from the buffer/glycerol media. Glycerol has an effect on CYP11A1 spin state conversion. Also, Headlam et al[64] have stated that glycerol will tend to convert CYP11A1 from high spin to low spin; perhaps this would cancel the effects of adding of substrates and adrenodoxin. In the present study, the aqueous buffer will be

used to illustrate the effects of CYP11A1 with different substrates with and without Adx in the high frequency and low frequency.

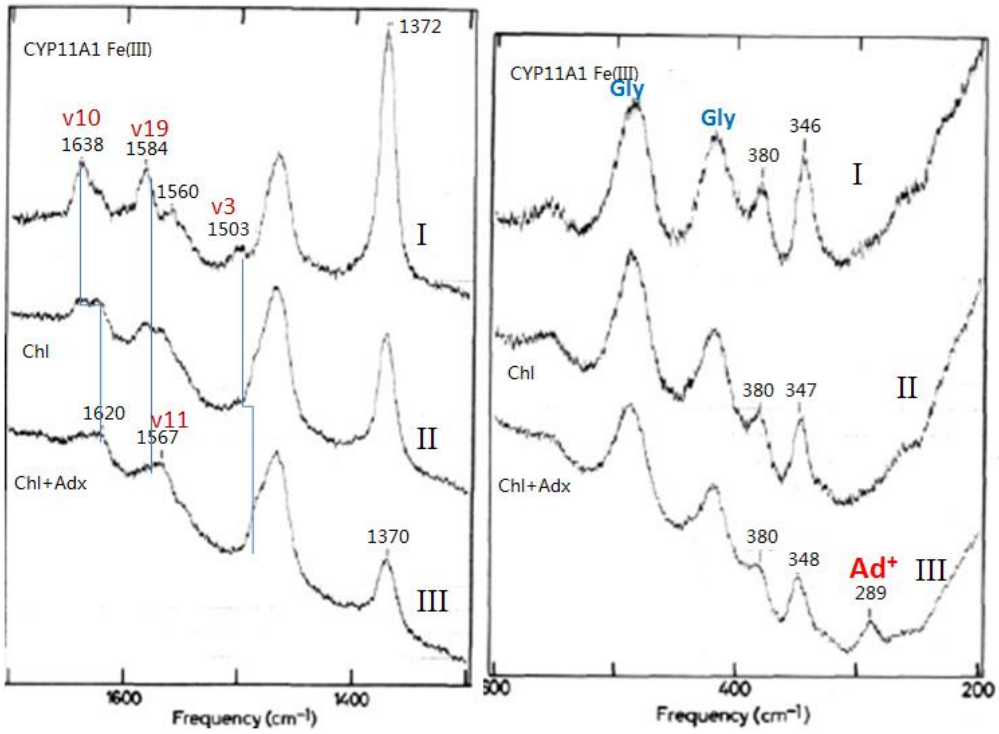

Figure 3.1.8 Resonance Raman spectroscopy of CYP11A1 with addition of cholesterol and cholesterol+adrenodoxin [105]

3.1.3 Adrenodoxin (Adx) 2Fe-2S cluster

Adx is a member of a class of redox proteins, called ferredoxins, which contain a [2Fe-2S] cluster. The Adx serves as an electron transport protein that provides electrons from a NADPH containing enzyme, adrenodoxin reductase (AdR), to the active site of CYP11A1. It has been reported that the inherent reduction potential of substrate-bound CYP11A1 is -284 mV, while that for Adx is -273 mV and that protein-protein complex formation caused the redox potential of Adx to undergo a small negative shift to -291 mV, while that of the CYP11A1 shifted to -312 mV. [106,107] The mechanism of electron transfer process is still not entirely clear. There are three main hypothesis: 1) Adx serves as a shuttle between AdR and CYP11A1; 2) a 1:1:1 complex of AdR, Adx and CYP11A1 is formed; 3) a 1:2:1 complex of AdR, Adx and CYP11A1 forms.[108–111] Although many attempts have been made to illustrate the exact mechanism and favor the shuttle model, none of these can be definitely ruled out.[109] The association of Adx and CYP11A1 is postulated arise from electrostatic interactions of charged surface residues of Adx and CYP11A1.[109] The recently reported crystal structure of the fusion protein between Adx and CYP11A1 revealed the presence of two salt bridges: Lys339 (CYP11A1)-Asp72 (Adx) and Lys 343 (CYP11A1)-Asp76(Adx). [40]

3.1.4 NADPH-AdR Adrenodoxin reductase

Adrenodoxin reductase (AdR) is also called ferredoxin NADP+ (nicotinamide adenine dinucleotide phosphate) reductase because AdR can reduce a ferredoxin Adx by using the electron provided by NADPH. AdR has a coenzyme flavin adenine dinucleotide (FAD) which can accept electron from NADPH and then transfer to Adx. Multiple electrons can be transferred but only one at a time.

3.1.5 Research purpose of CYP11A1

Resonance Raman (rR) spectroscopy has been applied to study various heme proteins and enzymes for decades.[71,112] Applications are focused on rR-based determinations of: spin population change;[113] distortions of the heme, as reflected in variations of the in-plane and out-of-plane macrocycle modes; [71,112,114,58,115–118] and interactions of the vinyl and propionate groups on the heme periphery, as reflected in the behavior of the propionate- and vinyl- bending modes appearing in the low-frequency region and the vinyl group ν(C=C) stretching modes that are observed near 1600-1640 cm^{-1} and are sensitive to out-of-plane disposition of these groups with respect to the mean heme plane.[114,119–123] In addition to these rR markers of heme structural changes, the technique is an especially powerful and direct probe of the strength of binding of various endogenous and exogenous heme axial ligands. For example, the behavior of the ν(Fe-C) and ν(C-O) for ferrous CO forms reveal detailed information about the polarity of the distal pocket and H-bonding interactions with molecular fragments of bound substrates or distal pocket protein residues.[72] Of special importance for this work, the ν(Fe-O) and

ν(O-O) modes of the oxy form of cytochromes P450 and certain other proteins bearing an axial cysteine-thiolate are efficiently rR enhanced and provide telltale vibrational data that reflect subtle, but functionally important, H-bonding differences with distal side molecular fragments.[72,124] Also important for the present application is the fact that rR is able to probe the status of the key ν(Fe-S) mode, using 356 nm excitation line, which is in close proximity to an S→Fe(III) LMCT transition occurring near 360 nm.[35,114,125–129] Moreover, rR measurements can monitor the effects of redox partners on the heme active sites for all of the above forms. It is also important to mention that rR measurements can be done at different temperatures; e.g., near room temperature for samples in natural, aqueous conditions (with varying pH and ionic strengths), as well as at cryogenic temperatures, under conditions in which unstable intermediates can be characterized.

Early rR studies of this enzyme were reported mainly by Tsubaki et al., for the ferric and ferrous CO states, providing valuable insight,[41-43] but also leaving some unexplained issues of interpretation unanswered (vide infra). In the present work we expand the rR investigation of CYP11A1 to studies of the dioxygen complexes, ordinarily fleeting intermediates within cytochrome P450 reactions cycles at ambient temperatures that must be prepared and stabilized under low temperature conditions.[124,130,131] Studies of such dioxy-intermediates by rR spectroscopy have recently been shown to be an especially effective approach to reveal even subtle active site structural changes that significantly impact the disposition of crucial intermediates and influence alternative reaction pathways that may occur within in these enzymatic cycles.[124,130] For example, the rR technique can reveal quite subtle, but highly significant differences in hydrogen bonding interactions with the Fe-O-O fragment, with H-bonding

to the proximal oxygen ($Fe\text{-}O_p$) leading to a lower ν(Fe-O)frequency, while H-bonding to the terminal oxygen ($Fe\text{-}O_p\text{-}O_t$) yields relatively higher ν(Fe-O) modes. [72,132] This is quite an important capability, because DFT computations,[133] as well as studies of the dioxygen adducts of NOS,[18,134,135] have indicated that hydrogen bonding to the proximal oxygen will stabilize this intermediate, thereby the hindering cleavage of the O-O bond, making it more likely that a (susceptible) substrate will be processed through the peroxo intermediate.[124,133] On the other hand, if hydrogen bonding is formed to the terminal oxygen atom of the Fe-O-O fragment, which favors the breakage of the O-O bond,[136,137] the reaction inevitably proceeds through the compound I intermediate.[130,133]

The original purpose of this project is to evaluate the activity of CYP11A1 with its natural substrates bound with redox partner Adx in nano-disc system in order to avoid the aggregation. Since the difficulty of collaboration, the results presented here is the CYP11A1 without nano-disc. CYP11A1 only have a few amino acids associated with the membrane so the aggregation is not a big issue during our experiments.[40] Detailed task was listed below.

1) Measure CYP11A1 ferric forms bound with its three natural substrates and their Adx effect;
2) Evaluate the proximal ligand effect by measuring the Fe-S linkage;
3) Stable ligation forms with CO of all three natural substrates and their Adx effect;
4) FTIR measurements with CYP11A1 bound with 22R-OHCH and 20R,22R-DiOHCH in ferrous CO form;

5) Most importantly, characterize the unstable intermediates oxy-forms and their Adx effect to predict the active catalysis during the hydroxylation cycles.

3.2 Methods and experiments

3.2.1 Bovine CYP11A1 purification

Fresh bovine adrenal glands were purchased from a local slaughter house and the connective tissue and fat was removed as much as possible. CYP11A1 is in the adrenal cortex which is a brownish layer between medulla (core part) and the capsule (skin part). Adrenal cortex was scraped by a scalpel to very small pieces. This material was then chopped to form a fine mash in order to obtain a successful homogenization. The adrenal cortex was suspended in 4 volumes of cold 0.25 M sucrose solution containing 10 mM phosphate pH 7.4, 0.1 mM ethylenediaminetetraacetic acid (EDTA) and 0.1 mM dithiothreitol (DTT). The homogenate was centrifuged (4℃) at 500xg for 10 minutes to remove the unbroken cells and nuclei. The supernatant was centrifuged again at 11,000xg for 30 minutes at 4℃, forming a brown pellet (called mitochondrial pellet), which were collected and stored.

The mitochondria pellets were resuspended in 20 mM phosphate buffer pH 7.5 containing 0.10 mM EDTA and 0.10 mM DTT. This solution was homogenized to fully mix. The solution was sonicated for 1 minute, using two 30 second bursts, with a 5 minute interval between bursts. The sonicated suspension was centrifuged at 100,000xg for 1 h at 4 ºC, using an ultracentrifuge (Beckman Coulter, Optima^{TM} L-90K ultracentrifuge). The supernatant, which contains adrenodoxin and adrenodoxin reductase, was stored. The Adx purification will be described in next section. The pellets, which are called sub-mitochondrial particles, were re-suspended by homogenization in 100 mM

phosphate buffer pH7.4, containing 0.1 mM EDTA and 0.1 mM DTT. The protein concentration was checked by using Bradford assay[138] and diluted to a concentration of 15 mg/ml. The suspended sub-mitochondrial particles were extracted for 1 h with 1% cholate by adding 10% sodium cholate stock dropwise while stirring. The cholate containing solution was centrifuged at 100,000xg for 1 h at 4℃ by using an ultracentrifuge. The supernatant which contains CYP11A1 and CYP11B1 was kept.

The volume of the supernatant was measured. The 18 g of the ammonium sulfate $(NH_4)_2SO_4$ per 100 ml supernatant was added for 0 - 32% saturation. The $(NH_4)_2SO_4$ was added slowly while stirring and making sure all $(NH_4)_2SO_4$ is dissolved. The solution stood for 30 minutes. The solution was centrifuged at 50,000xg for 10 minutes at 4℃. Discard the pellet which contains CYP11B. The volume of supernatant was measured. The 8 g ammonium sulfate was added per 100 mL of supernatant for 30 - 45% saturation, dissolve and stand for 30 minutes and centrifuge the solution at 50,000xg for 10 minutes at 4℃. The pellets were resuspended in 100 mM phosphate buffer pH7.2 containing 0.1 mM EDTA and 0.1 mM DTT and dialysis in this buffer for overnight.

After dialysis, the solution was centrifuged at 12000 rpm for 20 minutes at 4℃ to remove the undissolved or denatured protein. An Octyl sepharose column was equilibrated by washing with 100 mM phosphate buffer pH7.2 containing 0.1 mM EDTA and 0.1 mM DTT. The clear solution was loaded on the column and washed with the equilibrated buffer until no color elutes. Then the column was washed with 100 mM phosphate buffer pH7.2 containing 0.03% cholate, 0.5M KCl, 0.1 mM EDTA and 0.1 mM DTT until no color elutes and the major fraction was not eluted. The CYP11A1 was eluted by 100 mM phosphate buffer pH7.2 containing 0.3% cholate, 0.5M KCl, 0.1 mM

EDTA and 0.1 mM DTT. The product was collected in fractions and checked by UV. Fractions with absorption of A_{390nm} / A_{280nm} greater than ~0.6 were pooled as pure CYP11A1. The pure samples were dialysis overnight at 100 mM phosphate buffer pH7.2 containing 0.1 mM EDTA and 0.1 mM DTT in order to remove cholate and extra salt. The sample was measure by UV to check the concentration and its CO form to check the P420 amount. Then the sample was diluted and divided into small vials and stored at -80℃ for future use.

3.2.2 Bovine adrenodoxin purification

A DE52 column, equilibrated with 100 mM phosphate buffer pH7.4 containing 0.1 mM EDTA and 0.1 mM DTT, was prepared. The sub-mitochondrial supernatant containing the Adx and AdR, saved in section 3.2.1, was loaded to the column. The brown Adx binds to the top of the gel. The AdR, and other proteins, were eluted from the column with the 100 mM phosphate buffer, pH7.4 containing 0.1 mM EDTA and 0.1 mM DTT until no color elutes. The unwanted proteins were eluted through different buffers listed below. Then the column was washed with 200ml 10 mM phosphate buffer pH 7.4 containing 0.1 M KCl. The column was then washed with 200mL of 10 mM phosphate buffer pH 7.4 containing 0.12 M KCl. The column was washed with 200mL 10 mM phosphate buffer pH 7.4 containing 0.15 M KCl until the Adx band moves to the bottom of the gel. The Adx was eluted with 10 mM phosphate buffer pH 7.4 containing 0.3 M KCl. The product was collected in fractions, check UV, pooling the fractions with absorption of A_{414}/A_{280} larger than 0.1.

A new DE52 column equilibrated with 100 mM phosphate buffer pH7.4 was prepared. The above samples were diluted three times and loaded on the column. The column was washed with 100 mM phosphate buffer pH7.4. The column was washed with 200mL 10 mM phosphate buffer pH 7.4 containing 0.1 M KCl. The column was washed with 200mL 10 mM phosphate buffer pH 7.4 containing 0.15 M KCl until the Adx band moved to the bottom of the gel. The Adx was eluted with 10 mM phosphate buffer pH 7.4 containing 0.3 M KCl. The product was collected in fractions, checked by UV, and

the fractions with absorption of A_{414}/A_{280} larger than 0.4 were pooled. The samples were concentrated to approximate 4-5 ml for next step.

A 2 cm x 70 cm long column was prepared with gel Sephadex G100 in 100 mM phosphate buffer pH7.4. The samples collected from previous step were applied on the column. Slowly Adx moved down in the column and collected 2-3 mL fractions. The fractions were checked by UV and the fractions with absorption of A_{414}/A_{280} larger than 0.7 were pooled. The sample was concentrated and divided them in small amount and store at -80℃ for future use.

3.2.3 Preparation of ferric samples

The CYP11A1 purified from bovine adrenal glands naturally binds with cholesterol which gives majority of high spin. Since the binding affinity of the other two substrates, 22R-OHCH and 20R,22R-DiOHCH, are much higher than cholesterol, different substrates binding samples were made by adding from ethanol stock solution with 3-5 fold excess and incubated overnight to insure the fully exchange. The ratio of Adx to P450scc is 1.2:1 for those Adx containing samples. The samples containing redox partner were incubated overnight in order to insure the full binding of Adx. The concentration of all the ferric samples measured by excitation line 406.7 nm is 100 uM of CYP11A1 in buffer 100 mM phosphate buffer pH 7.4, 0.1 mM DTT and 0.1 mM EDTA.

CH bound with CYP11A1 ferric sample: dilute or concentrate the sample to 100 uM concentration;

CH bound with CYP11A1 containing Adx ferric sample: incubate purified CYP11A1 with 20% excess amount of Adx for overnight. Then concentrate the sample to 100 uM concentration of CYP11A1.

22R-OHCH bound with CYP11A1 ferric sample: add 3-5 fold excess amount of 22R-OHCH from ethanol stock solution with purified CYP11A1 and dilute the solution to lower the ethanol concentration be less than 1%. Incubate this solution for overnight then centrifuge to remove the denatured protein. Concentrate the sample to 100 uM.

22R-OHCH bound with CYP11A1 containing Adx ferric sample: add 3-5 fold excess amount of 22R-OHCH from ethanol stock solution and 20% excess amount of

Adx with purified CYP11A1. Dilute this solution to lower the ethanol concentration be less than 1%. Incubate this mixture for overnight then centrifuge to remove the denatured protein. Concentrate the sample to 100 uM.

20R,22R-DiOHCH bound with CYP11A1 ferric sample: add 3-5 fold excess amount of 20R, 22R-DiOHCH from ethanol stock solution with purified CYP11A1 and dilute the solution to lower the ethanol concentration be less than 1%. Incubate this solution for overnight then centrifuge to remove the denatured protein. Concentrate the sample to 100 uM.

20R, 22R-DiOHCH bound with CYP11A1 containing Adx ferric sample: add 3-5 fold excess amount of 20R, 22R-DiOHCH from ethanol stock solution and 20% excess amount of Adx to purified CYP11A1. Dilute this solution to lower the ethanol concentration be less than 1%. Incubate this mixture for overnight then centrifuge to remove the denatured protein. Concentrate the sample to 100 uM.

The only samples used to investigate the behavior of the ν(Fe-S) of the ferric forms, measured by excitation line 356.4 nm, were those bound with CH, with and without Adx. The preparation was the same as described above. The concentration is 200 uM in 10 mM phosphate buffer pH 7.4, 0.1 mM DTT and 0.1 mM EDTA, because in this lower buffer condition there is more difference for the Adx effect in high spin population.

3.2.4 Preparation of the ferrous-CO samples

3.2.4.1 Ferrous-CO samples for rR

Regarding preparation of the various ligated forms, the ferrous CO adducts were made by addition of an excess amount of reducing agent, sodium dithionite ($Na_2S_2O_4$), from stock solution. A 100 µL aliquot of a 100 µM sample of the enzyme was placed in an NMR tube (WG-5 Economy,Wilmad) and sealed with a rubber septum (Sigma-Aldrich, Milwaukee, WI). The tube was connected to a vacuum line with a needle connection. The sample was degassed three times by exchange with Ar gas and then exchanged with CO gas two times to ensure the sample was saturated by CO gas. A freshly prepared solution of sodium dithionite dissolved in an Ar degassed buffer was added to the solution of CYP11A1. The ferric sample can be reduced by addition of ~2 molar equivalents of sodium dithionite solution (8 µL). The electronic absorption spectrum (Q-band region) showed a sharp band rising at ~550 nm and a disappearing band at ~645 nm; the solution was allowed to incubate for 15 minutes to ensure full conversion.

3.2.4.2 Ferrous-CO samples for FTIR

Ferrous-CO adducts for FTIR measurements are only made with 22R-OHCH and 20R, 22R-DiOHCH-bound CYP11A1. Making the ferric form of 22R-OHCH and 20R, 22R-DiOHCH bound CYP11A1 was described in section 3.2.3. The samples were concentrated to higher than 200 uM since FTIR needs higher concentration to get better signal-to-noise. The ferrous CO samples were made by adding an excess amount of $Na_2S_2O_4$ to the CO saturated ferric sample in 2 ml glass vial sealed with rubber septum and then incubated for 15 minutes to ensure full conversion to ferrous CO. Then the ferrous CO sample was transferred, as quickly as possible, to the FTIR cell, which had already been flushed with CO gas. The concentration of the protein for FTIR sample was 200-300 μM.

3.2.5 Preparation of the oxy samples

Oxy samples were prepared on the vacuum line. The oxygenated samples were prepared from the ferric samples as described in the following manner. A 100 µL aliquot of concentration at 200 µM ferric CYP11A1 sample was placed in the NMR tube and connected to the vacuum line. The sample was degassed with Ar gas by evacuating the air out of the tube and filling Ar gas into the tube, repeating the process three times to make sure the sample was saturated with Ar gas but no oxygen present. Sodium dithionite, freshly made in Ar degassed the buffer, was added to the solution by using a gas sealed syringe through a rubber septum on the vacuum line system into the ferric sample, gently tapping the sample to mix well. The sample was titrated with small amounts of sodium dithionite solution while monitoring the rising the sharp band at ~550 nm and the disappearing band at ~645 nm. Then oxygen can be added to this ferrous sample by bubbling ^{16}O or ^{18}O gas, using vortex to spin the sample in order to mix well and let the oxygen bind with the complex well. The sample was placed in the cold bath temperature at 0 ℃. The mixing time is different according to the substrates; the oxygen complexes of the samples with the first two substrates, CH and 22R-OHCH, were prepared using 30 seconds mixing time, while the sample containing 20R, 22R-DiOHCH was mixed for 90 seconds. The oxygenated samples were frozen in the liquid N_2 immediately after mixing to avoid auto-oxidation.

3.2.6 Spectroscopy with CYP11A1

3.2.6.1 Resonance Raman with ferric samples at room temperature

Ferric CYP11A1 samples were measured using the 406.7 nm and 356.4 nm excitation lines from a Kr^+ laser (Coherent Innova Sabre Ion Laser). The rR spectra of all samples were collected using a Spex 1269 spectrometer equipped with Spec- 10 LN-cooled detector (Princeton Instruments). The slit width was set at 150 μm, and the 1200 g/mm grating was used; with this grating, the resultant spectral dispersion is 0.46 cm^{-1}/pixel. The laser power for the ferric sample was adjusted to ~10 mW. Moreover, to avoid laser-induced heating and protein degradation, the samples were contained in spinning NMR tubes (5 mm outside diameter, WG-5 ECONOMY, Wilmad). The 180° backscattering geometry was used for all measurements, and the laser beam was focused onto the sample using a cylindrical lens. Ferric samples were measured at room temperature. Fenchone was used to calibrate the spectrum processed by Grams. Rayleigh scattering was removed by Notch filter.

Two sets of samples having different buffer conditions were prepared: (1) 100 mM phosphate buffer pH 7.4 containing 0.1 mM DTT and 0.1 mM EDTA; (2) 10 mM phosphate buffer pH 7.4 containing 0.1 mM DTT and 0.1 mM EDTA. There were 24 samples prepared according to the buffer condition, substrates and Adx effect. All the ferric samples were measured using 406.7 nm, close to the maximum absorption, and were scanned for 60 minutes in low frequency region and 30 minutes for high frequency region.

Only two sets of samples were measured by 356.4 nm: CYP11A1 bound with CH with and without Adx in 10 mM phosphate buffer pH 7.4 containing 0.1 mM DTT and 0.1 mM EDTA. The ferric samples measured by 356.4 nm were scanned for 60 minutes. Since the electronic transition between the heme Fe and S of the proximal amino acid cysteine occurs at ~360 nm, the excitation line 356.4 nm was used to monitor the effect of Adx binding.

3.2.6.2 Resonance Raman spectra of ferrous-CO samples at room temperature

The Fe(II)-CO adducts were excited by the 441.6 nm line provided by a He-Cd laser (IK Series He Cd laser, Kimmon Koha CO., Ltd.). The rR spectra of all samples were collected using a Spex 1269 spectrometer equipped with Spec- 10 LN-cooled detector (Princeton Instruments). The slit width was set at 150 μm, and the 1200 g/mm grating was used; with this grating, the resultant spectral dispersion is 0.46 cm^{-1}/pixel.

The laser power for the ferrous CO adducts was kept at ~1 mW to minimize photodissociation. Moreover, to avoid laser-induced heating and protein degradation, the samples were contained in spinning NMR tubes (5 mm outside diameter, WG-5 ECONOMY, Wilmad). The 180° backscattering geometry was used for all measurements, and the laser beam was focused onto the sample using a cylindrical lens. Ferrous CO samples were measured at room temperature. These conditions are the same as measuring ferric samples except the power.

3.2.6.3 FTIR measurements of the ferrous-CO samples

The infrared spectra were obtained using a 4020 Galaxy Series FT-IR spectrometer, Matson Instruments. The Wilmad semi-permanent cell (IR OTTLE33) purchased from New Era, when equipped with a Teflon spacer with 0.1 mm width placed between two CaF_2 windows, requires only 60 uL of sample for each measurement. The infrared spectrophotometer was run in a single-beam mode. A spectrum was acquired with no sample cell present (i.e., air) to serve as a blank and then 6 scans of a ferric sample (each with 500 acquisitions) were collected; the same procedure was used for collection of the ferrous-CO samples. The presented data are the difference spectra between the ferrous-CO and ferric samples.

3.2.6.4 Resonance Raman spectra of the oxy samples

Multiple excitation lines, including the 356.4, 406.7 and 415.4 nm lines from a Kr^+ laser (Coherent Innova Sabre Ion Laser), as well as the 441.6 nm from the He-Cd laser, were employed to try to enhance the ν(Fe-O) and ν(O-O) modes of the oxy samples, but adequate signal to noise ratios were obtained for these modes only when using the 415.4 nm and 441.6 nm lines. The rR spectra of all samples were collected using a Spex 1269 spectrometer equipped with Spec- 10 LN-cooled detector (Princeton Instruments). The slit width was set at 150 μm, and the 1200 g/mm grating was used; with this grating, the resultant spectral dispersion is 0.46 cm^{-1}/pixel. The laser power for oxy samples was kept at ~1.0 mW minimize photodissociation. Moreover, to avoid laser-induced heating and protein degradation, the samples were contained in spinning NMR tubes (5 mm outside diameter, WG-5 ECONOMY, Wilmad). The 180° backscattering geometry was used for all measurements, and the laser beam was focused onto the sample using a cylindrical lens to form a line image. The oxy samples were measured at 77K, employing an in-house designed immersion dewar, fitted with a NMR tube sample spinning device. Spectra were calibrated with fenchone (Sigma-Aldrich, WI), and processed with Grams/32 AI software (Galactic Industries, Salem, NH). Conditions to measure oxy samples are almost the same except temperature.

3.3 Results and discussion

While the large majority of Cytochrome P450 mediated oxidations proceed through the Compound I intermediate arising from proton-assisted O-O bond cleavage of the precursor ferric peroxo- species, any conditions which effectively restrict protonation of the latter can facilitate its attack on susceptible bound substrates.[16,18,139,140] Indeed, rR evidence has been recently obtained for H-bonded proximal oxygen of the (Fe-O_p-O) fragment, which supports this mechanism in the case of the C-C bond cleavage reaction that occurs for 17-hydroxy-pregnenolone (17-OH PREG) processing by CYP17A1;[34]on the other hand, the rR confirmation of a H-bond interaction with the terminal oxygen of the Fe-O-O_t fragment disfavors such a mechanism for the C-C bond cleavage/aromatization process that occurs for CYP19 production of estrone and suggests the mediation of the Compound I species,[44] a conclusion which is in essential agreement with very recent kinetic studies by Sligar and coworkers.[141] Given that rR spectroscopy provides an effective probe of these functionally important H-bonding interaction with the Fe-O-O fragments of dioxy intermediate, it has herein been used to probe the dioxygen complexes obtained for CYP11A1 bound with each of its three natural substrates, CH, 22R-OHCH and 20R,22R-DiOHCH. Before proceeding to a discussion of the results obtained for the dioxygen adducts, rR studies undertaken to further define active site structural differences that exist for the ferric and ferrous CO-bound forms with each of these three substrates present and upon interaction with Adx are presented, these additional studies helping to clarify certain nebulous or incomplete results reported in previous studies and more clearly defining the effects of substrate and reductase binding

on the heme structure and its interactions with active site structural elements, including the critical Fe-S linkage between the heme and proximal heme pocket.

3.3.1 UV of purified CYP11A1 and its CO forms

The CYP11A1 was purified from adrenal glands. The procedure was described in section 3.2.1, pooling the fractions with absorption A_{394}/A_{280} larger than 0.7. The electronic absorption spectrum of purified CH-bound CYP11A1 and its complex with Adx are shown in Figure 3.3.1. The red line is for CYP11A1 bound with CH complex which shows two bands at 394 nm and 413 nm. This indicates that this complex is only partially high spin (band at 394 nm), with the low spin shown at 413 nm. After addition of Adx, the band at 413 nm disappeared and gave a relatively wider band at 394 nm which indicated the increasing of high spin population compared without Adx complex.

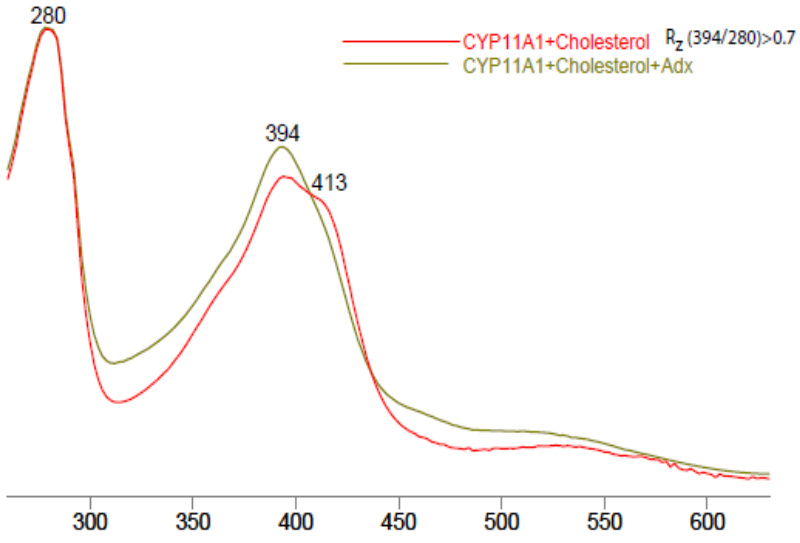

Figure 3.3.1 UV spectrum of purified cholesterol bound CYP11A1 with and without Adx.

In order to estimate the amount of P420 in this purified CYP11A1, the sample was reduced by adding $Na_2S_2O_4$ and bubbling CO in the solution. The results are shown in Figure 3.3.2. As can be seen, the intensity of 420 nm band is smaller when compared with 450 nm band. This indicated that there was some amount P420 generated during the purification process. However, it is emphasized that for most rR measurements, the contributions of P420 the the spectra is minimized by using excitation lines in resonance with the P450 (e.g., 442 nm).

The concentration of CYP11A1 was measured by UV-Vis absorption spectroscopy on ferrous-CO spectra using reduced form as reference. The difference between the absorbance measured at 450 nm and 490 nm of the absorption spectra was used to calculate the concentration, based on the reported differential extinction coefficient 91 cm^{-1} mM^{-1}. [64]

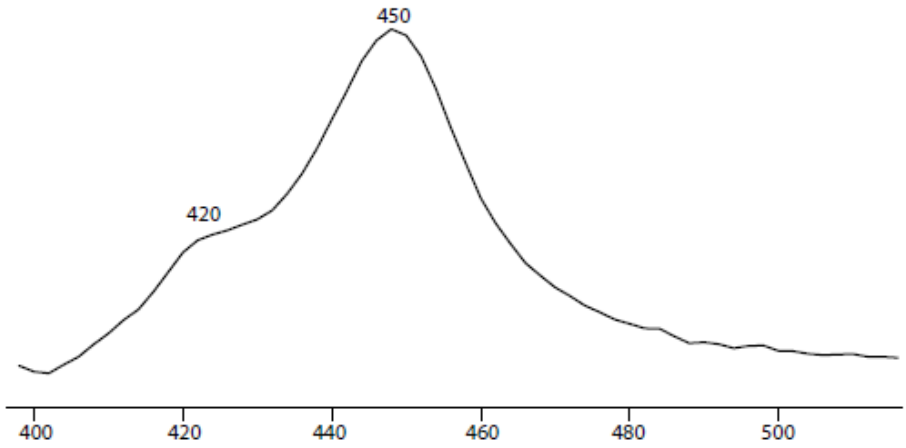

Figure 3.3.2 UV spectra of ferrous-CO CYP11A1 bound with cholesterol

3.3.2 Electronic absorption spectra of CYP11A1 bound with 22R-OHCH and 20R, 22R-DiOHCH and their Adx effect

CYP11A1 purified from Adrenal glands are naturally bound with CH, which showed the high population of high spin. Because the binding affinity of 22R-OHCH and 20R, 22R-DiOHCH with CYP11A1 are four times higher than CH with CYP11A1,[142] the addition of other substrates can be made by incubating the substrate with naturally CH bound CYP11A1. The detailed procedure was described in previous section.

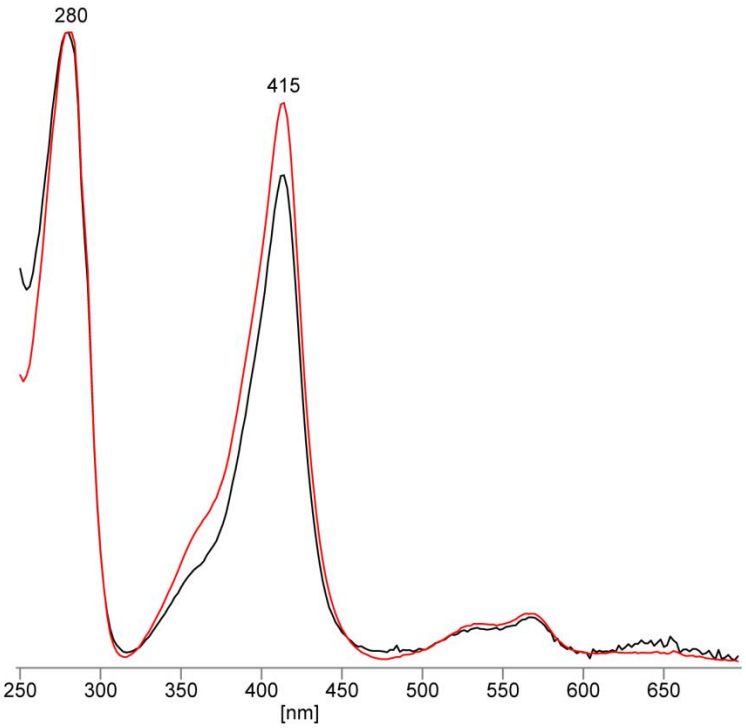

Figure 3.3.3 UV spectra of CYP11A1 + 22R-OHCH (red) and CYP11A1 + 22R-OHCH +Adx (Black)

The electronic absorption spectra of CYP11A1 bound with 22R-OHCH with and without Adx are shown in Figure 3.3.3. As can be seen, 22R-OHCH gave almost 100% of low spin with and without Adx. This finding means the exchange was successful and sufficient. The addition of Adx sample has lower intensity at 415 nm which indicates that the addition of Adx will affect the CYP11A1 complex even for this low spin substrate. This finding is confirmed by our resonance Raman data in section 3.3.4.

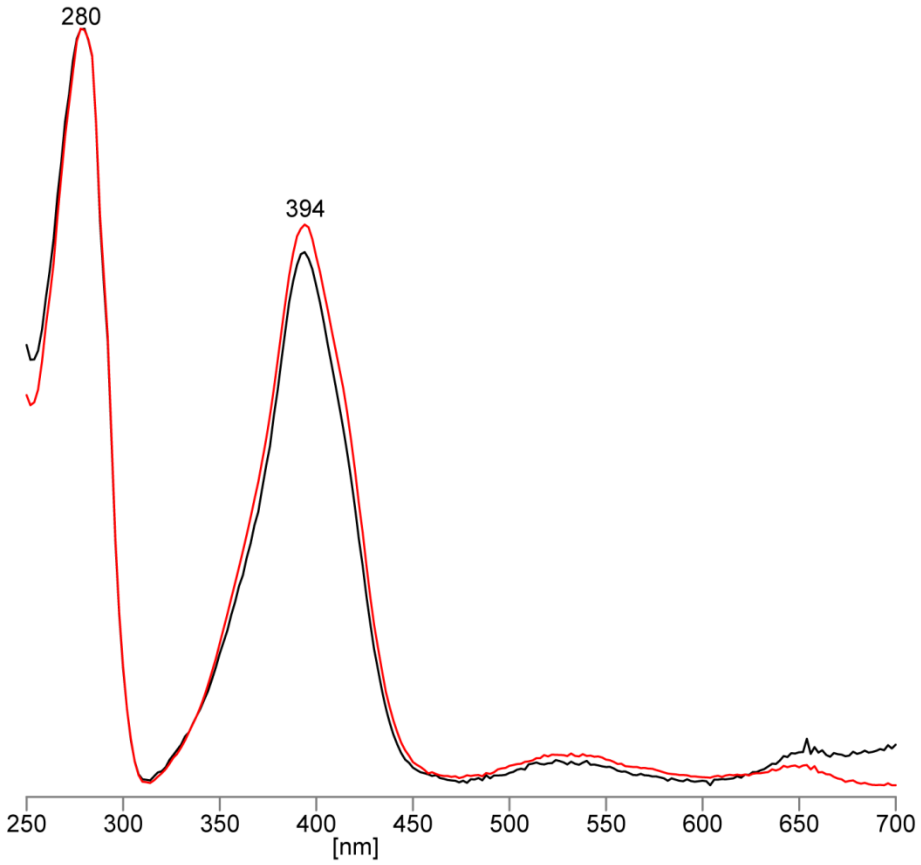

Figure 3.3.4 UV spectra of CYP11A1 + 20R, 22R-OHCH (red) and CYP11A1 + 20R, 22R-OHCH +Adx (black)

The electronic absorption spectra of CYP11A1 bound with 20R, 22R-OHCH with and without Adx are shown in Figure 3.3.4. As can be seen, 20R, 22R-OHCH gave 100% of high spin, showing only one band at 394 nm. This finding means the exchange was successful and sufficient compared with the electronic absorption spectrum of the original protein, CYP11A1 + CH complex. After addition of Adx, the intensity of 394 nm band is a little lower and narrower than the one without Adx. Situation here is complicated to judge which has more high spin population because both the increase intensity of 394 nm and narrower band width indicate the increasing of high spin population. Additional information about the spin population will be provided by resonance Raman in section 3.3.4.

3.3.3 Electronic absorption of purified Adx

The Adx was purified from the adrenal glands along with CYP11A1. The detailed procedure was described in section 3.2.2. The fractions with absorption ratio of A_{414}/A_{280} larger than 0.7 were pooled as pure samples. The electronic absorption spectrum of pure Adx is shown in Figure 3.3.5. The concentration of Adx is calculated based on the extinction coefficient 11 cm^{-1} mM^{-1} at 414 nm.

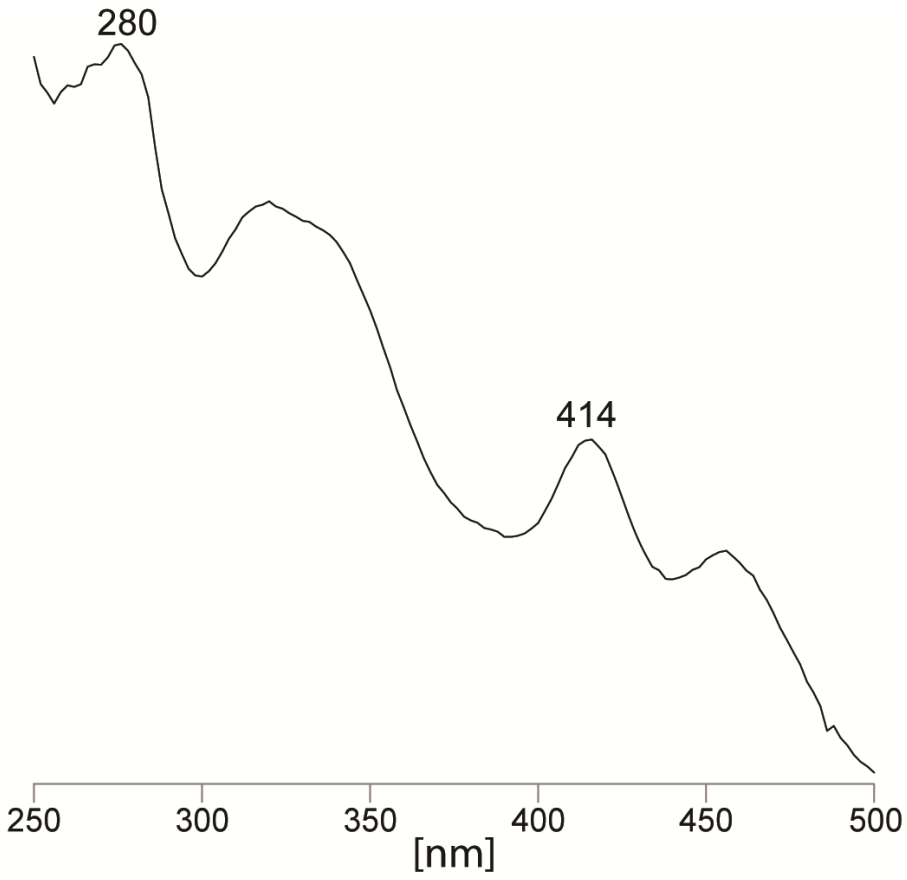

Figure 3.3.5 UV spectrum of purified Adx from bovine adrenal glands

3.3.4 Resonance Raman of ferric samples

Early rR studies of this enzyme were reported mainly by Tsubaki et al., for the ferric and ferrous CO states, providing valuable insight.[103,143,105] However, the interpretations of some of these data were hampered by the presence of strong glycerol bands that overlap with some heme rR modes, especially in the low frequency region. Another troubling issue occurred with the ferrous CO adducts, where it was reported that the rR spectrum of the 22R-OHCH bound sample contained only one ν(Fe-C) stretching frequency, while the IR data clearly revealed the presence of *two* ν(C-O) stretching modes, the most reasonable explanation of this unexpected behavior being unintentional photodissociation during the Raman experiment. In this work attempts are made to clarify the interpretation of the vibrational spectra of the ferric and ferrous CO adducts for all three physiologically important substrates and to further evaluate the effect of Adx binding to the CYP11A1 adducts.

Compared with previous data, the data presented below was acquired from samples prepared in aqueous condition without glycerol, ethylene glycol or detergent, all of which were contained in previous work and complicated the interpretation by the presence of the additives' Raman bands in both the low frequency and high frequency regions; e.g., a high intensity and wide glycerol band appearing at ~1467 cm^{-1} interferes with the ν_3 HS at around 1484 cm^{-1}, [103,143,105] an overlap that directly leads to the wrong interpretation of the spin population.

Now turning attention to the newly acquired data, the rR spectra of ferric CYP11A1 samples with CH, 22R-OHCH and 20R, 22R-DiOHCH substrates in high and

low frequency regions, as well as in the presence of the natural redox partner, adrenodoxin (Adx), are shown in Figure 3.3.6. The high frequency spectra were normalized to the ν_4 mode at 1370 cm^{-1} and the low frequency region was normalized to the ν_7 mode at around 674 cm^{-1} ; neither of these strong modes are included in these traces so as to allow a clearer presentation of the lower intensity structure-sensitive heme modes. The assignments of the modes were done according to the previous published data on cytochromes P450s and model compounds of Ni-octaethylporphyrin.[71,112]

High frequency region: The spectra of cholesterol (CH) bound samples (Figure 3.3.6 A, right panel) show components associated with both the high (HS) and low spin (LS) states. The population of high spin state is larger than the LS as seen by higher intensity of the high spin markers ν_3 at 1484 cm^{-1}, ν_2 at 1567 cm^{-1} and ν_{10} at around 1621 cm^{-1} as compared to the corresponding low spin makers, which are seen at 1500 cm^{-1}, 1581 cm^{-1} and 1637 cm^{-1}, respectively. It is noted that the HS ν_{10} mode overlaps with the vinyl stretching modes that are seen more clearly in the spectrum of LS.[58] Binding of 22R-OHCH induces almost complete low spin state conversion as seen by the presence of the dominant LS state markers ν_3 at 1500 cm^{-1}, ν_2 ~1582 cm^{-1}, and ν_{10} at 1637 cm^{-1}. The absence of the HS ν_{10} mode (1637 cm^{-1}) reveals existence of two vinyl stretching modes at 1618 and 1627 cm^{-1}, the lower frequency one being usually associated with the in-plane conformation of a vinyl group, with the higher frequency one being associated with the out-of-plane conformation. The fact that the 22R-OHCH substrate does not induce high spin conversion is not surprising, given the fact that the crystal structure of CYP11A1 with this substrate shows that there is a large amount of electron density between the O atom of the hydroxyl group attached to the 22 carbon of the substrate and

the heme Fe, with the distance between O and Fe being only 2.56 A, indicative of a covalent bond between heme iron and substrate; i.e., the presence of six coordinated, low spin state, in agreement with observed here rR data.[39,40] On the other hand, binding of 20R,22R-DiOHCH induces a mixture of spin states similar to, but slightly larger, than that seen for CH-bound sample (Figure 3.3.6 E). The stated spin state populations for all three enzyme/substrate complexes were calculated using previously published HS/LS cross section ratios for cytochromes P450.[113] Here it was found that the sample isolated with CH bound is 63 % HS, the sample prepared with 22R-OHCH is only 8 % HS and sample prepared with 20R,22R-DiOHCH is 76 % HS. The detail information will be addressed later.

Low frequency region: The low frequency spectrum of CH-bound sample (Figure 3.3.6 A, left panel) shows the presence of the propionate bending mode at 379 cm^{-1} and vinyl bending mode at 420 cm^{-1}. Addition of 22R-OHCH substrate to CYP11A1 causes activation of an additional propionate bending mode at 363 cm^{-1}, a frequency which is generally interpreted to signal the presence of a propionate group now experiencing a weaker H-bonding interaction with active site fragments (i.e., amino acid residues, water or possibly substrate fragments). Moreover, a small band appearing at 396 cm^{-1} was also enhanced and can be reasonably associated with weak activation of an in-plane vinyl bending mode. The presence of two vinyl bending modes associated with in-plane (396 cm^{-1}) and out-of-plane (420 cm^{-1}) vinyl group conformations in the low frequency region of the rR spectrum of the 22R-OHCH-bound sample is consistent with the presence of two vinyl *stretching* modes in the high frequency region assigned to the in-plane and out-of-plane orientations of vinyl groups, as was discussed above (Figure 3.3.6 C). The

binding of the third substrate (Figure 3.3.6 E, left panel) shows a spectral pattern quite similar to the CH-bound samples.

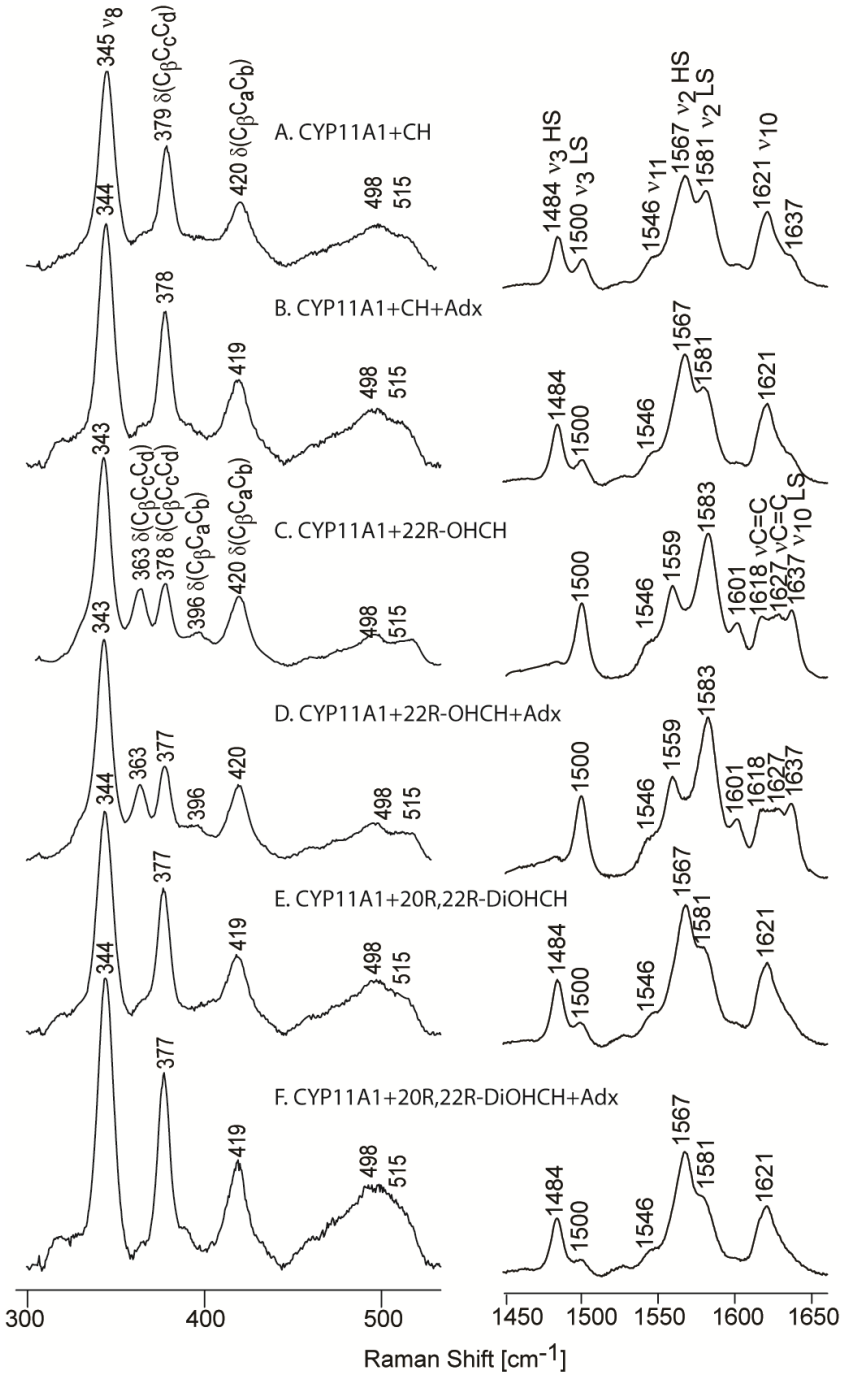

Figure 3.3.6 Ferric form for different substrates in buffer 100 mM phosphate buffer pH=7.4, 0.1 mM DTT and 0.1 mM EDTA. Excitation line 406 nm, acquisition time 60 mins for low frequency and 30 mins for high frequency at room temperature.

CYP11A1 bound with 22R-OHCH: CYP11A1 bound with substrate 22R-OHCH shows low spin population which is similar with type II inhibitor binding. The distance of Fe and the oxygen in C22 carbon is 2.6 A which is a very weak interaction and long bond distance compared with the bond length of covalent Fe-O that is 1.8 A and the distance for type II inhibitor of Fe-N is 2.2 A.[39] Also the redox potential of CYP11A1 bound with 22R-OHCH is similar with that bound with CH and 20R, 22R-DiOHCH. The former on is -285 mV and later two are -282 mV and -270 mV.[107]

Different ionic strength affect to spin population: When lower the ionic strength to 10 mM phosphate buffer pH 7.4, 0.1 mM EDTA and 0.1 mM DTT. Data are not shown because they are very similar with the listed ones. By using the cross section number found in section 2 which is I_{HS}/I_{LS}=1.25, I calculated the spin population in high spin percentage are listed in table 3.3.1. From the table, it is easy to see that after addition of Adx, the high spin population has increased for all three substrates and in both buffer conditions. Compared with the results in two buffers, the Adx brought more high spin population changes in the low ionic strength buffer because the high ionic strength buffet tends to push more substrates into the active site. Because of this finding, the strength of Fe-S linkage was measured in low ionic strength buffer.

Table 3.3.1 High spin population in percentage of HS effect of CYP11A1 with different substrates, w/o Adx and ionic strength

		resonance Raman (%HS)	
CYP11A1+substrate	Adx	100 mM[a]	10 mM[b]
CH	-	63	58
	+	73	73
22R-OHCH	-	8	7
	+	13	6
20R,22R-DiOHCH	-	76	72
	+	82	85

Note: a) 100 mM phosphate buffer containing 0.1 mM EDTA and 0.1 mM DTT; b) 10 mM phosphate buffer containing 0.1 mM EDTA and 0.1 mM DTT.

The iron-sulfur linkage: Obviously, the nature of the linkage between the heme prosthetic group and a given associated protein is quite important for dictating the reactivity patterns of the enzyme. [144–146] Indeed, the Fe-S linkage of cytochromes P450 and some related enzymes plays a key role in enabling these enzymes to mediate such remarkable chemical transformations under normal physiological conditions.[2,2] Fortunately, it has been well established that rR spectroscopy, when employing a near UV excitation wavelength (e.g., near 350-360 nm), is one of the most effective probes of the status of this key Fe-S fragment, providing an easily identifiable ν(Fe-S) band in the low frequency rR spectrum.[35] Specifically, the behavior of this mode can be documented to evaluate the linkage between the heme Fe and the endogenous cysteine thiolate ligand, the strength of which can be modulated by structural alterations within the proximal heme pocket, the most effective perturbations arising by interaction with natural reductases, such as Adx, that typically bind to the proximal side of the active site.

While several studies have consistently shown that the precise structure of substrates, all of which bind within the distal pocket of cytochromes P450, have little or no effect on the Fe-S linkage, [129,130,147,148] it is anticipated that interactions with reductases can impact the status of the Fe-S linkage. Results from the present work are shown in Figure 3.3.7, where the ν(Fe-S) is observed at 347 cm^{-1} for CYP11A1 bound with CH, with no detectable change being seen upon binding Adx. This is an unexpected result inasmuch as significant effects on the ν(Fe-S) mode are commonly seen for these types of interactions; i.e., binding of putidaredox to P450cam caused a strengthening of Fe-S, as witnessed by an up shift of ν(Fe-S) by ~3 cm^{-1}.[148] In addition, a differential effect on the Fe-S bond was seen in CYP2B4 interactions with Cyt b5 vs CPR. [129]

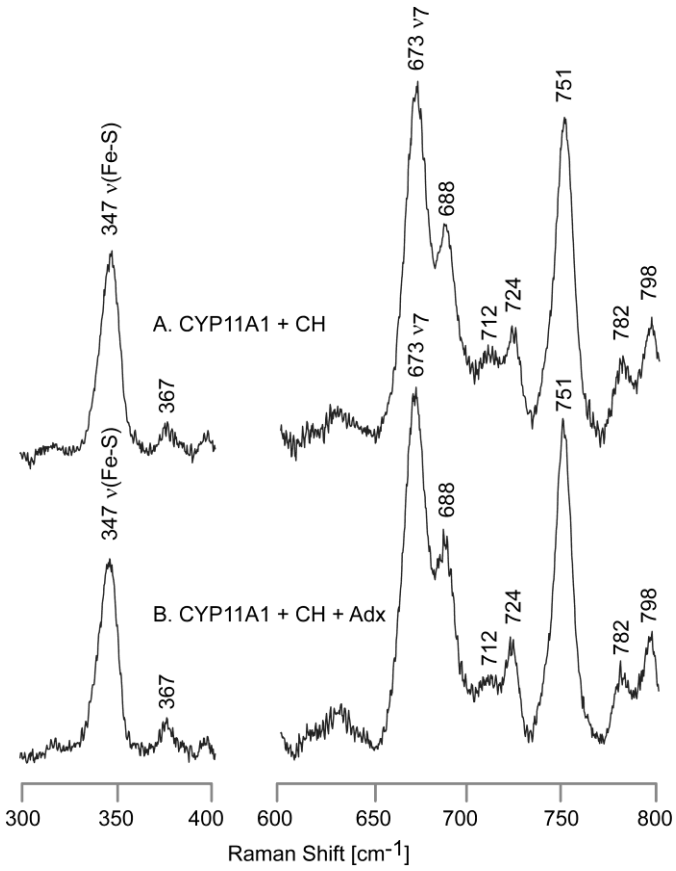

Figure 3.3.7 Low frequency RR spectra of ferric cholesterol bound CYP11A1 w/o Adx in buffer 10 mM phosphate buffer pH 7.4, 0.1 mM DTT and 0.1 EDTA. Excitation line 356.4 nm, acquisition time 60 mins at room temperature.

3.3.5 Ferrous-CO samples measured by resonance Raman and FTIR

Resonance Raman spectroscopic interrogation of the ferrous CO adducts of heme proteins has now long been established as an effective probe of proximal- and especially distal-pocket active site structure, with the internal modes of the Fe-C-O fragment reporting on th strength of the Fe-L linkage with the trans-axial proximal ligand and simultaneously reflecting steric and polar interactions with distal pocket residues, including those presented by enzyme-bound substrate,[63,72,114,129,147,149–153] the latter interaction being crucially important for cytochromes P450, such as the CYP11A1 being studied here. Basically, increases in the degree of $d\pi$(Fe) to CO(π^*) back-bonding in the Fe-C-O fragment, arising from weakening of the Fe-L bond or increases in positive polarity of the distal pocket environment, strengthen the Fe-C bond while simultaneously weakening the C-O bond, resulting in a negative correlation between the ν(Fe-C) and ν(C-O) vibrational modes.[72,149–151] In order to provide a more thorough characterization of the structural factors involved in CYP11A1 function, such studies have been conducted in this work, with a secondary purpose being to try to clarify somewhat confusing observations made in previous rR studies of this protein.[103] The rR spectra acquired for the low frequency region are shown in Figure 3.3.8.

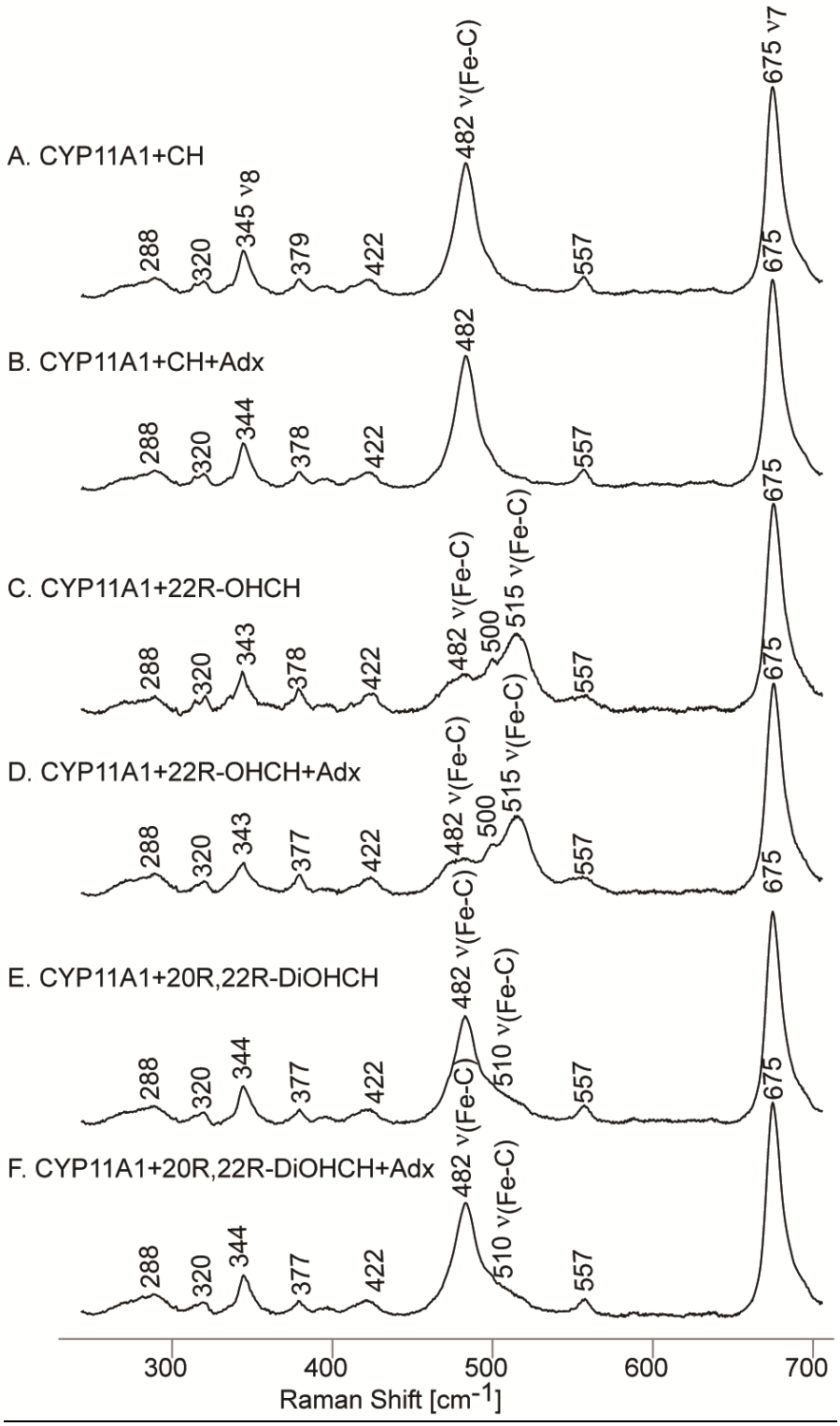

Figure 3.3.8 Low frequency RR spectra for CO adducts CYP11A1 with different substrates in 100 mM phosphate buffer pH 7.4, 0.1 mM DTT and 0.1 EDTA. Excitation line 442.4 nm, acquisition time 60 mins at room temperature.

The most obvious finding that is noted upon initial inspection of the data is that there are no observable effects of Adx binding upon the status of the Fe-C-O fragment. In similar studies reported earlier by other workers,[103]the changes for Adx binding were reported to be quite small (between 0 -1.5 cm^{-1}). However, the apparent existence of these small effects, along with the presence of some confusing results of those spectral studies, prompted us to reexamine this issue. For example, in those earlier studies it was reported that in some cases, including the sample containing the 22R-OHCH, while *two* ν(C-O) modes could be observed by FTIR, only a single ν(Fe-C) could be observed (by rR); as will be seen below, these confusing results can be readily explained by the presence of unintended photodissociation for the ferrous CO adducts by the rR laser excitation beam.

Now, returning to consider the effects of different substrates on the Fe-C-O fragment, the sample bound with cholesterol, a substrate that presents no hydrophilic R-OH fragments to the bound CO ligand, shows a clear and relatively sharp ν(Fe-C) mode appearing at 482 cm^{-1}, a value in good agreement with the previous work,[103] and the corresponding ν(C-O) being observed in the FTIR spectrum at 1952 cm^{-1}, again a value in reasonably good agreement with that reported earlier (i.e., 1954 cm^{-1}).[103] In contrast, to the relatively simple spectral signature displayed for the CO adduct of the CH-bound enzyme, the CO adduct formed for the enzyme bound with the more polar substrate, 22R-OHCH, whose C22-OH fragment is apparently close enough to the iron binding site to have induced a LS spin state by direct interaction with the heme iron, as evidenced in the rR data for the ferric state, gave *three* observed features appearing in the region where the

ν(Fe-C) modes are expected to appear: i.e., at 482 cm^{-1}, 500 cm^{-1} and 515 cm^{-1}. In order to clarify the interpretation of the spectra acquired for the 22R-OHCH substrate, the Fe(II)-$^{12}C^{16}O$ and Fe(II)-$^{13}C^{16}O$ samples were made and measured, the results being shown in Figure 3.3.9. From these results, it is clear that both 481cm^{-1} and 515 cm^{-1} bands seen in trace A, shifted down by 5 cm^{-1} in the spectra of $^{13}C^{16}O$ isotope, confirming their assignments to ν(Fe-C) modes. On the other hand, the feature observed at 500 cm^{-1} does not shift upon $^{12}C/^{13}C$ substitution, securing its assignment to a heme mode. The assignment of the 481cm^{-1} and 515 cm^{-1} bands to two different Fe-C-O conformers is supported by observation two high frequency ν(C-O) modes at 1952 cm^{-1} and 1934 cm^{-1} in the FTIR, as shown in Figure 3.3.10. In previous research,[103] the appearance of only one band in low frequency was reported for this complex, an observation which may be due to accidental photo dissociation perhaps owing to either high laser power (~5 mW) or ineffective spinning during the measurement. Indeed, results of experiments to verifying photosensitivity for this complex are shown in the bottom two traces of Figure 3.3.9, where it is seen there is a strong and wide heme mode overlapped with the ν(Fe-C) modes. From previously published data, it was reported that only one ν(Fe-C) mode could be detected (at 479 cm^{-1}) for the 22R-OHCH bound CYP11A1 complex; actually this could have arisen from a heme mode see at 479 cm^{-1} in the photo-disassociated sample we generated in the present work (Figure 3.3.9 traces C and D).

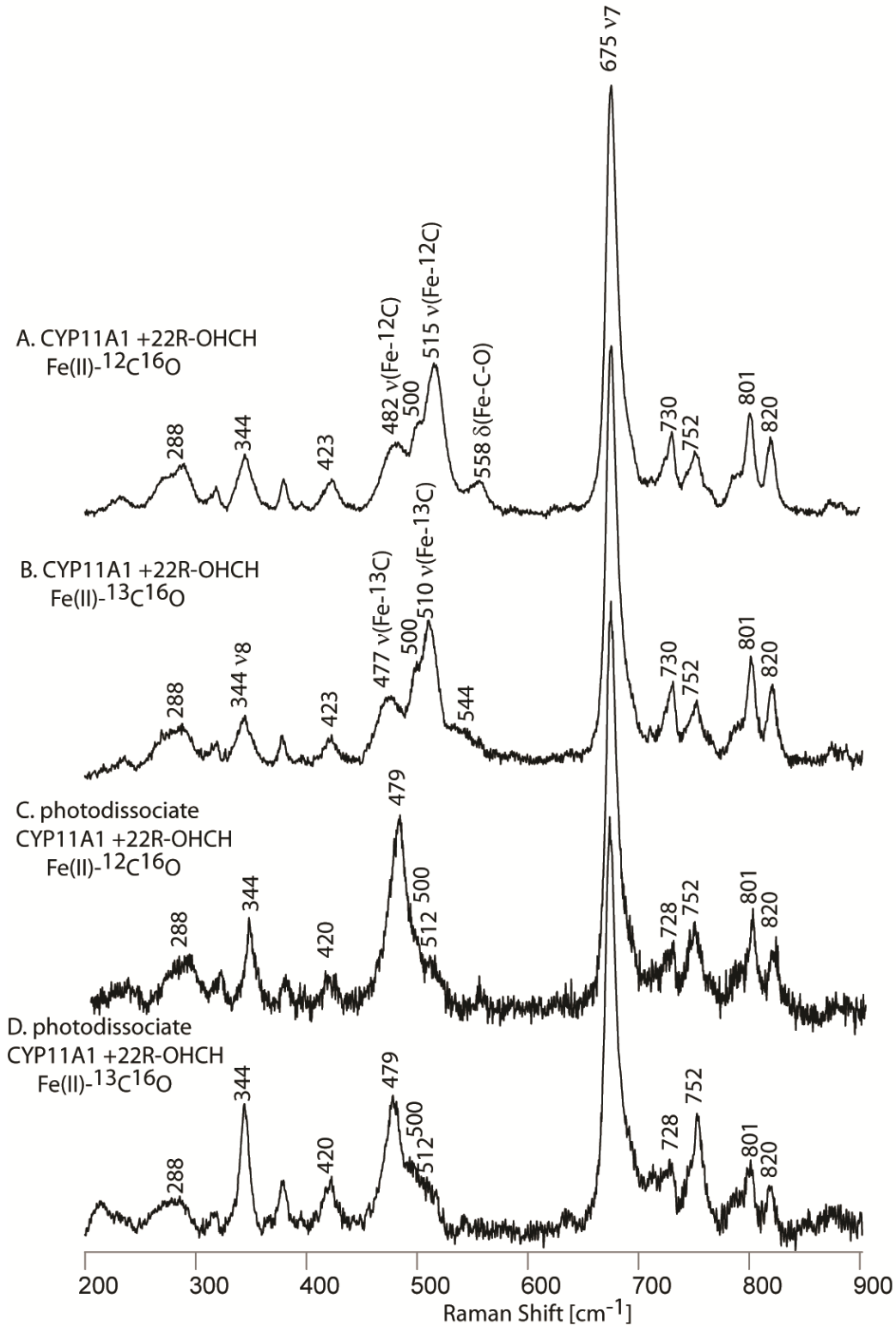

Figure 3.3.9. Isotope effect for 22R-OHCH CO adducts in buffer 100 mM phosphate buffer pH 7.4, 0.1 mM DTT and 0.1 EDTA. Excitation line 442.4 nm, acquisition time 60 mins at room temperature.

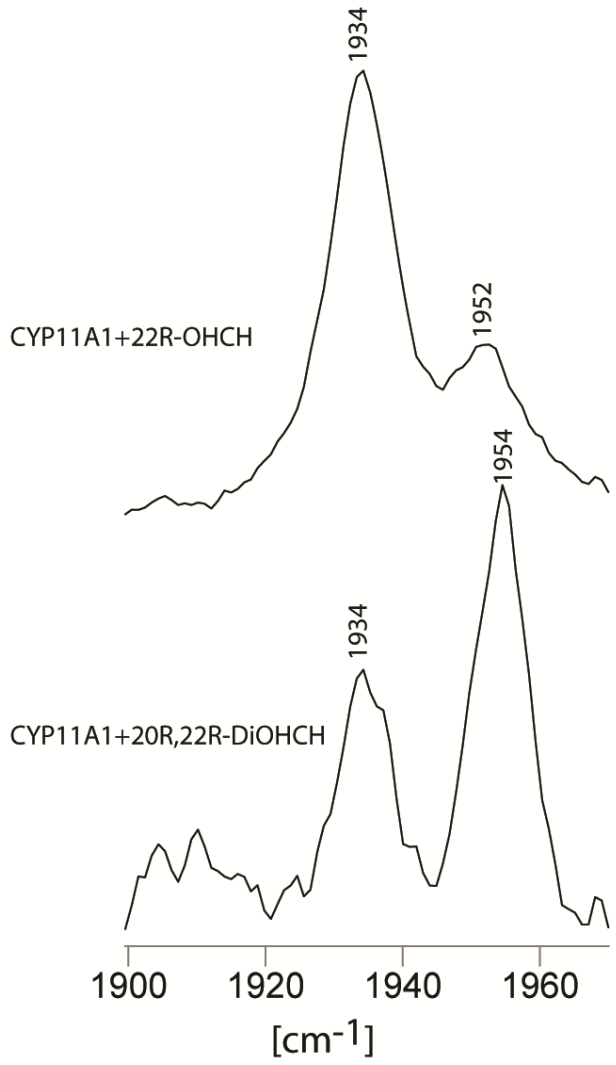

Figure 3.3.10 FTIR results for high frequency CYP11A1 with substrate 22R-OHCH and 20R, 22R-DiOHCH ferrous CO forms in 100 mM phosphate buffer pH 7.4, 0.1 mM DTT and 0.1 EDTA.

Given these clarified spectral traces for the 22R-OHCH-bound ferrous CO adduct, the most reasonable conclusion for this species is that this directed C-O-H group interacts with the Fe-C-O fragment to produce two different Fe-C-O conformers. Furthermore, it is also quite reasonable to conclude that the appearance of two ν(Fe-C) and two ν(C-O) modes for the 20R,22R-DiOHCH-bound substrate is also attributable to interactions of one or both C-OH groups with the Fe-C-O fragment; indeed, the two pairs of ν(Fe-C)/ν(C-O) frequencies are quite similar for both complexes. From this collective data set for the three substrates, it seems likely that (for the 2nd and 3rd substrates) the presence of one C-OH group positioned quite near the Fe-C-O fragment leads to two Fe-C-O conformers, one with a disposition similar to that of the "unperturbed" Fe-C-O conformer of the CH-bound enzyme and the other reflecting a reasonably strong H-bonding interaction with the C-OH group present on the substrate.

For all the data described in this section is summarized in Table 3.3.2. Because there are no so many data presented here, it is hard to get a linear inverse correlation between ν(Fe-C) and ν(C-O) but as can be seen from the table, there is a inverse correlationship for a specific substrate complex. The results were clarified compared with previous published data. As to evaluate the efficiency of exchange the substrates by incubate 22R-OHCH and 20R, 22R-DiOHCH, from the ν(Fe-C) and ν(C-O) data, we see the exchange is successful because the totally different pattern.

Table 3.3.2 Summary of ferrous- CO CYP11A1 complex with different substrates with and without Adx

		Raman shift (cm^{-1})	
CYP11A1+substrate	Adx	ν(Fe-C)	ν (C-O)
CH	-	482	1952
	+	482	1952
22R-OHCH	-	482	1952
		515	1934
	+	482	nd
		515	nd
20R,22R-DiOHCH	-	482	1954
		510	1934
	+	482	nd
		510	nd

3.3.6 Resonance Raman of oxy samples

As was discussed above, recent rR studies of the oxy intermediates of CYP17 and CYP19, [34,44] along with analogous studies of NOS,[16,18,137,140,154] have shown that this technique is effective in detecting subtle structural differences in H-bond interactions with the Fe-O-O fragment. Specifically, H-bond donation to the proximal oxygen (O_p) of the Fe-O_p-O_t fragment, which apparently persists upon reduction to the peroxo intermediate, stabilizing it for attack on susceptible substrates, exhibits a *relatively low* ν(Fe-O) mode. On the other hand, H-bonding to the terminal oxygen (O_t) of the Fe-O_p-O_t fragment, which exhibits relatively high ν(Fe-O) frequency, promotes formation of the hydroperoxo intermediate, ultimately leading to O-O bond cleavage and Compound I formation, an intermediate that effectively mediates the more typical hydroxylation reactions. Clearly, the rR technique is an important tool to document these structural variations that, though so subtle, carry profound functional consequences.[124] Given that ambiguity persists regarding details of the C-C bond cleavage process for 20R,22R-DiOHCH substrate efforts are made here, for the first time, to acquire rR spectra of these dioxygen adducts with all three natural substrates, seeking to detect any telltale differences in the RR spectra that might reveal H-bonding differences for the three cases. In order to study these relatively unstable oxy-intermediates encountered within the catalytic cycles for these three natural substrates of CYP11A1 special procedures were required, as summarized earlier in Methods and Materials. Inasmuch as no differential effects of the three substrates on the proximal Fe-S linkage were seen in the studies of the ν(Fe-S) modes (vide supra), all effects observed here are presumed to arise from *distal* side structural perturbations.

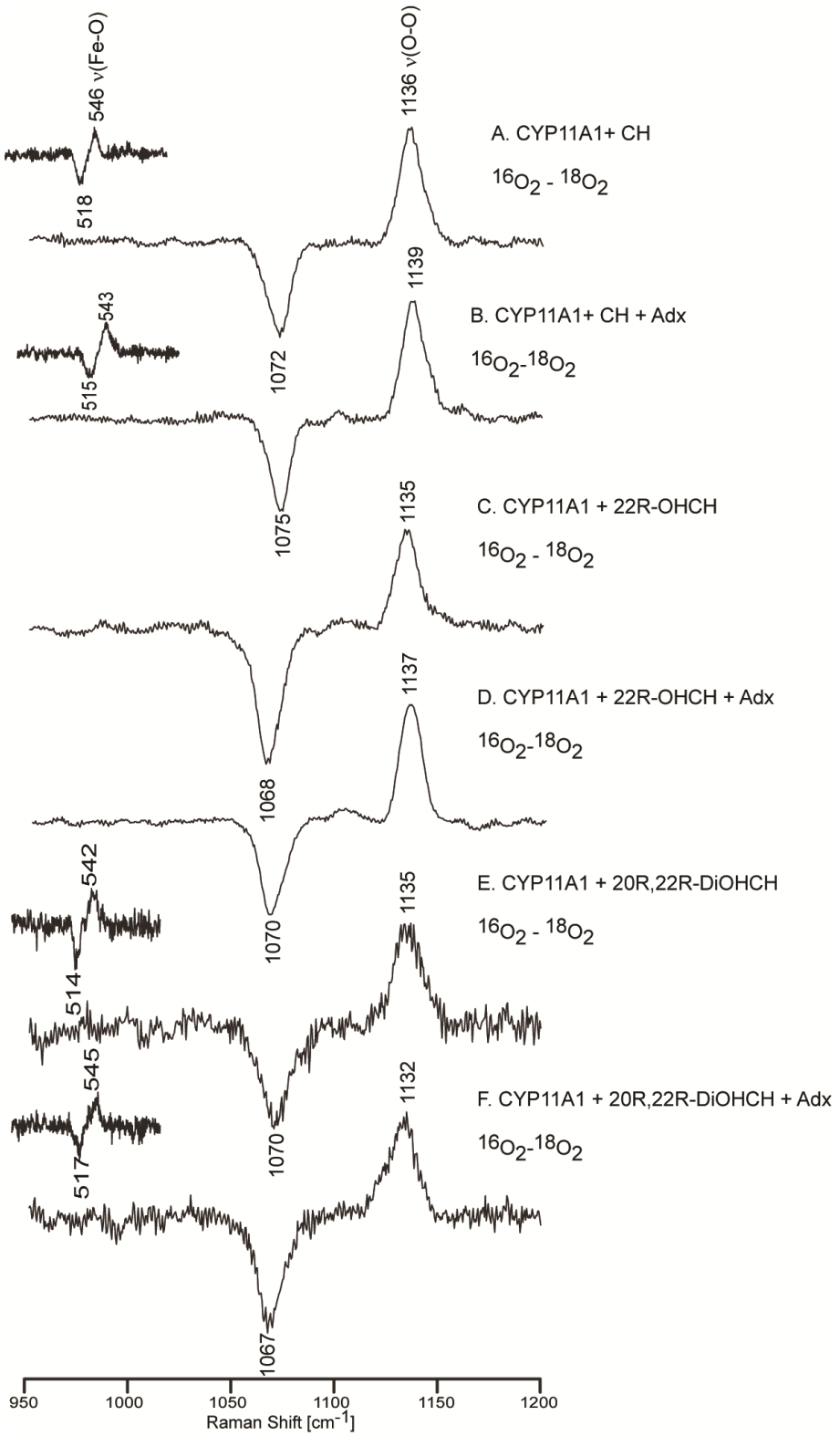

Figure 3.3.11 Oxy samples for all the substrate w/o Adx in 100 mM phosphate buffer containing 0.1 mM EDTA and 0.1 mM DTT. The insets above the ν(O-O) difference spectra show the difference $^{16}O_2$-$^{18}O_2$ for ν(Fe-O) modes.

Cholesterol bound oxy-CYP11A1: The 415.4 nm line from a Krypton ion laser, which in in resonance with the Soret transition of the CH-bound CYP11A1, was used to measure this complex. It is noted that, owing to relatively low S/N attainable for these frozen oxy- CYP samples, definitive identification of the key internal modes of the Fe-O-O fragments are only accessible via generation of the $^{16}O_2/^{18}O_2$ difference traces, which are shown in Figure 3.3.11. The ν(Fe-O) are seen in low frequency region shown in traces (A) and (B) (insets) for oxy-CYP11A1 with and without Adx. The ν(O-O) were seen in high frequency region, shown in traces (A) and (B) for samples with and without Adx, respectively.

In the low frequency spectra, the ν(Fe-^{16}O) is assigned at 546 cm^{-1} and the ν(Fe-^{18}O) at 518 cm^{-1} for the cholesterol-bound form, a shift of 28 cm^{-1} (calculated 25 cm^{-1}) As was outlined above in the first paragraphs of this section, this set of values for ν(Fe-O) and ν(O-O) is quite similar to that obtained for camphor-bound CYP101 and for oxyCYP17 and oxyCYP19 with those substrates that are known to converted via Compound I processing, the conclusion emerging form this being that conversion of CH to 22-OHCH also proceeds through a Compound I intermediate. This finding has long been generally been accepted, with recent EPR results providing strongly supporting data for the involvement of Compound I in this first step.[51] Significantly, the sample prepared including the Adx exhibits a ν(Fe-^{16}O) at 543 cm^{-1} and a corresponding ν(Fe-^{18}O) at 515 cm^{-1}, this ~3 cm^{-1} down shift upon addition of Adx reflecting a slight weakening of the Fe-O bond when Adx is present. On the other hand, the ν(^{16}O-^{16}O) (at 1136 cm^{-1}) and ν(^{18}O-^{18}O) (at 1072 cm^{-1}) modes shift *up* to 1139 cm^{-1} and 1075 cm^{-1}

upon addition of Adx, the combined results suggestion that the interaction with Adx might slightly lower the tendency for the O-O bond cleavage process.

22R-OHCH-bound oxyCYP11A1: Figure 3.3.11 shows the difference spectra for this species, both in the absence and presence of Adx. The high frequency region (right panel, traces C and D) shows the same pattern as was observed for the cholesterol-bound sample, exhibiting the $\nu(^{16}O\text{-}^{16}O)$ at 1135 cm^{-1}, with the $\nu(^{18}O\text{-}^{18}O)$ being observed at 1068 cm^{-1}. Also like the CH-bound sample, upon Adx binding, the $\nu(^{16}O\text{-}^{16}O)$ shifts up to 1137 cm^{-1}, with the corresponding $\nu(^{18}O\text{-}^{18}O)$ appearing at 1070 cm^{-1}, yielding only a slighter larger isotopic shift. Obviously, a key issue of interest is determining the status of the Fe-O bond for the enzyme bound with this 22R-OHCH substrate. Unfortunately, though numerous attempts to observe the telltale ν(Fe-O) mode were made, employing multiple excitation lines, including the 441.6 nm line from a He:Cd laser, no evidence was obtained for its enhancement. These efforts are summarized in the Supporting Information, along with a discussion of structural and electronic factors that can affect the degree of resonance enhancement of the internal modes of these Fe-O-O fragments. In the absence of observable ν(Fe-O) modes, it is not possible to draw conclusions about the status of the Fe-O-O fragment with regards to its disposition towards O-O bond cleavage vs the hydroxylation pathways, but the well-documented generation of the 20R,22R-DiOHCH product is entirely consistent with the proposal that a Compound I intermediate is involved.

20R, 22R-DiOHCH bound oxy-CYP11A1: Figure 3.3.11 also shows the difference spectra obtained for the oxy complexes of the 20R, 22R-DiOHCH-bound CYP11A1 complex with Adx and without Adx. The difference pattern for the spectral region

containing the ν(O-O) modes were measured by Soret excitation (415.4 nm), as was done for the previous substrates; however, using this line for this complex, no clear difference pattern for ν(Fe-O) could be observed in the low frequency region. The same efforts were employed as were used to try to enhance the ν(Fe-O) modes of the 22R-OHCH sample. Though no success was realized using available excitation lines from the krypton laser, the ν(Fe-O) mode was effectively enhanced by using the 441.6 nm excitation line from the He:Cd laser. The data acquired for the enzyme bound with the 3rd substrate, 20R,22R-DiOHCH, the ν(Fe-^{16}O) stretch at 542 cm^{-1} and the ν(^{16}O-^{16}O) at 1135 cm^{-1}. Interestingly, the effect of Adx binding on this species is opposite to its effect on the enzyme bound with the first two substrates; i.e., Adx binding to the samples containing the first two substrates increases the strength of the O-O bond, simultaneously decreasing the strength of the Fe-O bond, while the effect of Adx binding on the sample containing 20R,22R-DiOHCH is to increase the strength of the Fe-O bond and decrease the strength of the O-O bond. As can be seen from the CYP11A1+CH oxy complex, the frequencies here for ν(Fe-O) and ν(O-O) are very similar with oxy CYP11A1+CH and P450cam complexes with hydrogen bonding at terminal oxygen. This leads to the conclusion that the bond cleavage step proceeds through Compound I intermediate. With addition of Adx, the ν(Fe-O) increases[124,133,155] indicating the increase of back bonding between Fe-O and strength the Fe-O bond. The decrease ν(O-O) indicates the weakening the O-O bond. Both of these shifts are consistent with a slightly stronger hydrogen bond donation to the terminal oxygen, a change that would increase favorability of the O-O bond cleavage of the Fe-O-O fragment and formation of Compound I.

3.4 Summary

The results presented here show that the three natural substrates of CYP11A1 have quite different effects on the active site structure, including variations of spin state populations, reorientations of heme peripheral groups and, most importantly, substrate-mediated distortions of the Fe-XY fragments of bound exogenous ligands, including CO and O2, as revealed by telltale shifts of the ν(X-Y), ν(Fe-X) and δ(Fe-X-Y) vibrational modes. On the other hand, most significantly, our results reveal that the vibrational modes patterns observed for the Fe-O-O fragments of the dioxygan adducts obtained with the first and third substrates are almost identical, being consistent with H-bonding interactions to the terminal oxygen, a structural feature that tends to promote O-O bond cleavage and reactions mediated by the Compound I intermediate, as outlined above. Moreover, the effect of adrenodoxin binding to all three forms of CYP11A1 (ferric, ferrous CO and oxy forms) was studied and shows that, although Adx has small effect on ferric and ferrous CO states, it has a relatively stronger impact on the Fe-O-O fragments of the oxy complexes.

Our newly acquired data are partially consistent with what was published previously, but also clarified the confusion due to the apparent photo-dissociation during the measurement in case of 22R-OHCH with CYP11A1 complex in ferrous-CO form.[103] Our data clearly show that the enzyme bound with the non-H-bonding substrate, CH, yields only one set of vibrational modes for the CO adduct; i.e., ν(Fe-C) at 482 cm^{-1} and ν(C-O) at 1952 cm^{-1}. On the other hand, for the two substrates possessing hydroxyl substituents that are well positioned to H-bond with the bound Fe-C-O fragment, *two* sets

of Fe-C-O vibrational modes are seen. Thus, for both enzyme/substrate complexes, a ν(Fe-C)/ν(C-O) pair is seen at 482/1954 cm^{-1}, which is quite similar that that observed for the non-H-bonding CH substrate. On the other hand, the presence of one or two H-bonding hydroxyl groups near the Fe-C-O fragment generates a new set of modes having the ν(Fe-C) mode at 515 cm^{-1} (or 510 cm^{-1}) and the ν(C-O) mode at 1934 cm^{-1}. Our data also shows this is minimal effect of Adx in ferric and ferrous-CO forms.

Finally, a careful and thorough study of the rR spectra of the dioxygen adducts of CYP11A1 with all three substrates, revealed vibrational spectral patterns for the sample bound with 20R,22R-DiOHCH that were quite similar to those obtained for the first substrate, the non-H-bonding CH. Though it can be argued that the effective H-donor for these two cases might be different (water for CH and substrate hydroxyl for the DiOHCH), the Fe-O-O fragments in both cases are apparently well positioned to generate Compound I oxidative centers.

BIBLIOGRAPHY

(1) Les, A. M.; Lecomte, J. T. J. In *Protein Families*; Orengo, C.; Bateman, A., Eds.; 2014; pp. 207–235.

(2) Sigel, A.; Sigel, H.; Sigel, R. K. O. *"The Ubiquitous Roles of Cytochrome P450 Proteins", in Metal Ions in Life Sciences*; John Wiley & Sons, Ltd, 2007.

(3) Oohora, K.; Hayashi, T. *Curr. Opin. Chem. Biol.* **2014**, *19*, 154–161.

(4) Poulos, T. L. *Chem Rev.* **2014**, *114*, 3919–3962.

(5) Walker, F. A. *J. Inorg. Biochem.* **2005**, *99*, 216–236.

(6) Knipp, M.; He, C. *IUBMB Life* **2011**, *63*, 304–312.

(7) *Methods in Enzymology V76 Hemoglobins*; Antonini, E.; Rossi-Bernardi, L.; Chiancone, E., Eds.; Academic Press, 1981.

(8) Berg, J. M.; Tymoczko, J. L.; Stryer, L. In *Biochemistry*; W. H. Freeman and Company: New York, 2007; pp. 183–193.

(9) Jones, E. M.; Monza, E.; Balakrishnan, G.; Blouin, G. C.; Mak, P. J.; Zhu, Q.; Kincaid, J. R.; Guallar, V.; Spiro, T. G. *J. Am. Chem. Soc.* **2014**, *136*, 10325−10339.

(10) Reedy, C. J.; Gibney, B. R. *Chem Rev.* **2004**, *104*, 617–649.

(11) Degh, M.; Vries, S. De; Criml, M.; Ghelh, A.; Patarnello, T.; Meyer, A. *Biochim. Biophys. Acta* **1993**, *1143*, 243–271.

(12) Smith, L. J.; Kahraman, A.; Thornton, J. M. *Proteins* **2010**, *78*, 2349–2368.

(13) Soares, A. C.; Carvalho-Tavares, J.; Gontijo, N. D. F.; dos Santos, V. C.; Teixeira, M. M.; Pereira, M. H. *J. Insect. Physiol.* **2006**, *52*, 468–472.

(14) Bach, A.; Chodat, R. *Ber. Dtsch. Chem. Ges* **1903**, *36*, 600–605.

(15) Hamid, M. *Food Chem.* **2009**, *115*, 1177–1186.

(16) Rousseau, D. L.; Li, D.; Couture, M.; Yeh, S.-R. *J. Inorg. Biochem.* **2005**, *99*, 306–323.

(17) Liu, Q.; Gross, S. S. *Meth. Enzym.* **1996**, *268*, 311–324.

(18) Li, D.; Kabir, M.; Stuehr, D. J.; Rousseau, D. L.; Yeh, S. *J. Am. Chem. Soc.* **2007**, *129*, 6943–6951.

(19) Kikuchi, G.; Yoshida, T.; Noguchi, M. *Biochem. Biophys. Res. Commun.* **2005**, *338*, 558–567.

(20) Unno, M.; Matsui, T.; Ikeda-Saito, M. *Nat. Prod. Rep.* **2007**, *24*, 553–570.

(21) Antony, J.; Grodzicki, M.; Trautwein, A. X. *J. Phys. Chem. A* **1997**, *101*, 2692–2701.

(22) Schöneboom, J. C.; Lin, H.; Reuter, N.; Thiel, W.; Cohen, S.; Ogliaro, F.; Shaik, S. *J. Am. Chem. Soc.* **2002**, *124*, 8142–8151.

(23) Hofrichter, M.; Ullrich, R. *Appl. Microbiol. Biotechnol.* **2006**, *71*, 276–288.

(24) Axelrod, J. *J. Pharmacol. Exp. Ther.* **1955**, *114*, 430–438.

(25) Brodie, B.; Axelrod, J.; Cooper, J. R.; Gaudette, L.; LaDu, B. N.; Mitoma, C.; Udenfriend, S. *Science (80-.).* **1955**, *121*, 603–604.

(26) Garfinkel, D. *Arch. Biochem. Biophys.* **1958**, *77*, 493–509.

(27) Klingenberg, M. *Arch. Biochem. Biophys.* **1958**, *75*, 376–386.

(28) Hashimoto, Y.; Yamano, T.; Mason, H. S. *J. Biol. Chem.* **1962**, *237*, 3843–3844.

(29) Omura, T.; Sato, R. *J. Biol. Chem.* **1964**, *239*, 2379–2385.

(30) Omura, T.; Sato, R. *J. Biol. Chem.* **1964**, *239*, 2370–2378.

(31) Bayer, E.; Hill, H. A. O.; Röder, A.; Williams, R. J. P. *Chem. Commun.* **1969**, *109*.

(32) Hill, H. A. O.; Röder, A.; Williams, R. J. P. *Struct. Bond.* **1970**, *8*, 123–151.

(33) Hanson, L. K.; Keaton, W. A.; Sligar, S. G.; I. C. Gunsalus, M. G.; Connell, C. R. *J. Am. Chem. Soc.* **1976**, *98*, 2672–2674.

(34) Gunsalus, I. C.; Sligar, S. G. *Adv. Enzym. Relat. Areas Mol. Biol.* **1978**, *47*, 1–44.

(35) Champion, P. M.; Stallard, B. R.; Wagner, G. C.; Gunsalus, I. C. *J. Am. Chem. Soc.* **1982**, *104*, 5469–5473.

(36) Isin, E. M.; Guengerich, F. P. *Biochim. Biophys. Acta.* **2007**, *1770*, 314–329.

(37) Lewis, D. F. V. *Guide to cytochromes P450 structure and function*; Taylor & Francis Inc. New York, 2001.

(38) Nebert, D.; Nelson, D.; Feyereisen, R. *Xenobiotica* **1989**, *19*, 1149–1160.

(39) Mast, N.; Annalora, A. J.; Lodowski, D. T.; Palczewski, K.; Stout, C. D.; Pikuleva, I. a. *J. Biol. Chem.* **2011**, *286*, 5607–5613.

(40) Strushkevich, N.; MacKenzie, F.; Cherkesova, T.; Grabovec, I.; Usanov, S.; Park, H.-W. *Proc. Natl. Acad. Sci. USA* **2011**, *108*, 10139–10143.

(41) Meunier, B.; de Visser, S. P.; Shaik, S. *Chem. Rev.* **2004**, *104*, 3947–3980.

(42) Montellano, O. de. *Cytochrome P450: Structure, Mechanism, and Biochemistry*; Kluwer Academic/Plenum Publisher, New York, 2005.

(43) Song, W. N.; Ryu, Y. O.; Ju, W. *J. Biol. Inorg. Chem.* **2004**, *9*, 654–660.

(44) Champion, P. M. *Biological Applications of Raman Spectroscopy*; John Wiley and Sons: New York, 1988; pp. 249–292.

(45) Rittle, J.; Green, M. T. *Science (80-.).* **2010**, *330*, 933–937.

(46) Balding, P. R.; Porro, C. S.; McLean, K. J.; Sutcliffe, M. J.; Maréchal, J.-D.; Munro, A. W.; de Visser, S. P. *J. Phys. Chem. A* **2008**, *112*, 12911–12918.

(47) Conner, K. P.; Woods, C. M.; Atkins, W. M. *Arch. Biochem. Biophys* **2011**, *507*, 56–65.

(48) Peng, C.-C.; Pearson, J. T.; Rock, D. a; Joswig-Jones, C. a; Jones, J. P. *Arch Biochem Biophys* **2010**, *497*, 68–81.

(49) Gardiner, D. J. *Practical Raman Spectroscopy*; Springer-Verlag, 1989.

(50) McCleverty, J. A.; Meyer, T. J. *Comprehensive Coordination Chemistry II From Biology to Nanotechnology Vol. 2*; Elsevier: New York, 2004.

(51) Beekvelt, M. Van; Colier, W.; Wevers, R.; Engelen, B. Van. *J. Appl. Physiol.* **2001**, *90*, 511–519.

(52) Hu, S.; Kincaid, J. R. *J. Biol. Chem.* **1993**, *268*, 6189–6193.

(53) Macdonald, I. D. G.; Sligar, S. G.; Christian, J. F.; Unno, M.; Champion, P. M. *J. Am. Chem. Soc.* **1999**, *121*, 376–380.

(54) Complex, P.; Sjodin, T.; Christian, J. F.; Macdonald, I. D. G.; Davydov, R.; Unno, M.; Sligar, S. G.; Hoffman, B. M.; Champion, P. M. *Biochemistry* **2001**, *4*, 6852–6859.

(55) Kappl, R.; Hoehn-Berlage, M.; Huettermann, J.; Bartlett, N.; Symons, M. C. R. *Biochim. Biophys. Acta.* **1985**, *827*, 327–343.

(56) Davydov, R.; Macdonald, I. D. G.; Makris, T. M.; Sligar, S. G.; Hoffman, B. M. *J. Am. Chem. Soc.* **1999**, *121*, 10654–10655.

(57) Benson, D. E.; Suslick, K. S.; Sligar, S. G. **1997**, *2960*, 5104–5107.

(58) Mak, P. J.; Kaluka, D.; Manyumwa, M. E.; Zhang, H.; Deng, T.; Kincaid, J. R. *Biopolymers* **2008**, *89*, 1045–1053.

(59) Hu, S.; Schneider, A. J.; Kincaid, J. R. *J. Am. Chem. Soc.* **1991**, *113*, 4815–4822.

(60) Denisov, I. G.; Mak, P. J.; Makris, T. M.; Sligar, S. G.; Kincaid, J. R. *J. Phys. Chem A* **2008**, *112*, 13172–13179.

(61) Denisov, I. G.; Sligar, S. G. *Biochim. Biophys. Acta.* **2011**, *1814*, 223–229.

(62) Sligar, S. G.; Bayburt, T. H.; Schuler, M. A.; Civjan, N. R.; Grinkova, Y. V; Denisov, I. G. Membrane scaffold proteins for assembly of target membrane proteins into soluble nanoscale particles., 2004.

(63) Mak, P. J.; Denisov, I. G.; Grinkova, Y. V; Sligar, S. G.; Kincaid, J. R. *J. Am. Chem. Soc.* **2011**, *133*, 1357–1366.

(64) Headlam, M. J.; Tuckey, R. C. *Arch. Biochem. Biophys* **2002**, *407*, 95–102.

(65) Poulos, T. L.; Finzel, B. C.; Gunsalus, I. C.; Wagner, G. C.; Kraut, J. *J. Biol. Chem.* **1985**, *260*, 16122–16130.

(66) Guengerich, F. P. *Annu. Rev. Pharmacol. Toxicol* **1999**, *39*, 1.

(67) Miller, W. L.; Auchus, R. J. *Endocr. Rev.* **2011**, *32*, 81–151.

(68) Denisov, I. G.; Makris, T. M.; Sligar, S. G.; Schlichting, I. *Chem. Rev. (Washington, DC, United States)* **2005**, *105*, 2253–2277.

(69) Sligar, S. G.; Gunsalus, I. C. *Proc. Natl. Acad. Sci. USA* **1976**, *73*, 1078–1082.

(70) Fisher, M. T.; Sligar, S. G. *J. Am. Chem. Soc.* **1985**, *107*, 5018–5019.

(71) Kincaid, J. R. In *Porphyrin Handb.*; Academic Press, 2000; Vol. 7, pp. 225–291.

(72) Spiro, T. G.; Soldatova, A. V; Balakrishnan, G. *Coord. Chem. Rev.* **2013**, *257*, 511–527.

(73) Andersson, L. A.; Bylkas, S. A.; Wilson, A. E. *J. Biol. Chem.* **1996**, *271*, 3406–3412.

(74) Fisher, M. T.; Sligar, S. G. *Biochemistry* **1985**, *24*, 6696.

(75) Gunsalus, I. C.; Wagner, G. C. *Methods Enzym.* **1978**, *52*, 166–188.

(76) Manna, S. K.; Mazumdar, S. *Biochemistry* **2006**, *45*, 12715–12722.

(77) Das, A.; Grinkova, Y. V.; Sligar, S. G. *J. Am. Chem. Soc.* **2007**, *129*, 13778.

(78) Frank, D. J.; Denisov, I. G.; Sligar, S. G. *J. Biol. Chem.* **2011**, *286*, 5540–5545.

(79) Denisov, I. G.; Baas, B. J.; Grinkova, Y. V; Sligar, S. G. *J. Biol. Chem.* **2007**, *282*, 7066–7076.

(80) Nath, A.; Grinkova, Y. V; Sligar, S. G.; Atkins, W. M. *J Biol Chem* **2007**, *282*, 28309–28320.

(81) Guengerich, F. P. *Chem. Res. Toxicol.* **2008**, *21*, 70–83.

(82) Czarnecki, K.; Kincaid, J. R.; Fujii, H. *J. Am. Chem. Soc.* **1999**, *121*, 7953–7954.

(83) Lefranc, A.; Tournaire, C.; Martinez, A.; Berger, M.; Daoudal, S.; Tritsch, D.; Veyssie, G.; Jean, C.; Pascal, B.; Ce, L. *J Biol Chem* **1999**, *274*, 32875–32880.

(84) Rainey, W. E.; Saner, K.; Schimmer, B. P. *Mol. Cell. Endocrinol.* **2004**, *228*, 23–38.

(85) Pastel, E.; Pointud, J.-C.; Volat, F.; Martinez, A.; Lefrançois-Martinez, A.-M. *Front. Pharmacol.* **2012**, *3*, 148 (1–18).

(86) Martinez, A.; Aigueperse, C.; Val, P.; Tournaire, C.; Berger, M.; Jean, C.; Lefranc, A. *Chem. Biol. Interact.* **2001**, *130-132*, 903–917.

(87) Martinez, A.; Val, P.; Sahut-Barnola, I.; Aigueperse, C.; Veyssière, G.; Lefrançois-Martinez, A.-M. *Endocrinology* **2003**, *144*, 2111–2120.

(88) Baumann, C.; Davies, B.; Peters, M.; Kaufmann-Reiche, U.; Lessl, M.; Theuring, F. *Reproduction* **2007**, *134*, 97–109.

(89) Groves, J. T. *J. Inorg. Biochem.* **2006**, *100*, 434–447.

(90) Krest, C. M.; Onderko, E. L.; Yosca, T. H.; Calixto, J. C.; Karp, R. F.; Livada, J.; Rittle, J.; Green, M. T. *J Biol Chem* **2013**, *288*, 17074–17081.

(91) McQuarters, A. B.; Wolf, M. W.; Hunt, A. P.; Lehnert, N. *Angew. Chem. Int. Ed.* **2014**, *53*, 4750–4752.

(92) Groves, J. T. *Nat. chem.* **2014**, *6*, 89–91.

(93) Groves, J. T.; McClusky, G. A. *J. Am. Chem. Soc.* **1976**, *98*, 859–861.

(94) Murray, R. I.; Sligar, S. G. *J. Am. Chem. Soc.* **1985**, *107*, 2186–2187.

(95) Okamoto, T.; Sasaki, K.; Oka, S. *J. Am. Chem. Soc.* **1988**, *110*, 1187–1196.

(96) Lieberman, S.; Lin, Y. Y. *J. Steroid Biochem. Mol. Biol.* **2001**, *78*, 1–14.

(97) Byon, C.; Gut, M. *Biochem Biophys Res Commun* **1980**, *94*, 549–552.

(98) Duque C, Morisaki M, Ikekawa N, Shikita M, T. B. *Biochem. Biophys. Res. Commun.* **1978**, *85*, 317–325.

(99) Hochberg, R.; McDonald, P.; Feldman, M.; Lieberman, S. *J Biol Chem* **1974**, *249*, 1277–1285.

(100) Larroque, C.; van Lier, J. *J Biol Chem* **1986**, *261*, 1083–1087.

(101) Van Lier, J. E.; Rousseau, J. *FEBS Lett.* **1976**, *70*, 23–27.

(102) Larroque, C.; Rousseau, J.; Lier, J. E. Van. *Biochemistry* **1981**, *20*, 925–929.

(103) Tsubaki, M.; Yoshikawa, J. S.; Ichikawa, Y.; Yull, N. *Biochemistry* **1992**, *31*, 8991–8999.

(104) Tuckey, R. C.; Kamin, H. *J Biol Chem* **1983**, *258*, 4232–4237.

(105) Tsubaki, M.; Hiwatashi, a; Ichikawa, Y. *Biochemistry* **1986**, *25*, 3563–3569.

(106) Lambeth, J. D.; Pemberg, O. S. *J. Biol. Chem.* **1983**, *258*, 5596–5602.

(107) Lambeth, J. D.; Kriengsiri, S. *J. Biol. Chem.* **1985**, *260*, 8810–8816.

(108) Lambeth, J. D.; Seybert, D. W.; Kamin, H.; Chem, J. B.; David, J.; Seybert, W. *J. Biol. Chem.* **1979**, *254*, 7255–7264.

(109) Ewen, K. M.; Kleser, M.; Bernhardt, R. *Biochim Biophys Acta* **2011**, *1814*, 111–125.

(110) Kido, T.; Kimura, T. *J Biol Chem* **1979**, *254*, 11806–11815.

(111) Turko IV, Adamovich TB, Kirillova NM, Usanov SA, C. V. *Biochim Biophys Acta* **1989**, *996*, 37–42.

(112) Spiro, T. G. *biological applications of raman spectroscopy*; Spiro, T. G., Ed.; John Wiley and Sons, New York, 1988.

(113) Mak, P. J.; Zhu, Q.; Kincaid, J. R. *J. Raman Spectrosc.* **2013**, *44*, 1792–1794.

(114) Chen, Z.; Ost, T. W. B.; Schelvis, J. P. M. *Biochemistry* **2004**, *43*, 1798–1808.

(115) Smulevich, G.; Feis, A.; Howes, B. D.; Ivancich, A.; Edited by Kadish, Karl M. Smith, K. M.; Guilard, R. *Hand. Porphyr. Sci.* **2010**, *6*, 367–453.

(116) Friedman, J. M. *Meth. Enzym.* **1994**, *232*, 205–231.

(117) Kitagawa, T.; Mizutani, Y. *Coord. Chem. Rev.* **1994**, *135/136*, 685–735.

(118) Terner, J.; Palaniappan, V.; Gold, A.; Weiss, R.; Fitzgerald, M. M.; Sullivan, A. M.; Hosten, C. M. *J. Inorg. Biochem.* **2006**, *100*, 480–501.

(119) Marzocchi, M. P.; Smulevich, G. *J. Raman Spectrosc.* **2003**, *34*, 725–736.

(120) Peterson, E. S.; Friedman, J. M.; Chien, E. Y. T.; Sligar, S. G. *Biochemistry* **1998**, *37*, 12301–12319.

(121) Hu, S.; Smith, K. M.; Spiro, T. G. *J. Am. Chem. Soc.* **1996**, *118*, 12638–12646.

(122) Rwere, F.; Mak, P. J.; Kincaid, J. R. *Biopolymers* **2008**, *89*, 179–186.

(123) Cerda-Colon, J. F.; Silfa, E.; Lopez-Garriga, J. *J. Am. Chem. Soc.* **1998**, *120*, 9312–9317.

(124) Gregory, M.; Mak, P. J.; Sligar, S. G.; Kincaid, J. R. *Angew. Chem. Int. Ed. Engl.* **2013**, *52*, 5342–5345.

(125) Galinato, M. G. I.; Spolitak, T.; Ballou, D. P.; Lehnert, N. *Biochemistry* **2011**, *50*, 1053–1069.

(126) Yoshioka, S.; Tosha, T.; Takahashi, S.; Ishimori, K.; Hori, H.; Morishima, I. *J. Am. Chem. Soc.* **2002**, *124*, 14571–14579.

(127) Lang, J.; Santolini, J.; Couture, M. *Biochemistry* **2011**, *50*, 10069–10081.

(128) Sabat, J.; Stuehr, D. J.; Yeh, S.; Rousseau, D. L. **2009**, *131*, 12186–12192.

(129) Mak, P. J.; Im, S.-C.; Zhang, H.; Waskell, L. A.; Kincaid, J. R. *Biochemistry* **2008**, *47*, 3950–3963.

(130) Mak, P. J.; Luthra, A.; Sligar, S. G.; Kincaid, J. R. *J. Am. Chem. Soc.* **2014**, *136*, 4825–4828.

(131) Davydov, R.; Gilep, A. A.; Strushkevich, N. V; Usanov, S. A.; Hoffman, B. M. *J. Am. Chem. Soc.* **2012**, *134*, 17149−17156.

(132) Spiro, T. G.; Soldatova, A. V. *J. Inorg. Biochem.* **2012**, *115*, 204–210.

(133) Visser, S. P. De; Cohen, S.; Sharma, P. K.; Shaik, S. *J. Am. Chem. Soc.* **2002**, *124*, 2806–2817.

(134) Cho, K.-B.; Gauld, J. W. *J. Phys. Chem. B* **2005**, *109*, 23706–23714.

(135) Pant, K.; Crane, B. R. *Biochemistry* **2006**, *45*, 2537–2544.

(136) Lu, C.; Egawa, T.; Wainwright, L. M.; Poole, R. K.; Yeh, S.-R. *J Biol Chem* **2007**, *282*, 13627–13636.

(137) Chartier, F. J. M.; Couture, M. *J Biol Chem* **2007**, *282*, 20877–20886.

(138) Compton, S.; Jones, C. *Anal Biochem* **1985**, *151*, 369–374.

(139) Khatri, Y.; Gregory, M. C.; Grinkova, Y. V.; Denisov, I. G.; Sligar, S. G. *Biochem. Biophys. Res. Commun.* **2014**, *443*, 179–184.

(140) Couture, M.; Stuehr, D. J.; Rousseau, D. L. *J Biol Chem* **2000**, *275*, 3201–3205.

(141) Khatri, Y.; Luthra, A.; Duggal, R.; Sligar, S. G. *FEBS Lett.* **2014**, *588*, 3117–3122.

(142) Lambeth, J. D.; Kitchen, E.; Farooqui, A. A.; Tuckey, R.; Kamin, H. *J. Biol. Chem.* **1982**, *257*, 1876–1884.

(143) Tsubaki, M.; Hiwatashi, a; Ichikawa, Y. *Biochemistry* **1987**, *26*, 4535–4540.

(144) Antonini, E.; Brunori, M. *HEMOGLOBIN AND MYOGLOBIN IN THEIR REACTIONS WITH LIGANDS*; NORTH-HOLLAND, 1971.

(145) Pruitt, K.; Tenovuo, J. *The Lactoperoxidase System: Chemistry and Biological Significance*; Marcel Dekker: New York, 1985.

(146) Reiter, B.; Perraudin, J. P. Everse, J.; Everse, K. E.; Grisham, M. B., Eds.; CRC Press: Boca Raton, FL, 1991; pp. 143–180.

(147) Mak, P. J.; Gregory, M. C.; Sligar, S. G.; Kincaid, J. R. *Biochemistry* **2014**, *53*, 90–100.

(148) Unno, M.; Christian, J. F.; Benson, D. E.; Gerber, N. C.; Sligar, S. G.; Champion, P. M. *J. Am. Chem. Soc.* **1997**, *119*, 6614–6620.

(149) Ibrahim, M.; Xu, C.; Spiro, T. G. *J. Am. Chem. Soc.* **2006**, *128*, 16834−16845.

(150) Ray, G. B.; Li, X. Y.; Ibers, J. A.; Sessler, J. L.; Spiro, T. G. *J. Am. Chem. Soc.* **1994**, *116*, 162–176.

(151) Li, X. Y.; Spiro, T. G. *J. Am. Chem. Soc.* **1988**, *110*, 6024–6033.

(152) Wells, A. V; Li, P.; Champion, P. M.; Martinis, S. A.; Sligar, S. G. *Biochemistry* **1992**, *31*, 4384–4393.

(153) Uno, T.; Nishimura, Y.; Makino, R.; Iizuka, T.; Ishimura, Y.; Tsuboi, M. *J. Biol. Chem.* **1985**, *260*, 2023–2026.

(154) Chartier, F. J. M.; Blais, S. P.; Couture, M. *J Biol Chem* **2006**, *281*, 9953–9962.

(155) Harris, D. L.; G. H. Loew. *J. Am. Chem. Soc.* **1998**, *120*, 8941–8948.

(156) Antonini, E.; Luigi Rossi-Bernardi; Chiancone, E. *Methods in Enzymology*; volume 76.; Academic Press, 1981.

Appendix I Preparation of meso/proto hybrids

1. Isolation hemoglobin from blood

One unit of out-dated human blood around 300 ml was obtained from blood center in Marquette University. The blood was kept in the foam box contained with ice bag when transferring from blood center to our lab. Pour around 150 ml of blood in 250ml centrifuge tube and then mix with 0.9% NaCl solution which is prepared in deionized water and cooled down to 4 °C. Centrifuge the mixture at 4 °C, 8000 rpm for 10 minutes. The supernatant was removed with the white coating on the top of the red cells through a pipette connected with aspirator. Waste flows to the flask contained with bleach. This procedure was repeated three times and the final suspensions were centrifuged at 4 °C, 10,000 rpm, 10 minutes.

Mix 3 volume of 4 °C deionized water with the red cells. Use glass rod to mix the solution well and keep at 4 °C for one hour and then centrifuge at 4 °C, 12,000 rpm for 1.5 hours. The cell debris sticks on the wall of the bottle. Decant solution into a flask with cautious to avoid transfer any cell debris. Saturate with CO for 30 minutes with stir bar added in the solution. Separate the pure CO-hemoglobin into different tubes for storage purpose. Store the CO-hemoglobin in -80 °C freezer for long term storage and -20 °C freezer for relatively short period storage.

2. Make apo-hemoglobin

Run CO-hemoglobin through an AG 501-X8 (D) Resin 20-50 mesh column with 4 °C deionized water in order to remove the heavy cation metal impurities. Adjust the concentration to be less than 1 mM determined by UV-vis spectrum. Acidic acetone was prepared by mix 1 L of HPLC grade acetone with 3 ml of 2 M HCl. Cool this solution to -20 °C in a dry ice bath with constant stirring. Around 30 ml of CO-hemoglobin was added to the acidic acetone solution. The solution turned into a rust color which is due to the removal of heme into the solution. Incubate this solution for around 10 minutes. Centrifuge the solution for 20 minutes at -20 °C, 10,000 rpm. Remove the apo-hemoglobin which sticks on the wall and bottom of centrifuge tube. Dissolve this acetone contained apo-hemoglobin in deionized water. Dialysis apo-hemoglobin for three hours in deionized water. Then change to fresh deionized water to dialysis for overnight. The next morning, change dialysis buffer with 20 mM phosphate buffer (PB) pH=7.0 for three hours. Dialysis will allow to move any residual acetone and denatured protein.

3. Make meso-hemoglobin

Check UV-vis spectrum for previously prepared apo-hemoglobin and determine its concentration. Weigh 1.2 molar excess of meso-heme and dissolve in a minimal amount of 0.1 M KOH. Dilute that solution with deionized water to reduce its basicity. Apo-hemoglobin was placed in a round flask with gentle stir on the ice bath. Dropwisely add the meso-heme solution into the flask. Keep the pH=6.0 by using 0.1 M KCl and 0.1

M KOH. When the addition was complete, allow the solution to stir for 5 minutes and then the mixture was saturated with Ar for 30 minutes to create an inert atmosphere. The mixture was kept at 4 °C for three days to allow heme flipping in the active site which is the stable form of meso-heme.

After three days, saturate under CO for 30 minutes. Excess amount of sodium dithionite $Na_2S_2O_4$ was added to the solution. The color of the solution changed from brown to brilliant red. That is because the Fe^{3+} was reduced to Fe^{2+} by $Na_2S_2O_4$. Let the solution stay under CO for another 5 minutes. Then run the sample through a G25 with 20 mM PB pH=7.4 to remove excess $Na_2S_2O_4$. This is the pure meso-hemoglobin.

4. Make alpha and beta subunits

Dialysis CO-hemoglobin in 20 mM PB pH=7.4 for overnight and then dilute to approximately 1 mM if the concentration is higher than 1 mM. The concentration was determined by UV-vis spectrum. Meso-hemoglobin is already in 20 mM PB pH=7.4. Calculate the amount of 4-hydroxymercuribenzoic acid sodium salt needed for separation of alpha and beta chain. For each gram of CO-hemoglobin or meso-hemoglobin with molecular weight 64 KDa is needed 100 mg of PMB. The PMB is used to break the thiol group thus reducing the affinity of subunits from one another. Put CO-hemoglobin or meso hemoglobin in a beaker with stir bar inside on the ice bath and stir. Add NaCl to make the NaCl concentration 0.25 M and mix well. Adjust the pH to 6.0 with 1 M KH_2PO_4.

Dropwise add minimum amount of 0.1 M KOH to dissolve PMB. A clear/yellow solution will appear when PMB dissolves. Dropwise add 0.1 M acetic acid and mix well until a slight turbidity persisted. Add this PMB solution into CO-hemoglobin or meso-hemoglobin solution. Adjust the pH=6.0 by using 0.1 M acetic acid and 0.1 M KOH. After addition, mix well and then wrapped with aluminum foil. Keep the mixture at for 4 °C for overnight.

The next day, centrifuge the PMB-hemoglobin solution for 10 minutes at 4 °C 6,000 rpm to remove excess PMB. Load the sample to P-6 Biogel column with 50 mM Tris buffer pH=8.4 (at room temperature pH=7.8). The entire sample was applied to a DE53 column equilibrated with 50 mM Tris buffer pH=8.4. The alpha-PMB subunit was eluted with the buffer and collected. The buffer was changed to 30 mM PB pH=7.4 to elute any unreacted hemoglobin. The buffer was changed to 100 mM PB pH=7.4 to elute beta-PMB subunit. Concentrate each PMB contained subunit.

Run alpha-PMB subunits through a P-6 Biogel column with 100 mM PB buffer pH=7.4 contained 25 mM 2-Mercaptoethanpol (BME). PMB will be not bind with alpha subunit after treating with BME. After collection of BME treated alpha-PMB subunit, incubate for around 45 minutes and then run through a P-6 Biogel column with 100 mM PB pH=7.4 to remove PMB and BME. The sample is pure alpha subunit. Pure beta subunit can be obtained by same process just with 50 mM BME instead of 25 mM. Alpha and beta subunits are concentrated and stored at -20 °C freezer for making hybrids.

5. Make proto and meso hybrids

The Meso/Proto hemoglobin hybrids were made by mixing a 1.2 molar excess of beta subunits to alpha subunits. Slowly stir the mixture for 30 minutes to allow the hybrid mix adequately and then incubate the mixture at 4 °C for overnight.

The next day, run the sample through a P-6 Biogel column with 20 mM PB pH=6.4. Then the entire sample was applied on a CM52 column equilibrated by 20 mM PB pH=6.4. Excess beta subunit will pass through the column with buffer. Elute the tetrameric hybrids by changing buffer to 30 mM PB pH=7.0. Residual alpha subunit can be eluted by 50 mM PB pH=7.0.

Appendix II Preparation of Co/Fe hybrids

1. Make Co/Fe hybrids

Isolation of hemoglobin, preparation of apo-hemoglobin and separation of proto-Fe subunits are described in previous section. The rest of the steps for preparation of oxy-Co(II) hemoglobin will be addressed below.

2. Preparation of oxy-Co(II) hemoglobin

Prepare a degassed G-25 column which is washed by large amount of degassed 10 mM PB pH=6.0 buffer. The column is placed in the glove bag at 4 °C. The bag is also degassed by vacuuming the air out and filling the Ar in. That process will be repeated three times to insure no oxygen in the glove bag.

An anaerobic equipment was set up to proceed reduce Co(III) in Co(III) protoporphyrin IX chloride (PPIX) complex to Co(II) and then reconstitute into apo-hemoglobin. The set up was made by connecting two round bottom flask with stir bar inside and two air-tight vial with Ar. The round flasks and vials were sealed with rubber septa. They were connected with long needles to let Ar flow or transfer reactants from one to another. Apo-hemoglobin was placed in the round bottom flask which was in the ice bath with slowly continuous stirring. Weight 1.2 molar excess of Co(III) PPIX and place in another round bottom. Use minimum amount of pyridine to dissolve Co(III) PPIX and then add additional 10 mM PB pH=7.0 to reach a volume which is 1/10 the

volume of the apo-hemoglobin. This flask was also place on ice bath with slowly continuous stirring. Place 1 ml of 10 mM PB pH=7.0 in one vial and about 12 molar excess of $Na_2S_2O_4$ in another vial. Seal the flasks and vials and connect them with needles attached with Ar gas. Degas the whole thing for 40 minutes.

After 40 minutes degassing, immerse the needle in the vial which contains 1 ml of buffer. This will allow the buffer to transfer to another vial which contains 12 molar excess of $Na_2S_2O_4$. Shake the vial so the $Na_2S_2O_4$ will dissolve in the buffer. The same process is repeated to transfer the $Na_2S_2O_4$ solution to Co(III) PPIX solution. Because Co(III) complex is inert due to its electron configuration, its t_{2g} orbital is filled by electron. Fully reducing Co(III) to Co(II) will be insured by taking UV-vis spectrum. 12 molar excess is usually enough to reduce Co(III) to Co(II). If there is some Co(III) residual detected by UV-vis, then more $Na_2S_2O_4$ will be added following the above procedure. Degas some 1 M KH_2PO_4 and then store in a degassed syringe. Penetrate the syringe in the rubber septa on the round flask which contains apo-hemoglobin. Completely reduced Co(II) PPIX complex was transferred to apo-hemoglobin by immerse the needle in the Co(II) PPIX solution which was confirmed by UV-vis at different stage to make sure all Co(III) has been reduced to Co(II) by $Na_2S_2O_4$. This process will be done slowly and in the mean time, add the solution in the syringe to let the apo-hemoglobin in the neutral or weak acidic environment. This will decrease the precipitate. Leave the flask on the ice bath for 5 minutes to let the reaction complete. The color is dark-red after the reaction completed.

Apply the entire sample on the degassed G-25 column. This will allow to remove excess amount of $Na_2S_2O_4$. Deoxy Co(II) hemoglobin will be collected and some of the

deoxy Co(II) hemoglobin will become oxy form when expose in the air. The solution will be placed on ice bath and saturated with O_2 for one hour. The sample is applied on CM52 column which is previously equilibrated with 10 mM PB pH=6.0. Pure oxy Co(II)-hemoglobin will be eluted with buffer 100 mM PB pH=7.0. The sample is dialysis overnight against 20 mM PB pH=7.4 in order to proceed PMB treatment for subunits separation.

3. Make alpha and beta subunits

The PMB treatment to oxy Co(II) hemoglobin is identical to the previous procedure described in section 2.1.4. After incubating the PMB contained oxy Co(II) hemoglobin for overnight, centrifuge the sample for 10 minutes, at 4 °C 6,000 rpm to remove excess amount of PMB. Run the sample through P-6 Biogel column with 10 mM PB pH=8.0. Then apply the entire sample to DE53 column previous equilibrated with 10 mM PB pH=8.0. Alpha subunits is eluted with buffer 10 mM PB pH=8.0. Elute unreacted oxy-Co(II)-Hb with 30 mM PB pH=8.0. Then beta subunits was eluted with 100 mM PB pH=8.0. Concentrated subunits to around 10 ml. Add each subunit to a round bottom flask sealed with rubber septum, stir on ice bath and degas with Ar for 30 minutes. Add catalase to make the solution at concentration 5 µM catalase and DDT[156] to make the concentration 20 mM. The addition process needs to be done in anaerobic environment created by flowing Ar around the flask. After addition, the solution is saturated with Ar for 5 minutes without stirring and then placed under Ar for 15 minutes with stirring. Incubate for 90 minutes at 4 °C. Alpha subunits were applied on P-6 Biogel column with

10 mM PB pH=6.6. And then apply the entire sample to CM52 column previous equilibrated with 10 mM PB pH=6.6. Excess catalase will be eluted with the buffer 10 mM PB pH=6.6 and pure alpha subunits is eluted with 50 mM PB pH=7.4. Beta subunits are applied on P-6 Biogel column with 10 mM PB pH=8.0. And then apply the entire sample to DE53 column previous equilibrated with buffer 10 mM PB pH=8.0. Pure beta subunits are eluted with 50 mM PB pH=7.4.

The procedure of making Fe/Co hybrids are the same as described in previous section. Each hybrid is applied under O_2 with a photolysis lamp to remove CO ligated for 30 minutes. Oxygenated Fe/Co hybrids are obtained.